To the Graduate Council:

I am submitting herewith a thesis written by Bulent Aydogan entitled "Uncertainty Analysis for Absorbed Dose of a Brain Receptor Imaging Agent." I have examined the final copy of this thesis for form and content and recommend that it be accepted in partial fulfillment of the requirements for the degree of Master of Science, with a major in Nuclear Engineering.

Dr. Larry F. Miller, Major Professor

We have read this thesis
and recommend its acceptance:

Dr. K. Eckerman, Committee Member

Dr. P. Groer, Committee Member

Accepted for the Council

Associate Vice Chancellor and
Dean of The Graduate School

UNCERTAINTY ANALYSIS FOR

ABSORBED DOSE OF A BRAIN RECEPTOR IMAGING

AGENT

A Thesis
Presented for the
Master of Science Degree
The University of Tennessee, Knoxville

Bulent Aydogan

May 1996

DEDICATION

This thesis is dedicated to

my teachers

and to my parents

Mr. Ahmet Aydogan

Mrs. Anahanim Aydogan

my sister

Fatma Aydogan

and

my brother

Halit Aydogan

who are constant sources of inspiration in my life.

ACKNOWLEDGMENT

I would like to thank my major professor Dr. L.F. Miller, and technical advisors Dr. J. Stubbs and Richard Sparks for their guidance and patients. I would also like to thank the other committee members, Dr. K. Eckerman and Dr. P. Groer for their comments and assistance. I would like to express my thanks to the staff of the Internal Radiation Dose Center (RIDIC/ORAU) for their assistance. My life got richer by knowing each one of you. Special thanks go to R. Sparks for his invaluable assistance in this thesis. Without your technical guidance and editorial support this work would not be completed.

ABSTRACT

Radiation absorbed dose is calculated in order to predict the risk in a nuclear medicine procedure. However, it is not possible to calculate the true absorbed dose a patient would receive as a result of the exposure to ionizing radiations. Although absorbed dose estimates are known to contain uncertainty, no rigorous work which investigated the uncertainty associated with absorbed dose estimates existed before this study.

A method of uncertainty analysis for absorbed dose calculations was developed and calculations were performed for a brain imaging agent ^{123}I-IPT. The two major sources of uncertainty considered in this research were the inter-patient organ mass variabilities and uncertainty associated with the determination of residence times. The latter included the uncertainty associated with inter-patient biokinetic variabilities and the uncertainty associated with the least squares parameter estimation procedure. In this research the classical approach of statistics was employed.

Absorbed dose uncertainties for a seven patient population and for each patient sepaerately were determined by the use of a "Latin Hypercube Sampling" method. The upper bound of the 95% confidence interval of the dose distribution for an individual was found to be 2.5 times larger than the estimated mean absorbed dose. Neglecting the variability in organ masses, the upper bound of the 95% confidence interval of the dose distribution was about 45% more than the estimated population mean. Incorporation of the inter-patient organ mass variabilities, without including correlations to absorbed fraction, into uncertainty calculations almost doubled the range of the 95% confidence intervals of the population dose distributions. For instance, the 95% confidence interval of the population liver dose distribution was between 5.6E-05 rad/μCi and 1.7E-04 rad/μCi with a mean of 9.3E-05 rad/μCi. This study concluded that a new patient who is similar to the study group might receive an absorbed dose of twice as large as the estimated population mean due to the considered uncertainties.

Although there are several cases where diagnostic imaging may involve risk, in general, it is believed that diagnostic imaging entails little or no risk. Therefore, the determination of uncertainty is potentially more important in therapy applications of radiopharmaceuticals due to the much larger absorbed dose. Uncertainty information for a patient population can be used to predict the maximum dose (with the desired confidence such as 90% or 95%) a new patient who is similar to the study group might receive. The physician can then include the uncertainty information in his risk/benefit

evaluation in radiation therapy. The physician might be aided in estimating potential patient radiation doses by the construction of absorbed dose data bases which also include absorbed dose uncertainties for the frequently used therapeutic agents in nuclear medicine. The method established in this work can be used in order to construct such absorbed dose data bases. Future studies should include correlation of absorbed dose with mass variabilities.

TABLE OF CONTENTS

1. INTRODUCTION.....1

1.1Background.....1

1.2 Statement of the problem.....3

1.3 Overview of the methodology.....5

1.4 Organization of Thesis.....7

2. PRINCIPLES OF NUCLEAR MEDICINE.....9

2.1 Introduction.....9

2.2 Imaging Techniques.....11

2.3 Radiopharmaceuticals.....13

2.3.1 Radionuclides for nuclear imaging.....15

2.3.2 Production of radionuclide.....16

2.4 Pharmaceutical selection.....18

3. ABSORBED DOSE.....22

3.1 Introduction.....22

3.2 Absorbed dose.....23

3.3 The mean dose per unit cumulated activity, S-value.....26

3.3.1 Radionuclide data: The mean energy emitted per nuclear transition, Δ_i.....28

3.3.2 Anatomic data: The specific absorbed fraction, Φ_i 29

3.4 Biokinetics of radiopharmaceuticals and cumulated activity 34

3.5 Cumulated activity, $\tilde{A}_h$ 36

3.5.1 Residence time, τ_h 41

4. BIOKINETIC MODELING AND PARAMETER ESTIMATION 45

4.1 Introduction 45

4.2 Biokinetic modeling 47

4.2.1 Tracers 49

4.2.2 Compartments 49

4.3 Mathematics of compartmental modeling 51

4.4 Parameter estimation 58

4.5 Estimation of parameter uncertainties 66

4.6 Statistical analysis of estimated parameters through the asymptotic approach. 67

5. DETERMINATION OF UNCERTAINTIES IN THE ABSORBED DOSE CALCULATIONS 70

5.1 Introduction 70

5.2 Residence time calculations 74

5.2.1 Biokinetic data analysis 75

5.3 Methodology for the determination of residence times and associated uncertainties. 78

5.4 S-values and error propagation 96

5.4.1 The specific absorbed fraction, Φ_i 97

5.4.2 Statistical evaluation of the determination of absorbed dose by Monte Carlo method. 99

5.4.3 Methodology 101
5.4.3.1 For penetrating radiations: photons 102
5.4.3.2 Calculations 103
5.4.4 Nonpenetrating particles 105
5.4.5 The S-value uncertainties with the incorporation of inter-patient mass variability 107
5.5 Remainder of the body correction 110
5.6 Calculation of absorbed dose and determination of uncertainty 112
5.6.1 Determination of uncertainty when mass variabilities were neglected. 115
5.6.2 Determination of uncertainties when mass variabilities were considered as an additional source of uncertainty. 124

6. CONCLUSIONS AND RECOMMENDATIONS FOR FUTURE STUDIES 137

6.1 Conclusions 138
6.2 Recommendations for future studies 141

REFERENCES 143

APPENDICES 152

APPENDIX A. SAAM 153

APPENDIX B. Crystal Ball 165

VITA 172

LIST OF FIGURES

Figure 2.1 A hypothetical time-activity curve which illustrate the normal and abnormal biodistribution for a patient with blood brain barrier defect.....10

Figure 2.2 A time activity curve and a static posterior image from a flow study. The time activity curve demonstrates reduced portal flow (curve 2) which can not be determined from the static image shown in figure (b).....14

Figure 2.3 Biodistribution of four different ^{99m}Tc labeled drugs. Sulfur colloid for liver and spleen imaging, macroaggregates for lung perfusion imaging, DTPA for kidney-ureter-bladder imaging. andmethylene diposhonate for skelatal imaging 19

Figure 3.1 Pictorial illustration of absorbed dose concept.....31

Figure 3.2 The plot of the specific absorbed fraction as a function of photon energy for source organ liver and target organs, lung and stomach (based on Snyder *et al*'s SAF values).....35

Figure 3.3 The plot of the self organ specific absorbed fraction as a function of photon energy for liver (based on Snyder *et al*'s SAF values).....35

Figure 3.4 Hypothetical time-activity curves which illustrate the normal and abnormal activity distributions for a patient with a) blood brain barrier defect, b) low blood flow to the liver, and c) myocardial hypertrophy.....37

Figure 3.5 Pictorial illustration of the residence time.....43

Figure 3.6 Two hypothetical time-activity curves which illustrate rapid uptake with different removal phases. 44

Figure 3.7 A plot of a hypothetical time-activity curve with a slow uptake phase. 44

Figure 4.1 A typical compartmental model used in internal dosimetry applications 50

Figure 5.1 Simplified compartmental model for ^{123}I-IPT dosimetry 80

Figure 5.2 Illustration of the lung dose distribution for the seven-patient population with 95% confidence interval (mass variabilities were neglected). 121

Figure 5.3 Illustration of the liver dose distribution for the seven-patient population with 95% confidence interval (mass variabilities were neglected) 121

Figure 5.4 Illustration of the heart dose distribution for the seven-patient population with 95% confidence interval (mass variabilities were neglected). 122

Figure 5.5 Illustration of the brain dose distribution for the seven-patient population with 95% confidence interval (mass variabilities were neglected). 122

Figure 5.6 The 95% confidence interval of the liver absorbed dose distribution for patient PT (mass uncertainty was included). 128

Figure 5.7 Illustration of the lung dose distribution for the seven-patient population with 95% confidence interval (mass variabilities were included). 130

Figure 5.8 Illustration of the liver dose distribution for the seven-patient population with 95% confidence interval (mass variabilities were included). 130

Figure 5.9 Illustration of the brain dose distribution for the seven-patient population with 95% confidence interval (mass variabilities were included). 131

Figure 5.10 Illustration of the heart dose distribution for the seven-patient population with 95% confidence interval (mass variabilities were included). 131

Figure B. 1 Crystal Ball distribution gallery. 166

Figure B. 2 An example of assumption window for lognormal distribution. 167

Figure B. 3 Crystal Ball correlation window. 168

Figure B. 4 An example of Crystal Ball forecast window. 169

Figure B. 5 Run preference dialog window. 170

Figure B. 6 A forecast chart. 171

LIST OF TABLES

Table 5.1 A comparison of the multiexponential curvefit and compartmental model solutions for the residence time.....82

Table 5.2 A SAAM output for the patient BS.....84

Table 5.3 Parameter estimates, associated standard deviations, and 95% confidence intervals of mean parameter values for brain and liver.....86

Table 5.4 Two SAAM parameter estimates and their associated uncertainties for BS liver, and their comparison which indicate the nonuniquenesse of the solution.....89

Table 5.5 Some examples of the parameter uncertainties and the sum of squared error of the curvefits. 90

Table 5.6 Residence times for the source organs and their associated standard deviations calculated by both FOEP and LHS sampling method.....94

Table 5.7 An example table which shows the specific absorbed fractions and associated uncertainties for discrete photon energies and for ^{123}I spectrum, S-values and their estimated uncertainties.....106

Table 5.8 The list of the mean organ masses and their approximate standard deviations for American population.....108

Table 5.9 The S-values and associated standard deviations for source/target organ pairs and for the remainder of the body when mass variabilities were ignored. 113

Table 5.10 The S-values and associated standard deviations for source/target organ pairs and for the remainder of the body when mass uncertainties were included into calculations. 114

Table 5.11 The organ doses and associated standard deviations for each patient mass variabilities were neglected 117

Table 5.12. The mean organ doses for the seven-patient population and associated uncertainties for the mean doses and population doses when mass variabilities were neglected..... 120

Table 5.13 The maximum and minimum target organ doses for the seven-patient population with 95% confidence when mass variabilities were neglected..... 123

Table 5.14 List of the organ doses and associated uncertainties for each patient when the mass variabilities were included in uncertainty calculations..... 125

Table 5.15 The mean organ doses for the seven-patient population and associated uncertainties for mean doses and population doses when mass variabilities were included..... 127

Table 5.16 The maximum and minimum target organ doses for the seven-patient population with 95% confidence when the mass variabilities were considered as an additional source of uncertainty..... 132

Table 5.17 Comparison of the absorbed dose uncertainties and 95% confidence intervals when including and neglecting mass variabilities..... 134

Table A. 1 A SAAM input deck. 154

Table A. 2 SAAM dictionary..... 157

Table A. 3 An example output of SAAM. 158

Table A. 4 Available mathematical models in SAAM 161

Chapter 1

INTRODUCTION

1.1 Background

Since their discovery by Roentgen, external sources of X-rays for imaging have become a widely used tool in medicine. Their primary usefulness is, however, in obtaining anatomical information. Little or no information concerning organs' physiological functions can be obtained using external X-ray beams. To obtain information concerning organs' physiological functions one of the tools physicians use is radionuclide imaging. Physiological information is gathered by administering a radio-labeled substance to the patient and obtaining images with some sort of radiation camera. The use of radioisotopes in tracer quantities for the clinical diagnosis of human diseases as well as larger quantities for therapeutic procedures, has grown rapidly in the last two decades and has become a recognized medical specialty known as nuclear medicine. Nuclear imaging involves a variety of techniques to produce images of distribution of radio-labeled agents in the body. These agents, known as radiopharmaceuticals, are

designed to show biologic function of an individual organ or system of the body. Nuclear medicine physicians are then able to diagnose diseases quite accurately and rapidly, which is very important for quality medical care. Nuclear imaging replaces the diagnostic methods which make use of the symptoms of diseases, biopsy, and surgical methods which in some cases are very hard to perform, such as a brain biopsy.

Although it is highly expensive to maintain some nuclear imaging units such as positron emission tomography (PET), these nuclear imaging units significantly aid in the diagnosis of diseases. Nuclear imaging has become a routine medical diagnosis procedure. In 1993, approximately 664,000 nuclear medicine procedures including therapy and noninvasive physiologic and metabolic studies were performed in United States [1, 2]. This number is believed to be doubled every year.

On the other hand, risk can be involved in the use of a radiopharmaceutical in nuclear medicine studies. There is a direct relationship between the risk a patient incurs and the absorbed dose to the patient from a nuclear medicine procedure. Absorbed dose is the physical quantity describing the amount of energy from ionizing radiation absorbed by a unit mass of tissue. A nuclear medicine physician must know the absorbed dose distribution a patient will receive as a consequence of the administration of the radiopharmaceutical and then decide whether the benefit the patient will receive justifies the risk of the radiation exposure from the procedure.

1.2 Statement of the problem

Internal radiation dosimetry is the scientific methodology used to estimate the radiative energy absorbed in various tissues from a deposition of radioactive substance in the body. For nuclear medicine purposes, absorbed dose is calculated using a method developed by the Medical Internal Radiation Dose Committee (MIRD) of the Society of Nuclear Medicine (SNM). The MIRD method calculates the absorbed dose from two components [3]:

1. The time dependent biokinetic distribution of the radiopharmaceutical which is used to calculate the total number of transition in the source organ *h,* the cumulated activity $\tilde{A}_h$.

2. A physical quantity, absorbed fraction which is the fraction of energy emitted from the source organ that is absorbed in the target organ.

Being empirical data these quantities are subject to uncertainty. It is not possible to measure the data and estimate the absorbed dose with 100% certainty. Therefore, several questions arise about the absorbed dose calculation and MIRD method. These are some that first come to mind :

- How large is the uncertainty associated with the MIRD method of absorbed dose calculation?

- What are the possible sources of uncertainty?

- How can the uncertainty in the absorbed dose calculations be reduced?

Although the absorbed dose calculation methods seem to have large uncertainties, there has been no rigorous attempt to calculate the uncertainties in the absorbed dose calculations. In his book *Uncertainty*, G. M. Morgan says, "To people trained in the physical sciences, dealing with uncertainty is almost second nature. Serious physical scientists would not report an experimental result without giving an associated estimate of uncertainty, nor would they design an experiment without giving careful attention to uncertainties"[4].

The present work has been performed to determine possible sources and quantitative information of uncertainty and establish a method for uncertainty analysis in the absorbed dose estimation.

1.3 Overview of the methodology

In the present study the classical uncertainty approach and "Sampling Theory" were used to estimate uncertainty associated with the calculations of absorbed dose as a result of internally administered brain imaging agent ^{123}I-IPT (Cocaine analog pturine). Other than the sampling method, first order error propagation method (FOEP) was utilized to propagate the error when it is theoretically applicable, in order to make comparison between the two method of error propagation.

In order to assess uncertainty in the estimated absorbed dose, the uncertainty associated with the cumulated activity and the *S-values* were first determined and then propagated through the result of absorbed dose calculation.

The biodistribution of the compound as a function of time was measured in several normal adults. Time-activity curves for several significant source organs were mathematically simulated using multiexponential functions. The SAAM computer software (Simulation, Analysis, And, Modeling) [2] was used for curvefitting procedure. SAAM software is a computer program which uses a "least squares algorithm" to estimate the parameters of the mathematical models. The parameters of the exponential function are adjusted such that the "best fit" of the data set is obtained, in a statistical sense. The estimated model parameters are used to compute the residence times and their

associated uncertainties. The error propagation was carried out by the use of sampling theory. Sampling theory seeks to identify the procedure that has a good "average" distribution property, in terms of the sampling over potentially repeated data sets of the same kind [4,6]. The distributions of the organ activities were simulated at least 10,000 times in order to obtain a good distribution of the residence times. The latter part was performed by the use of Crystal Ball software which is a graphically oriented risk analysis computer program [7]. Crystal Ball uses a Latin Hyper Cube sampling method to perform statistical analysis of data sets.

Uncertainty information of the specific absorbed fractions, and organ masses were used to propagate the error in the *S-values*. The *S-value* uncertainties were determined by FOEP.

Using the residence times, *S-values*, and their estimated uncertainties, uncertainty in the absorbed dose estimates were assessed for each patient. Then the target organ absorbed dose distributions for the population of seven-volunteers are obtained by sampling from the absorbed dose distributions of each patient. The 95% confidence interval of the absorbed dose distributions were determined in order to be able to predict the dose for the next patient who is very similar to the sudy group with 95% confidence. At every step, possible sources of uncertainties are discussed. Several approaches which would reduce the magnitude of the uncertainties are also presented.

1.4 Organization of Thesis

Principles of nuclear medicine, including instrumentation and radiopharmaceutical properties, are explained in Chapter 2.

A brief description of the MIRD method of absorbed dose calculations is presented in Chapter 3. This chapter includes the conceptual development of absorbed dose calculation.

Chapter 4 is designed to explain mathematical and biokinetic modeling for linear and nonlinear systems. The assumptions of modeling and associated uncertainties are discussed. The computational methodology of SAAM, which is a least squares method, is defined. The mathematical algorithm of the least squares method for the parameter estimation for linear and non linear models are presented in detail. A list of available computer programs for parameter identification and some information about the programs can be found in Chapter 4.

In Chapter 5, the methodologies and calculations for the estimation of uncertainty for specific absorbed fractions, residence times, and absorbed doses are presented. Sampling theory and methods of sampling are discussed.

Chapter 6 discusses the results of the uncertainty analysis for the radiopharmaceutical ^{123}I-IPT dosimetry. Summary, conclusion, and recommendations for future work are presented in this last chapter.

Appendix A and *Appendix B* present more detail about the computer packages used during the course of this study SAAM (Simulation, Analysis, And Modeling) and Crystal Ball risk analysis program respectively.

Chapter 2

PRINCIPLES OF NUCLEAR MEDICINE

2.1 Introduction

Nuclear medicine has become an important diagnostic and treatment modality that is practiced in almost all hospitals nationwide. The main goal of nuclear medicine is to study organs and tissue systems in the body. Diagnostic nuclear medicine has the unique ability to asses whether an organ is functioning properly without disturbing the organ under observation. A photon emitting radionuclide is first attached to a specific drug or other biologically important chemical structure such as glucose, which will be used by the organ to be observed. The resulting product, called a radiopharmaceutical, is then administered to the patient by intravenous injection, inhalation or oral ingestion. Then the behavior of the administered radiopharmaceutical is monitored by the use of a gamma camera. A gamma camera detects the photons escaping the body, thus, creating an image of the radiopharmaceutical distribution in the body. Then the knowledge of the drug biodistribution can be used to diagnose pathologies. Figure 2.1 [3] is a good

example of a time-activity curve obtained in a dynamic study of a drug distribution can be of help in determining the abnormalities.

As shown in Figure 2.1, the behavior of the radiopharmaceutical is quite different in normal and abnormal organs [3]. This information is used to interpret the pathologic state of an organ or system. The ability of showing physiological function of organs or systems rather than organ anatomy (X-rays, CT scans are used to obtain information of the organ anatomy) makes nuclear medicine procedures very useful in diagnosis.

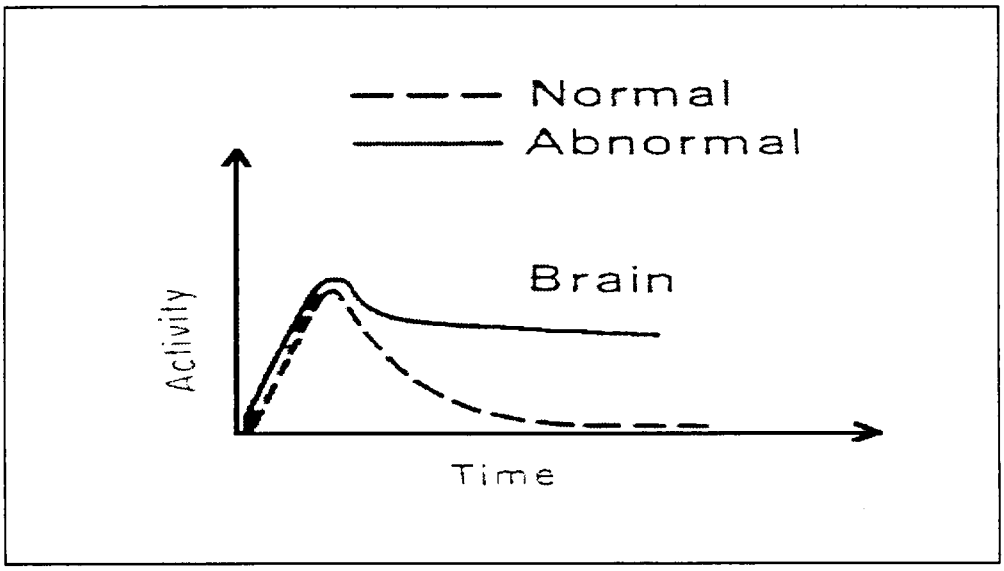

Figure 2.1 A hypothetical time-activity curve which illustrate the normal and abnormal biodistribution for a patient with blood brain barrier defect.

Source: Loevinger R., Budinger T.F., Watson .E., *MIRD primer for absorbed dose calculations*, revised edition. The Society of Nuclear Medicine, New York, 1991

2.2 Imaging Techniques

Imaging is generally carried out by the use of a gamma camera to detect photons escaping the body. When an ionizing radiation enters a gamma camera, it causes ionization and/or excitation of atoms and molecules of the detector material. Thallium-activated sodium iodide crystal, NaI (Tl), is the mostly used detector material in gamma cameras. The energy transferred to detector material is dissipated by the emission of photons as visible or near-visible light, a technique called scintillation. These photons are then converted into electronic signals and recorded, thus, creating counts or images [8].

Scintillation detectors were first introduced in the late 1940s, but they were insufficient in providing good images of the radioactivity distribution in the body. With the introduction of rectilinear scanners in the early 1950s image quality was improved significantly. These devices became widely available after the mid 1960s. Primitive rectilinear scanners consisted of one or two NaI (Tl) crystals and lead collimators. Since the sizes of the early detectors were very small, the images were taken while the gamma camera was scanned in a rasterlike pattern over the area of interest. The early images of a radiopharmaceutical distribution in the organ being observed were very poor due to the detector shortcomings, resulting in very limited and unsatisfactory radiation absorbed dose estimations [9]. The development of large-area NaI (Tl) crystals led to production of the gamma camera, known as the Anger camera in the 1960s. Radioisotope imaging

became more efficient with these new detection systems. Today's Anger cameras are comprised of a large NaI (Tl) detector coupled with heavy focused lead collimators, a series of photomultiplier tubes (PMT), and a logic circuit. The advantage of NaI (Tl) crystals is that they are highly sensitive at low photon energies (about 80-200 keV) which is very desirable in a nuclear medicine procedure to avoid delivering larger absorbed doses to patients [10]. This imaging technique is highly successful where the precise knowledge of activity is important and the source organ contains low activity. Other nuclear medicine imaging devices include single-photon emission computed tomography (SPECT) and positron emission tomography (PET) devices.

There are primarily two types of imaging methods used in nuclear medicine: dynamic and static. In static imaging, the activity is allowed to reach to a final biodistribution level by waiting a sufficient time after the administration of the radiopharmaceutical. Then a static image of the region of interest can be acquired by the use of a gamma camera. In some cases, more detailed information can be obtained by a series of static images from different views such as anterior and posterior. If necessary a three-dimensional static image can be obtained by the acquisition of planar images at multiple angles while rotating the camera around the patient. On the other hand, dynamic imaging involves the acquisition of the time dependent activity distribution of a radiopharmaceutical illustrating the physiologic functioning of the organ being observed. A time-activity curve can be generated showing the number of counts as a function of

time within the region of interest (ROI). Since, such curves represent the quantitative and qualitative information of the activity present in ROI in very simple form, they are invaluable in the evaluation of physiologic functions. Static images are very good in imaging anatomy. However, they are of limited help in some aspects of imaging the physiologic functions of the body organs. Figure 2.2 displays the capability of dynamic imaging in clinical diagnosis by comparing two flow studies (i) a time-activity curve from dynamic imaging and (ii) static imaging performed in a patient with "portal hypertension" [11]. Data obtained from dynamic image sequence, i.e., time-activity curves suggest that the diagnosis for this patient is "reduced portal tension" which would not have been suspected from the static posterior scan.

2.3 Radiopharmaceuticals

Radiopharmaceuticals are prepared by incorporating an appropriate radioisotope into a pharmaceutical. In a radiopharmaceutical, the radioactive label and the pharmaceutical carry out different functions. The radio-label makes it possible to trace the distribution of a radiopharmaceutical by emitting detectable radiations. The chemical properties of the pharmaceutical, on the other hand, enable the radiopharmaceutical to localize in the region of interest.

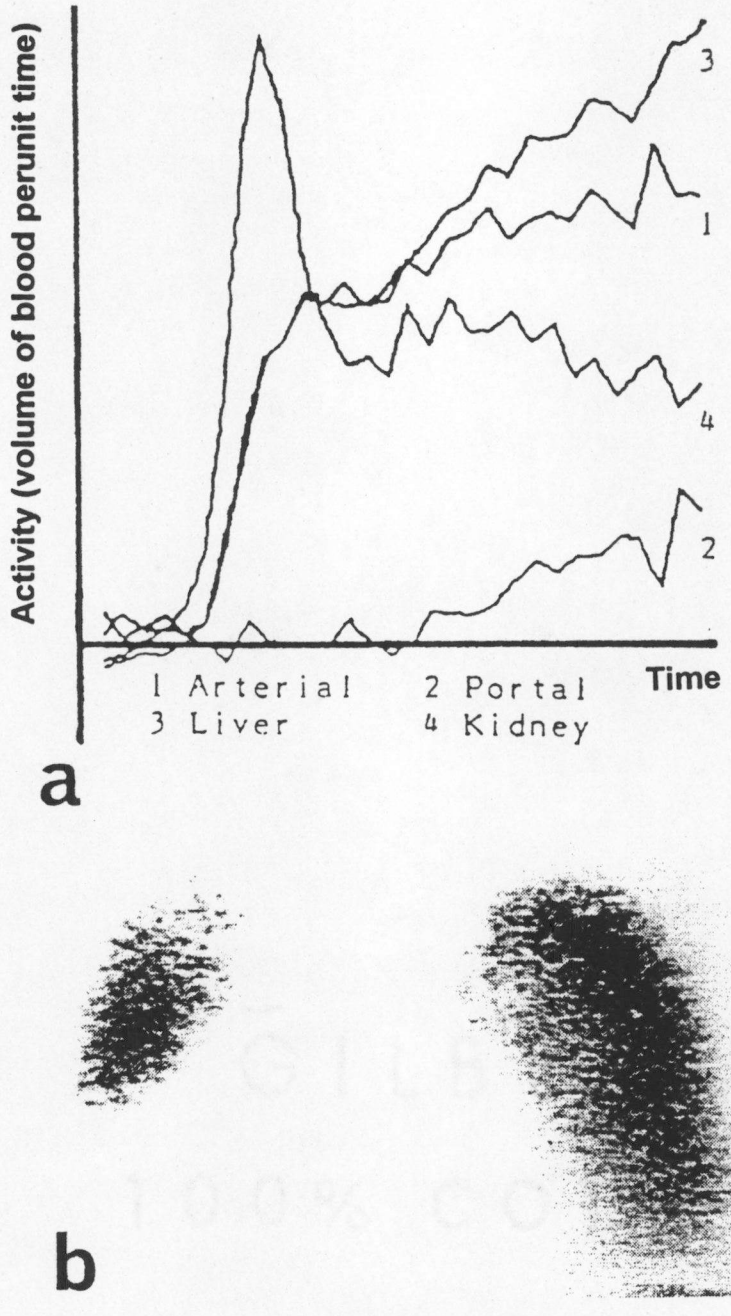

Figure 2.2 A time activity curve and a static posterior image from a flow study. The time activity curve demonstrates reduced portal flow (curve 2) which can not be determined from the static image shown in figure (b).

Source: Sharp P.F., H.G. Gemmell F.W. Smith., *Practical Nuclear Imaging*. IRL Press at Oxford University Press, 1989.

2.3.1 Radionuclides for nuclear imaging

There is no ideal radiopharmaceutical for imaging, however, the desired properties of the "best available" radiopharmaceutical with regard to its cost efficiency, availability, and performance for the particular imaging process can be defined as follows [10, 11, 12]:

- It should emit gamma rays and no charged particles (α *or* β). Since the charged particles deposit all their energy within a short distance, they increase the absorbed radiation dose to the patient without contributing to the image quality. However, gamma radiation, γ , is accompanied by the emission of charged particles, usually a β-ray [8]. The way to avoid from the emission of charged particles is to select a radionuclide which will decay by the electron capture or isomeric transition [1]. For instance, ^{125}I and ^{99m}Tc are examples of the above two decay processes respectively.

- It should be appropriate for the tagging to a pharmaceutical and it should not change the chemical properties or the biologic behavior of the pharmaceutical.

- It should be easily obtainable in the hospital environment

- The energy of the emitted gamma rays should be between 50 to 300 keV. However the ideal energy is around 150 keV. A photon with a higher energy is better for penetrating tissue, but harder to stop and detect. This would require more activity to be administered in order to obtain enough counting event for mapping the distribution of radiopharmaceutical, thus, resulting in larger doses to the patient.

- The half-life of the radionuclide is to be selected according to the particular nuclear medicine procedure. It should be long enough to trace the distribution of the radiopharmaceutical and, if possible, no longer than the necessary to obtain good clinical information.

- The cost-benefit ratio should justify the use of radiopharmaceutical.

- The radiopharmaceutical should localize mostly in the tissues of interest, and not in the other organs or systems as much as possible.

2.3.2 Production of radionuclide

There are primarily four ways to produce radioisotopes which are appropriate for imaging purposes [9, 10]. These are:

1. Neutron capture: the production of a new radionuclide thorough the absorption of a neutron by a nucleus.

2. Nuclear fission : irradiation of heavy unstable nuclei like ^{235}U and ^{239}Pu with thermal neutrons results in breaking up the heavy nuclei into two light nuclei.

3. Charged particle bombardment : the production of radionuclide by the interaction of energetic charged particles like deuterium (D^+) and helium (^4_2He, ^3_2He) with stable atoms.

4. Radionuclide generator: the production of radionuclide based on the concept that some radioactive isotopes of long half life decay into stable or short half life radionuclides. For example, the widely used radioisotope Technetium-99m (^{99m}Tc) is a generator produced radionuclide, with 6 hour of physical half-life, from Molybdenum-99 (^{99}Mo) which is a fission product having a physical half-life of 66 hours via the reaction

$$^{99}Mo \xrightarrow{\beta^-} {}^{99m}Tc \xrightarrow{IT} {}^{99}Tc + \gamma \qquad (2.1)$$

The sources of radionuclides are nuclear reactors (neutron capture and nuclear fission), cyclotrons (charged particle bombardment) and radionuclide generators (radioactive decay). Reactor generated radionuclides are vulnerable to transportation problems. These problems are generally solved by employing on-site radioisotope generators and some times by employing on-site cyclotrons in hospitals.

2.4 Pharmaceutical selection

The distribution of a radiopharmaceutical within the body strongly depends upon its chemical properties and the pathologic state of the patient. Radiopharmaceuticals with different chemical compositions result in different biodistributions. This behavior enables physicians to investigate the physiology of different parts of the body. The variability in regional distribution of a radiopharmaceutical is a significant source of variation in absorbed dose. For example, Figure 2.3 shows how the radiopharmaceutical carrier can alter biodistribution of radiopharmaceutical [3]. ^{99m}Tc is an extensively used radionuclide in nuclear medicine procedures. It is used in various diagnostic procedures with different chemical carriers. Figure 2.3 illustrates the distribution of four different ligands labeled with ^{99m}Tc. As shown, ^{99m}Tc can be used for kidney imaging with DTPA, for skeletal imaging with diphosphonate, for lung perfusion imaging with sulfur colloid, and kidney-ureter-bladder imaging with macroaggregates.

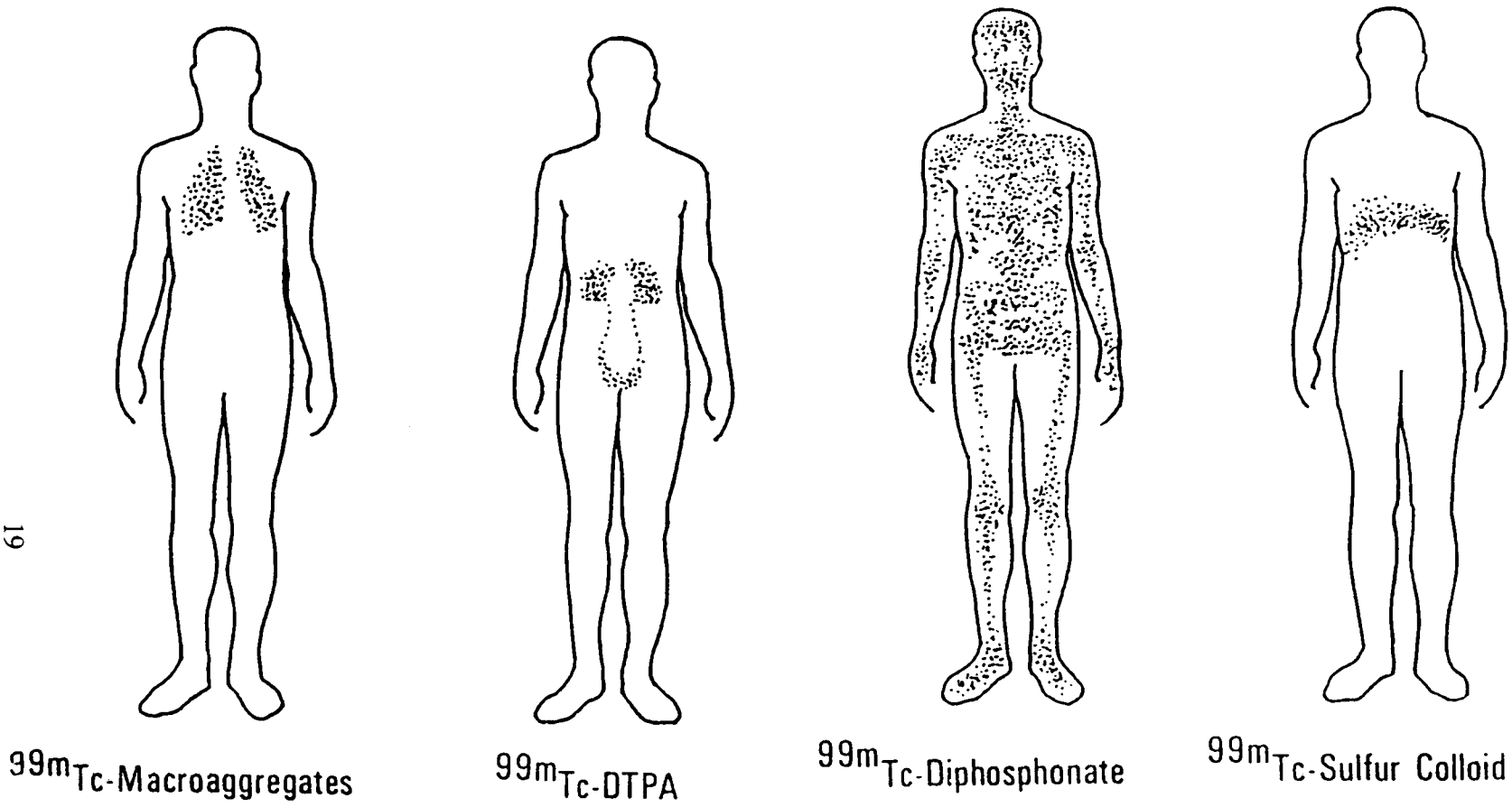

Figure 2.3 Biodistribution of four different ^{99m}Tc labeled drugs. Sulfur colloid for liver and spleen imaging, macroaggregates for lung perfusion imaging, DTPA for kidney-ureter-bladder imaging, and methylene diphosphonate for skeletal imaging

Source: Loevinger R., Budinger T.F., Watson .E., *MIRD primer for absorbed dose calculations*, revised edition. The Society of Nuclear Medicine, New York, 1991

There are three important aspects of an ideal pharmaceutical for nuclear medicine procedures.

- The pharmaceutical should behave in a manner which allows the physiology of interest to be determined. Otherwise the activity in the region of interest may be obscured by the activity present in the other parts of the body resulting in poor imaging and undesirable additional absorbed doses to other organs

- It should be taken up rapidly and mostly by the biologic system of interest, and not by the other organs and tissues in order to avoid delivering radiation doses to other organs. It should be eliminated completely from the body with a half-life comparable to the length of nuclear medicine procedure.

- It should have no physiologic effect whatsoever on the organs or tissues being studied.

The time period during which the radiopharmaceutical remains in the body is related to its effective half life. The effective half life of a radiopharmaceutical is the time period at which radioactivity decreases by half of its initial value. It depends both. upon the physical half life of the radionuclide and the biologic half life of the radiopharmaceutical. The biological half life is a characteristic property of the chemical

form of a radiopaharmaceutical and is defined as the time taken for a radiopharmaceutical to be excreted biologically from the body by half of its initial amount. The effective half life of a radiopharmaceutical can be given by the following equation:

$$\frac{1}{T_{Eff}} = \frac{1}{T_p} + \frac{1}{T_b} \tag{2.2}$$

where T_{Eff} is the effective half life for the radiopharmaceutical, T_p is the physical half life of the radionuclide, T_b is the biologic half life of the radiopharmaceutical.

Frequently of the time the biologic removal of a radiopharmaceutical is governed by more than one process with different removal rates. If this is the case, one needs to calculate effective half-lives for each removal process separately using *Equation 2.2*.

Chapter 3

ABSORBED DOSE

3.1 Introduction

One of the criteria for the acceptability and the clinical usefulness of a nuclear medicine procedure is the potential risk incurred by the patient. The risk involved in the clinical use of radiopharmaceuticals is mainly from the radiation exposure rather than toxicity of the drug [9, 10. 11]. Therefore, the main concern with the use of internally administered radiopharmaceuticals is the potential risk, specifically, somatic and genetic effects from radiation rather than the toxicity of the drug [11]. There is a direct relationship between the dose a patient receives as a consequence of the nuclear medicine procedures and the risk. Hence, the radiation exposure must be kept as low as possible to reduce the potential risk. The US Food and Drug Administration (FDA) requires the absorbed dose calculation be made correctly and the dose a patient may receive justifies the risk before approving the legal use of any radiopharmaceutical. Consequently, the

determination of the absorbed dose is essential when the procedure involves radioactivity. This chapter is devoted to conceptual development of the absorbed dose and its calculation.

3.2 Absorbed dose

In internal radiation dosimetry, the absorbed dose is defined as the amount of energy imparted by ionizing radiation per unit mass of tissue from internally deposited radioactive substances. In medical applications, it is generally calculated by a method introduced by the Medical Internal Radiation Dose Committee (MIRD) of the Society of Nuclear Medicine (SNM) [3]. This method was originally introduced by Loevinger in the mid 1950s [14] and developed by Loevinger and Berman [15] in 1960s. The MIRD dose calculation schema is the most widely accepted and used method for calculating internal radiation doses in medical applications. The FDA also requests that dose calculations be made according to the MIRD schema or a similar method [13]. Some other methods are presented in ICRP 26, ICRU Report 32, and ICRP Publication 30 [16, 40, 41]. This present work employs the MIRD method for the internal radiation dose calculations, and investigates the uncertainty associated with the calculations.

The MIRD radiation dose calculation method requires information describing the physics of radiation transport and the biologic distribution of the radiopharmaceutical in

the body. The radiation transport information includes decay characteristics of the radionuclide, mass of the organs under scrutiny, and the absorbed fractions of emitted energy from all sources to all target organs. The absorbed fraction calculations require the knowledge of the composition, shape and geometrical arrangement of the organs within the body and is performed statistically by a Monte Carlo radiation transport method. The quantitative determination of the radiopharmaceutical's biologic distribution and time-dependent amount of activity that an individual organ contains comprises the biokinetic part of the MIRD schema for dose calculation.

The calculation of the absorbed dose requires two steps: (i) the measurement of the amount of activity present in the source organs and (ii) radiation transport calculations in order to determine the fraction of the energy emitted from the source organ that is absorbed by the target organ. The latter needs a number of factors which can be lumped into one factor which is known as the *S-value*. The dose that an organ would receive can be expressed as

$$\overline{D} = \tilde{A} \times S \tag{3.1}$$

where $\overline{D}$ is the average absorbed dose in rad/μCi, $\tilde{A}$ is the cumulated activity in μCi-h, and S is the *S-value* in rad/μCi-h.

The administered activity generally localize in more than one organ. The total dose an organ may receive will be sum of the contributions from each of the organs containing activity, which are referred to as source organs. Considering all possible contributions, the equation for calculating the radiation absorbed dose can be expressed as

$$\overline{D}_k = \sum_h \overline{D}(r_k \leftarrow r_h)$$

$$\overline{D}_k = \sum_h \tilde{A}_h \; S(r_k \leftarrow r_h) \qquad (3.2)$$

where $\overline{D}(r_k \leftarrow r_h)$ is the dose to the target organ r_k from source organ r_h,, $S(r_k \leftarrow r_h)$ is the mean absorbed dose in the target organ per unit cumulated activity in the source organ, and $\tilde{A}_h$ is the cumulated activity in the source organ *h*.

The *Equation 3.2* describes the general formalism for the absorbed dose concept. However, it is not the equation which is used in MIRD methodology. The absorbed dose itself is a function of the administered amount of activity to the body.. Therefore, it would be more convenient to express the radiation dose as the dose per unit administered activity (i.e., rad/mCi or mGy/MBq). The MIRD Committee introduced a new term, residence time, τ, to perform the absorbed dose calculation in terms of administered activity.

$$\tau_h = \frac{\tilde{A}_h}{A_0} \tag{3.3}$$

where τ_h is the source organ residence time and A_0 is the administered activity. The equation which is in use in MIRD method of absorbed dose calculation can then be expressed as

$$\frac{\overline{D}(r_k \leftarrow r_k)}{A_0} = \sum_h \tau_h \; S(r_k \leftarrow r_k) \tag{3.4}$$

3.3 The mean dose per unit cumulated activity, S-value

The mean absorbed dose per unit cumulated activity compromises the physical component of the MIRD schema for calculating the absorbed dose. The decay characteristics of the radionuclide and anatomical properties of the body are combined together in one parameter, namely the *S-value.*

The mean absorbed dose per unit cumulated activity is the absorbed dose in the target organ r_k per unit cumulated activity in the source organ r_h and may be calculated using following equation:

$$S(r_k \leftarrow r_h) = \sum_{i=1}^{N} \Delta_i \times \Phi_i(r_k \leftarrow r_h) \tag{3.5}$$

where Δ_i is the mean energy emitted by the ith emission per nuclear transition and $\Phi_i(r_k \leftarrow r_h)$ is the specific absorbed fraction *(SAF)* in the target organ r_k for i^{th} emission.

The *S-values* for many source/target organ pairs are calculated and published for more than 100 radionuclides in MIRD Pamphlet No. 11 by Snyder *et al* [17]. In the *S-value* calculations, the radioactivity is approximated by the homogenous isotropic model which will be discussed in a later section of this paper. As a result of this approximation, the *S-value* is assumed to be independent from which organ is labeled as the source organ and which is labeled as the target organ for an organ pair. For instance, if the organ pair is brain and liver, then the following reciprocity relationship would hold.

$$S(brain \leftarrow liver) = S(liver \leftarrow brain) \tag{3.6}$$

This approximation is not exact; however, it reduces the complexity of the dose calculation without causing much uncertainty in calculations [3, 18].

3.3.1 Radionuclide data: The mean energy emitted per nuclear transition, Δ_i

Most of the radionuclides used in medical imaging emit more than one type of radiation in different quantities per transition. The mean energy per unit nuclear transition, Δ_i, is designated to carry all the information concerning the characteristics of the radionuclide decay (i.e., the type of radiation, the yield of each of the emissions, and the energy emitted per transition). Within the MIRD schema, the mean energy of ith emission per unit transition is given by

$$\Delta_i = Kn_iE_i \tag{3.7}$$

where, K is a unit conversion constant, n_i is the number of emitted particles per i^{th} emission, and E_i is the mean energy per particle. The absorbed fraction from nonpenetrating particles will be unity for most relatively large source organs. Therefore, it is more convenient to calculate the total mean energy emitted per unit transition which is the sum of the mean energies of all types of nonpenetrating particles.

$$\Delta_{np} = \sum_{i=1}^{N} Kn_iE_i \tag{3.8}$$

If E_i is expressed in joules per particle, the unit for Δ will be joules per transition

(Joule/transition=Gy-kg/Bq-s). The values of Δ_i for a number of radionuclides were published by the MIRD Dose Committee in 1989 [19]. This radionuclide decay schema does not include the complete list of the emitted particles for a given radionuclide; however, it is a good compilation of the major emitted particles. For instance, for Iodine-123 (^{123}I), the ratio of the energy of the omitted radiations to that of the listed radiations is approximately 4.1E-03.

3.3.2 Anatomic data: The specific absorbed fraction, Φ_i

The energy absorption in an organ from an emitted radiation is strongly correlated with (i) the geometry and composition of the source/target organ pairs and properties of the intervening tissues, (ii) the radionuclide decay characteristics such as the energy of the emitted radiation and the type of the radiation. Hence, only a fraction of the emitted radiation, namely the absorbed fraction ϕ_i, is absorbed by the target organ. For instance, γ -rays are penetrating radiations and only a small fraction of their energy might be absorbed by the source organ itself. They generally deposit a part of their energies to each organ along their path. For example, only 16 percent of the Iodine-123 (^{123}I) γ rays' energy emitted in brain are absorbed in brain. On the other hand, β particles are absorbed within a few millimeters. For source organs large relative to the mean free path of β particles, all

the β particles emitted in the source organ are absorbed by that source organ, thus, contributing only to the organ self-dose.

Figure 3.1 illustrate the concept of absorbed fraction and importance of the knowledge of radionuclide data. In Figure 3.1, the absorbed fraction is only 0.16 of the total emitted γ -rays from Iodine-123 (^{123}I) and Carbon-11 (^{11}C), while all nonpenetrating charged particles

(β and β^+) emitted from Carbon-11 (^{11}C) and Carbon-14 (^{14}C) are absorbed within the brain, thus resulting in an absorbed fraction of 1. Within the MIRD schema the absorbed fraction, ϕ_i is expressed by the following equation:

$$\phi_i(r_k \leftarrow r_h) = \frac{absorbed\ energy\ of\ i^{th}\ emission\ in\ target\ r_k}{total\ energy\ of\ i^{th}\ emission\ from\ source\ r_h} \tag{3.9}$$

The values of the absorbed fraction for penetrating particles are between 0 and 1 while non-penetrating particles (β, α) have a value of 1 where the source organ is large relative to the mean free path of the particles. Nonpenetrating particles lose all their energies through collisions and get absorbed by the source organ, thus, contribute only to self organ dose.

The values of absorbed fraction can be generalized as follow:

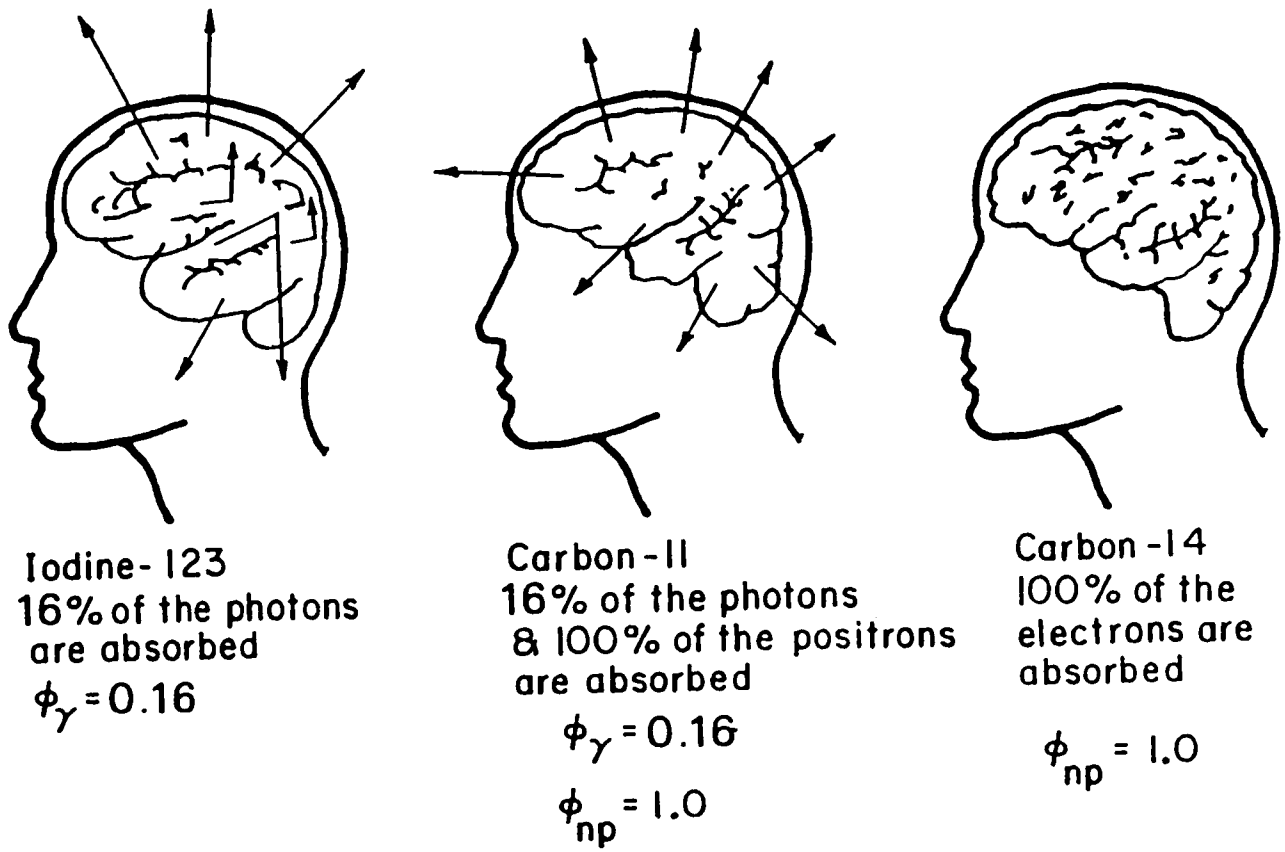

Figure 3.1 Pictorial illustration of absorbed dose concept.

Source: Loevinger R., Distributed radionuclide sources. Attix F.F., and Tochilin E., *Radiation dosimetry,* 2nd edition, pp. 51-90. Vol. III. New York; Academia Press, 1969.

$$\phi_{np} = \begin{cases} 1; if & r_k = r_h \\ 0; f & r_k \neq r_h \end{cases}$$

$$0 < \phi_p < 1 \tag{3.10}$$

The values of absorbed fraction estimates for 12 monoenergetic photon energies between 10 keV and 4 MeV for several source/target organ pairs in a "anthropomorphic phantom" were calculated by Snyder *et al.* and tabulated in MIRD Pamphlet No. 5 [20].

Although, $\phi_i(r_k \leftarrow r_h)$ represents the absorbed fraction in the target organ, it is somewhat insensitive to anatomical properties, mostly the size and composition of the organs. The specific absorbed fraction *(SAF)* was introduced in order to calculate the fraction of the energy absorbed per unit mass of the target organ. The specific absorbed fraction *(SAF)* in any target organ r_k is defined as the absorbed fraction in the target per unit mass of the target and given by

$$\Phi_i(r_k \leftarrow r_h) = \frac{\phi_i(r_k \leftarrow r_h)}{m_k} \tag{3.11}$$

where m_k is the mass of target organ in grams and $\phi_i(r_k \leftarrow r_h)$ is the fraction of energy emitted from the source organ that is deposited in the target organ.

The values of specific absorbed fraction are available for a variety source/target organ pairs in the revised MIRD Pamphlet No. 5 [21]. In this study, the uniform isotropic model was used to represent organs. In the uniform isotropic model, the activity is assumed to be uniformly distributed in a region of infinite, homogenous material of constant mass density. This approximation suggests that the specific absorbed fraction for a source/target organ combination is independent from which organ is labeled as the source organ and which is labeled as the target organ. Therefore, the specific absorbed fraction for i^{th} emission can be expressed as

$$\Phi_i(r_k \leftarrow r_h) = \frac{\phi_i(r_k \leftarrow r_h)}{m_k} = \frac{\phi_i(r_h \leftarrow r_k)}{m_h} \tag{3.12}$$

Some other approximations such as the "uniform homogenous model of finite size, and "uniform scatterless model" were also used in order to yield more accurate estimates [18, 22]. For instance, Cristy and Eckerman used phantoms consisting of different absorbing media representing lung, soft tissues and skeleton [18]. They performed a Monte Carlo transport calculation in a vacuum such that there was a tissue-vacuum boundary. In this case the reciprocity theorem dose not hold. Nevertheless Cristy's empirical studies showed that the differences between his results and *SAF* estimates which use the reciprocity theorem, in general, were no more than 10% for the soft tissue organs. If skeleton comprises one of the organs of an organ pair, the reciprocity theorem is no longer valid at energies of 10-200 keV. The reciprocity

approximation clearly is not exact but it is believed that it considerably reduces the complexity of the absorbed dose calculations resulting in reasonable error for absorbed dose calculations. [3]. More detail can be found in the work of Cristy, 1987 and Loevinger, 1969 [18, 22]. Further assumptions and uncertainties will be discussed in succeeding chapters.

The *SAF* values depend upon the energy and the type of the emission, organ size and density, and the geometric arrangement of the organs. Figure 3.2 and 3.3 delineate the photon *SAF* distribution with respect to photon energies (Snyder *et al'* s SAF values were utilized). Figure 3.2 is a plot of *SAF* where the source organ and target organ are different. This figure shows how the *SAF* estimates decreases as the separation between source and target organ increases. Figure 3.3 shows a plot of the *SAF* versus photon energy where the source and target organ are the same. The figure reveals that *SAF* values are very large at low photon energies and decreases as a function of increasing photon energy. From this plot, one may conclude that the lower the energy, the higher the self organ specific absorbed fraction which is not desirable.

These two figures suggest that the choice of radionuclide should be the intermediate energy gamma emitters (80-200 keV) in order to decrease the absorbed dose a patient may receive.

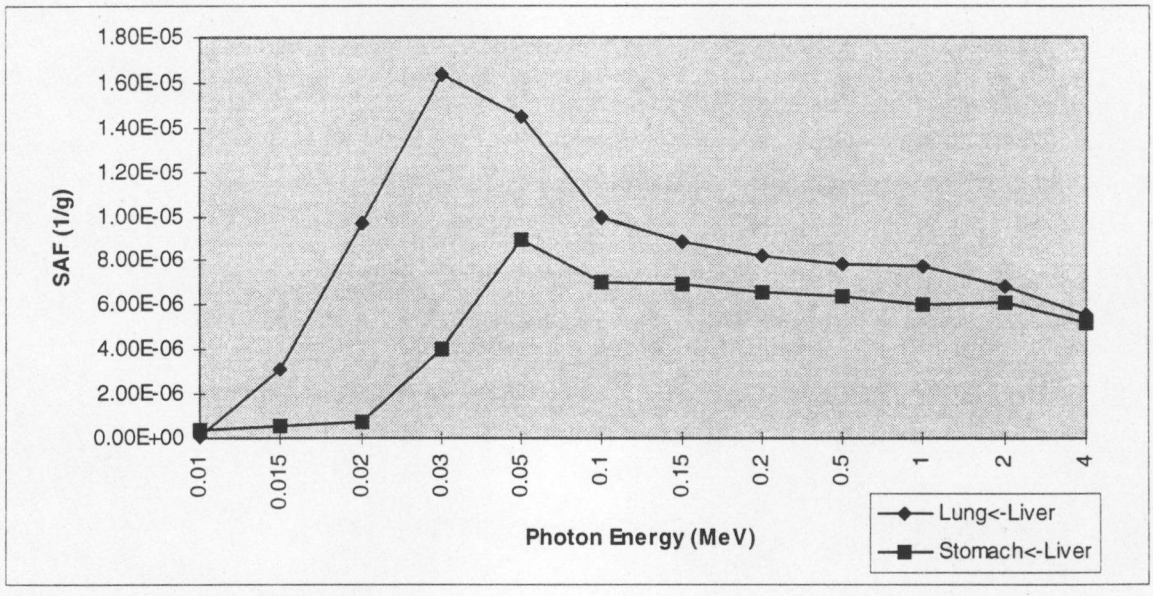

Figure 3.2 The plot of the specific absorbed fraction as a function of photon energy for source organ liver and target organs, lung and stomach (based on Snyder *et al*'s SAF values).

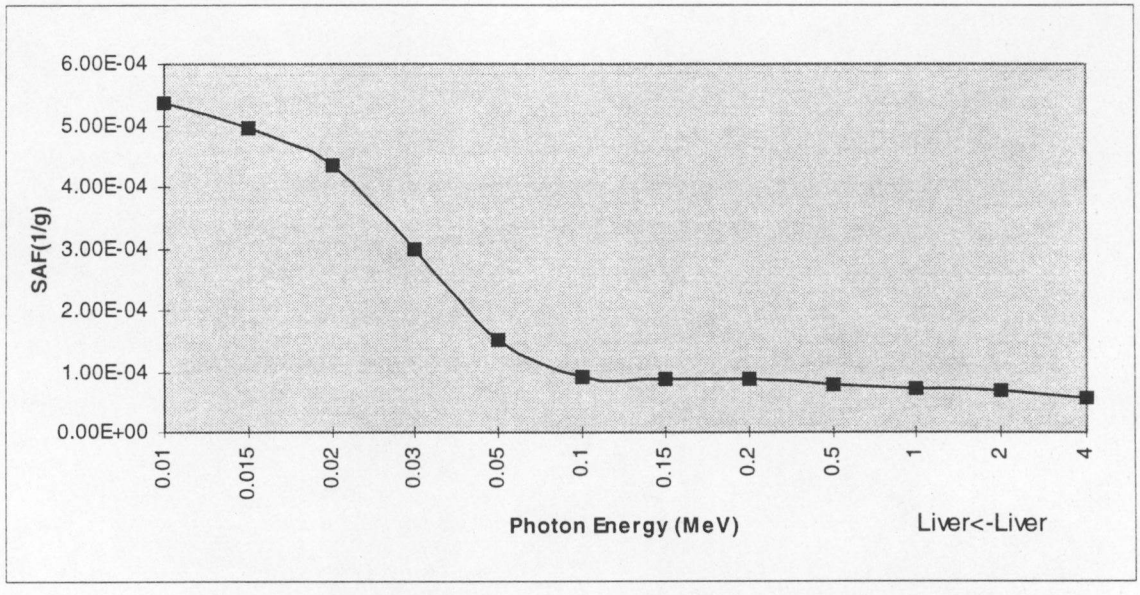

Figure 3.3 The plot of the self organ specific absorbed fraction as a function of photon energy for liver (based on Snyder *et al*'s SAF values).

3.4 Biokinetics of radiopharmaceuticals and cumulated activity

In internal radiation dosimetry, it is essential to determine the amount of activity present in the region of interest as a function of time. This knowledge comprises the biologic component of the MIRD formalism for calculating the absorbed dose given by *Equation 3.2*. The metabolism of the drug by body may show a large variability among species, and among individuals of a population of the same species. Reasons for inter-subject variability of the activity distribution within the body might be characterized as the metabolic differences, pathologic conditions, age, gender, dietary history and the modality of administration such as injection, ingestion, or inhalation [3, 23]. For instance, the variability of the radiopharmaceutical biodistribution relative to the pathologic status has been illustrated in Figure 3.4

In Figure 3.4, each time activity plot shows the normal and abnormal kinetics of the radiopharmaceutical for a patient with (a) blood-brain barrier defect , (b) low blood flow to the liver, and (c) myocardial hypertrophy [3]. These figures compromise good examples of how nuclear medicine images can yield information that allow a physician to make a diagnosis.

3.5 Cumulated activity, $\tilde{A}_h$

The total number of nuclear transitions in a region of interest is known as the

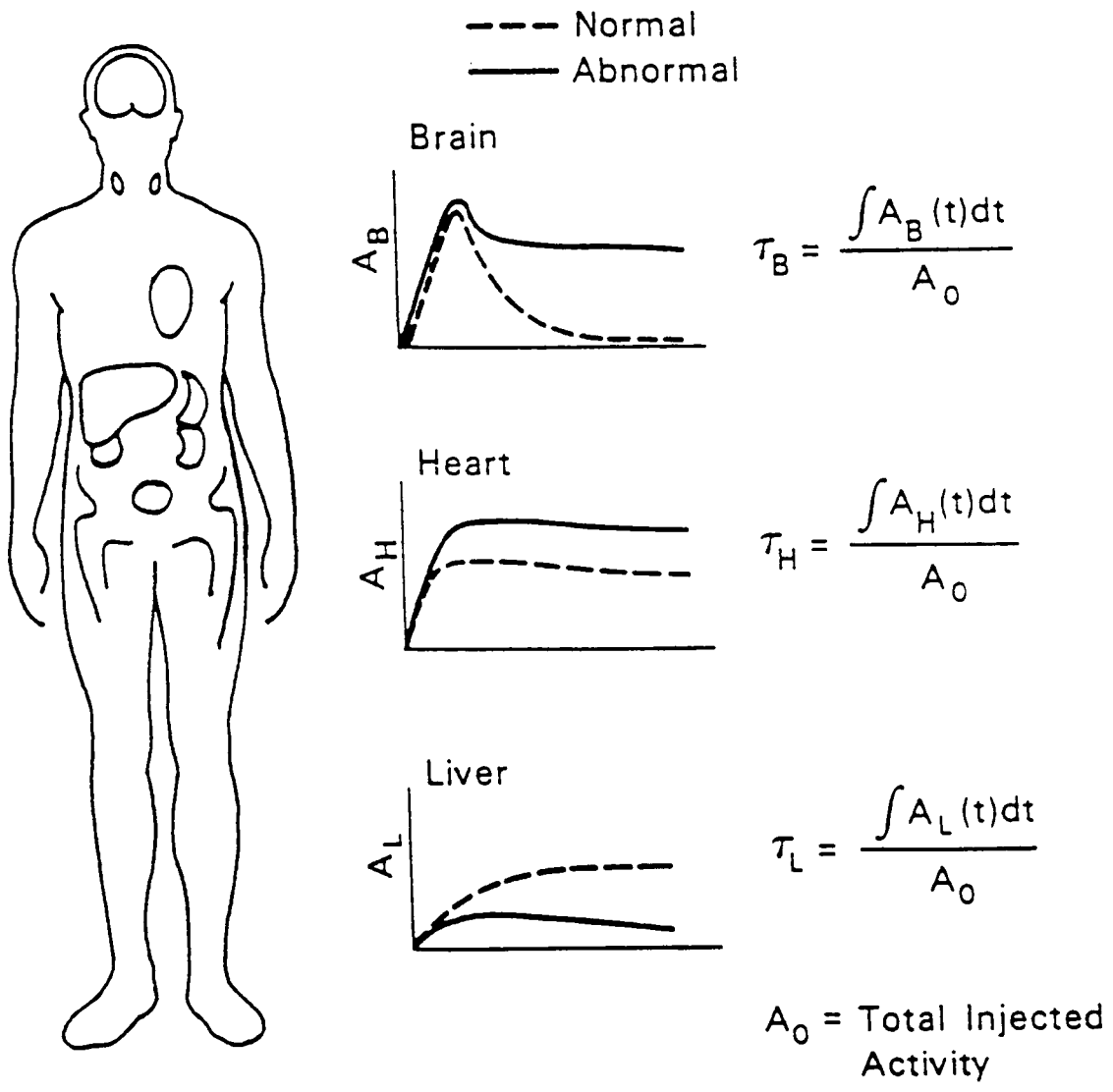

Figure 3.4 Hypothetical time-activity curves which illustrate the normal and abnormal activity distributions for a patient with a) blood brain barrier defect, b) low blood flow to the liver, and c) myocardial hypertrophy.

Source: Loevinger R., Budinger T.F., Watson .E., *MIRD primer for absorbed dose calculations*, revised edition. The Society of Nuclear Medicine, New York, 1991

cumulated activity $\tilde{A}_h$. Its determination is one of the major concerns of the absorbed dose calculation. It can be calculated by summing all nuclear transitions in the source organ h. Radioactive decay and the metabolic process are factors affecting the amount of activity in a region at a given time. The activity information is generally displayed as a time-activity curve. Some examples of time-activity curve were displayed in Figure 3.4.

The total number of transitions occurring in a given organ or region during the time interval (t_1, t_2) is equal to the area under the time activity curve. If the time activity curve can be approximated by a mathematical function, let us say $A_h(t)$, then the cumulated activity in organ h will be approximately equal the integral of this function over the time interval (t_1, t_2).

$$\tilde{A}_h = \int_{t_1}^{t_2} A_h(t)dt \tag{3.13}$$

where $\tilde{A}_h$ is the cumulated activity, and $A_h(t)$ is the mathematical function which describes activity present in a source organ as a function of time.

In internal dose assessment, one would definitely want to have good quantitative and qualitative knowledge about the distribution of activity in the body to estimate the

absorbed dose with high accuracy. One of the consequences is that the time interval $r(t_1, t_2)$ of the integral given in *Equation 3.13* must be chosen relatively large with expect to the effective removal half life of the radiopharmaceutical to ensure that all transitions occurring within the body are taken into account. In nuclear medicine practices, generally, radiopharmaceuticals with a short physical half-life are used to reduce the potential risk from radiation exposure. It will be convenient to set the upper limit to infinity in order to simplify the calculations. For the short-lived radionuclides, *Equation 3.12* can be modified as

$$\tilde{A}_h = \int_0^{\infty} A_h(t)dt \tag{3.14}$$

On the other hand, for any long lived isotope the upper limit should be chosen as 50 years to calculate the 50 year dose commitment in both occupationally exposed workers and those who undergo a nuclear medicine procedure [23].

The distribution of the activity in source organ *h* can be approximated by a sum of exponentials [3, 24, 25].

$$A_h(t) = \sum_i A_i \, e^{-(\lambda_p + \lambda_i)\, t} \tag{3.15}$$

where A_i is the coefficient of exponential term representing the amount of initial activity in that exponential component, λ_p is the physical half-life of the radionuclide, and λ_i is the biologic removal constant of the ith exponential component. Each exponential component can be thought as a sub-compartment inside the source organ which has a somewhat different removal process than the others. The exponential components do not necessarily relate to physiological parameters. They are used because of their considerable simplification in the dose calculation. These models are constructed only to simulate the biodistribution of the radiopharmaceutical in the body. The parameters of the model should not be taken to represent physiological information.

Inserting *Equation 3.14* into *Equation 3.13*, the cumulated activity can be expressed as

$$\tilde{A}_h = \int_0^\infty \sum_i A_i \, e^{-(\lambda_p + \lambda_i)\, t} \, dt \tag{3.16}$$

The integral of *Equation 3.15* from zero to infinity for radiopharmaceuticals with short-half-life will yield

$$\tilde{A}_h = \sum \frac{A_i}{\lambda_p + \lambda_i} \tag{3.17}$$

The solution can be written in terms of effective half-life $(T_i)_{eff}$ of the radiopharmaceutical as

$$\tilde{A}_h = 1.443 \sum_i A_i (T_i)_{eff} \tag{3.18}$$

where

$$(T_i)_{eff} = \frac{ln2}{\lambda_p + \lambda_{b_i}} \tag{3.19}$$

and

$$\frac{1}{(T_i)_{eff}} = \frac{1}{T_p} + \frac{1}{T_{b_i}} \tag{3.20}$$

where T_p is the physical half-life of the radionuclide and T_{b_i} is the ith biologic removal half-life.

3.5.1 Residence time, τ_h

The cumulated activity is the total area under the time-activity curve and is computed by the integral of the activity function from zero to infinity.

$$\tilde{A}_h = \int_0^\infty A_h(t)dt \tag{3.21}$$

The residence time, as explained in Section 3.2, was introduced to calculate the absorbed dose in terms of administered activity and given in *Equation 3.2* as

$$\tau_h = \frac{\tilde{A}_h}{A_0}$$

$$\tau_h = \frac{1}{A_0}\int_0^\infty A_h(t)dt \tag{3.22}$$

From the definition of the residence time, one can conclude that the area under the rectangle in Figure 3.5 must be equal to the area under the activity curve. This can be expressed as

$$\tilde{A}_h = \tau_h \times A_0 . \tag{3.23}$$

Hence, the cumulated activity in organ h is the same as it would be if the total administered activity A_0 were to remain in an organ for a time numerically equal to the value of τ_h, without decay or biological removal [8].

The shape of the time activity curves reveals the metabolism of the drug by the body and it is generally governed by the uptake, radiological decay and biologic removal

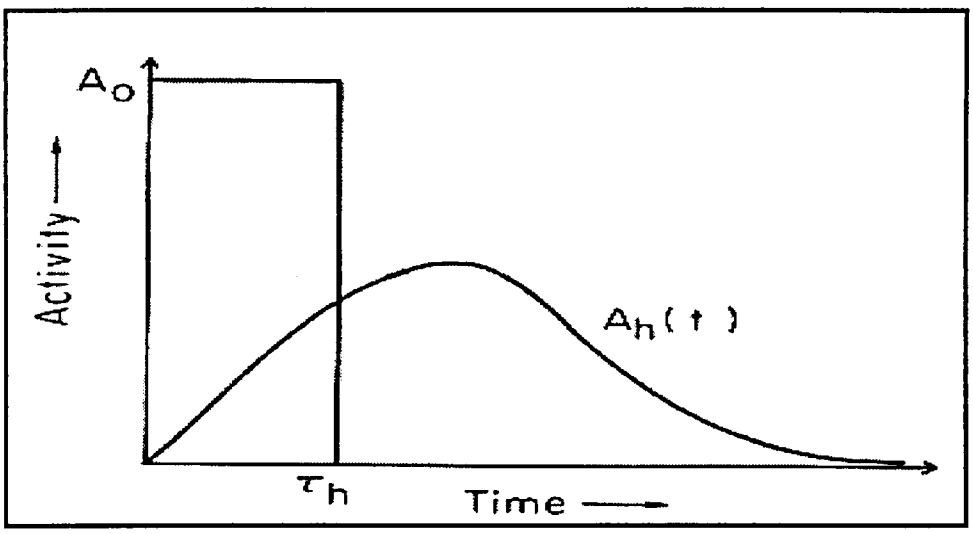

Figure 3.5 Pictorial illustration of the residence time.

Source: Loevinger R., Budinger T.F., Watson .E., *MIRD primer for absorbed dose calculations*, revised edition. The Society of Nuclear Medicine, New York, 1991

rates. Usually, at time zero *(t=0)* the bolus of activity is administered into the blood stream. All the other organs are considered to have no activity at *t=0*. The plots of hypothetical time-activity curves in Figure 3.6 and 3.7 shows the changes in the distribution of the radipharmaceutical as a function of time with different rates of uptake and biologic removal which, governs the shape of the time-activity curves. In Figure 3.6 the solid curve demonstrate a rapid uptake and long-term removal phase while the dashed-line represent a rapid uptake and a rapid washout phase. On the other hand, the time activity curve shown in Figure 3.7 reveals a slow take-up phase. One may infer quantitative as well as qualitative information about the kinetics of a radiopharmaceutical in the region of interest by examining time-activity curves.

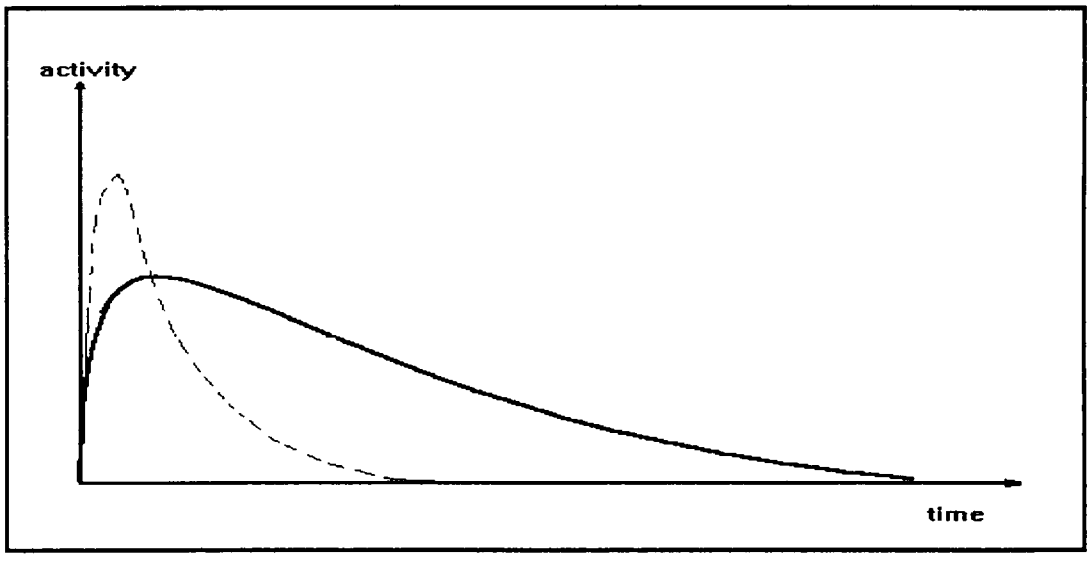

Figure 3.6 Two hypothetical time-activity curves which illustrate rapid uptake with different removal phases.

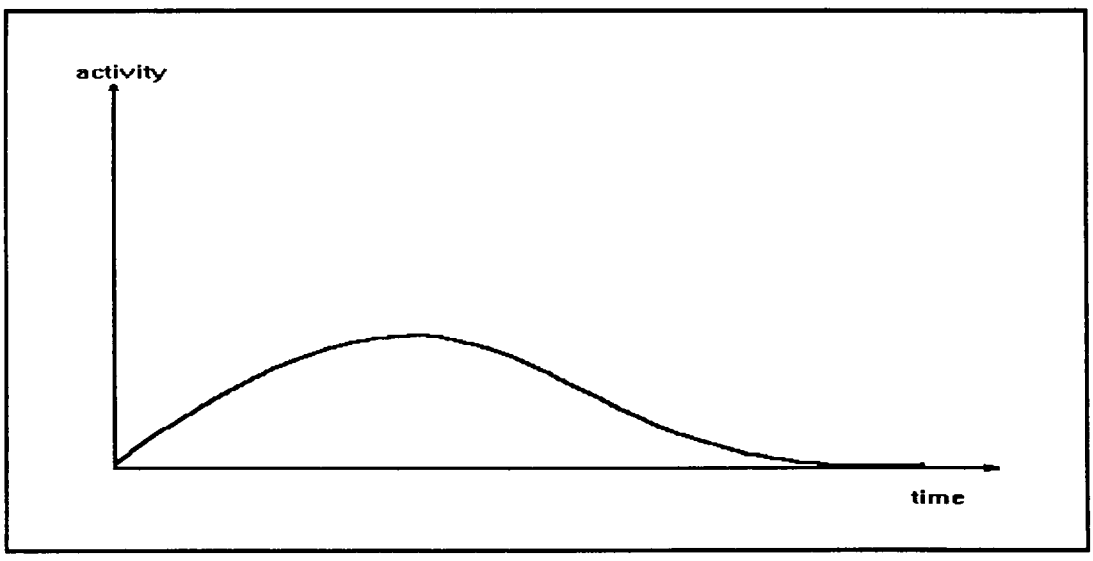

Figure 3.7 A plot of a hypothetical time-activity curve with a slow uptake phase.

Chapter 4

BIOKINETIC MODELING AND PARAMETER ESTIMATION

4.1 Introduction

A solution to a problem is not always attainable directly from the available empirical data. For instance, residence time, which is required for the absorbed dose calculations, cannot be obtained directly from the measurement of activity present in the body. One needs to make some assumptions and to construct a model which in turn can be used to estimate residence time.

Mathematical modeling can be defined as a simulation of the real world events in mathematical terms. The first step of the mathematical modeling is the identification of the problem with as much detail as possible. Translation of all available knowledge into mathematical formalism comes second. The latter is the more difficult part which is, more often than not, quite impossible without some assumptions [26].

After the model construction, the model validation is essential. This generally involves empirical tests of the model in so called "real world" situations. However, the validation to a large extent is subjective and involves personal judgment as to whether the model is appropriate. A mathematical model is, indeed, a simplified form to simulate real world situations. The form of the simplification is obtained by ignoring insignificant features of the problem. An originally complex and unattainable problem is idealized to one that is mathematically tractable. Such idealized models may not have real existence, they are, indeed, abstractions. However, they may represent an acceptable approximation of the real process rather than leaving the problem unanswered.

A major concern of the modeling is the nature of the mathematical variables involved. There are two types of variables in nature. First there are deterministic variables which represent, in theory, known features. The other illustrate a random features, namely stochastic variables. The latter infers that the real values of these parameters can not be determined precisely because of their inherent probabilistic nature. It is essential to determine the type of the variables involved at the very outset of modeling. A statistical and probabilistic method should accompany the modeling where a stochastic variable involved [4, 26].

The final stage of mathematical modeling is the interpretation of the model parameters. A model without such interpretation could be misleading, since the model

output parameters may not be exact representation of the real situation as discussed earlier. Therefore the implication of the output parameters must be clearly spelled out as a final stage of the modeling.

4.2 Biokinetic modeling

The study of biological systems and mathematical model development has been one of the prime considerations of the scientists since the early 19th century. Studies suggested that physiology of living systems could be observed by attaching a detectable material to a drug which will be absorbed by the system to be observed. This technique, namely the tracer technique led to the use of radioactive material in science and medicine as noninvasive studies of biological systems. The first known study with a radioactive tracer was performed by Hevesy in order to determine the uptake of lead by bean seedlings in the late 1920s. Some other studies including red cell labeling, clinical investigation with thorium-B, iron metabolism, and radioactively labeled water studies were conducted by Hevesy and his colleagues between 1925 and late 1930s [27, 28]. Later in 1943 Hevesy received the Nobel prize for his contribution to nuclear medicine and biochemistry. He is also known as "the father of the nuclear medicine." After the late 1940s the tracer method had become a widely used biologic study procedure with various applications. The availability and potential merit of the tracer method in the study of biologic systems called for new studies in order to refine the mathematics and theory of radiotracer kinetics in living systems [27]. In the early days most of the studies

were done in the area of mathematical model development. Among them, compartmental modeling has become an accepted method for biokinetic studies. Some of the basic mathematical principles of the kinetic of tracer and compartmental modeling were established by Torell [30, 32]. Torell proposed that the absorption , excretion, and variation of activity can be represented by linear differential equations. He not only developed and refined the theory and mathematics of compartmental analysis, but also performed some experimental studies to prove the validity of his theories. These efforts indicated that the theory was in agreement with the experimental results in predicting tissue concentration of the body organs. Development of the three-compartment and four-compartment models that can be solved in closed form, followed Torell's studies. Solutions to the higher-order models are relatively hard and requires correspondingly higher order differential equations for which there are no analytic solutions [27]. Nevertheless, approximate solutions can be obtained by advanced digital computers using well-established computer codes which will be discussed in the succeeding sections of this chapter. A number of studies have been performed to refine biokinetic modeling including the fundamental treatment of the mathematical principles involved in compartmental modeling and the computer software development. These studies allowed scientists to use compartmental modeling approach to investigate many problems which had previously been considered to be unsolvable. Principles of biokinetic modeling in terms of theory and computation will be discussed in the rest of this chapter.

4.2.1 Tracers

The word "tracer" in nuclear medicine, is meant to be a radioactively labeled substance to study certain properties of the labeled substance in biological systems. Some of these properties include exchangeable mass or volume of the material, its localization, and transfer rate coefficients between compartments. Useful information describing the physiology of the system being studied can then be deduced from the behavior of tracer in the system.

4.2.2 Compartments

A compartment is an interconnected subdivision of a system that is assumed to be homogenous with regard to the substance of interest, i.e., the tracer. A human body can be modeled as a system that consists of a finite number of interconnected compartments. Figure 4.1 depicts a typical compartmental model designed to model biokinetics of a radiopharmaceutical in the human body [32]. A compartment does not have to necessarily be a well-defined organ of the body. It is sufficient to be a kinetically distinguishable entity with regard to the substance of interest, i.e., radiotracer in nuclear medicine.

In terms of a mathematical modeling, a compartment, in linear compartmental modeling, is a part of the system whose mass is transferred into another compartment by a

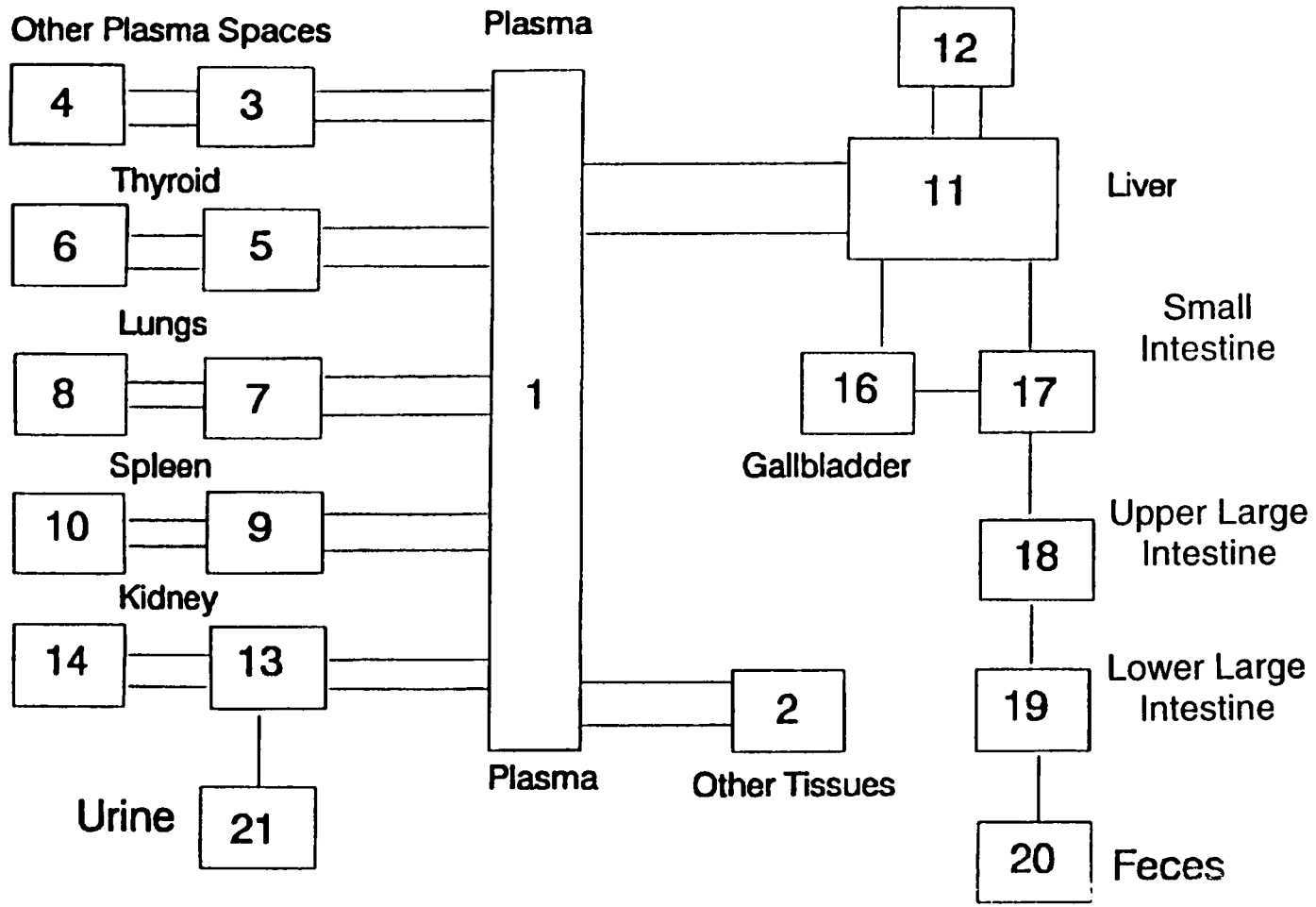

Figure 4.1 A typical compartmental model used in internal dosimetry applications.

Source: Loevinger R., Distributed radionuclide sources. Attix F.F., and Tochilin E., *Radiation dosimetry,* 2nd edition, pp. 51-90. Vol. III. New York; Academia Press, 1969.

first order process, i.e., elimination rate K is constant, not a function of time [27, 29, 44]. In such models, the flux of material between two compartments depends, linearly, upon the mass of material concentration in the source compartment only.

4.3 Mathematics of compartmental modeling

In a deterministic approach, a compartment is considered as a mass of substance whose concentration at time t, $q(t)$, can be represented by a linear differential equation which represent the mass balance, or activity balance in radiotracer studies, for a compartment

$$\begin{pmatrix} \textit{Rate of change in} \\ \textit{compartment } i \end{pmatrix} = - \begin{pmatrix} \textit{outflow} \\ \textit{from } i \end{pmatrix} + \begin{pmatrix} \textit{inflow} \\ \textit{to } i \end{pmatrix} \tag{4.1}$$

$$\frac{dq}{dt} = -Kq(t) + f(t). \tag{4.2}$$

where K is the relative rate of elimination from the compartment and $f(t)$ is the rate of entry into that compartment. In linear compartmental modeling K is generally considered to be linear, i.e., it is not a function of time.

A system of n interconnected compartments as shown in Figure 4.1 can be

described by a set of n linear differential equation:

$$\frac{dq_1}{dt} = -Kq_1 + k_{21}q_2 + k_{31}q_3 + \ldots\ldots\ldots + k_{n1}q_n + f_1(t)$$

$$\frac{dq_2}{dt} = k_{12}q_1 - K_2q_2 + k_{32}q_3 + \ldots\ldots\ldots + k_{n2}q_n + f_2(t) \qquad (4.3)$$

$$\vdots$$

$$\frac{dq_n}{dt} = k_{1n}q_n + k_{2n}q_2 + \ldots\ldots\ldots - K_nq_n + f_2(t)$$

where

q_i is the concentration or mass of compartment *i*,

K_i is relative rate of elimination from compartment *i*

k_{ij} is relative rate of transfer from compartment *j* to compartment *i*,

$f_i(t)$ is feeding rate into compartment *i*

.

Using elementary matrix notation *Equation 4.3* shall be expressed as

$$\underline{\dot{q}} = -\underline{\underline{K}}\underline{q} + \underline{F}(t)$$

$$q(0) = q_0 \qquad (4.4)$$

where

$$\underline{\underline{K}} = \begin{bmatrix} K_1 & -k_{21} & -k_{31} & \ldots\ldots & -k_{n1} \\ -k_{12} & K_2 & -k_{32} & \ldots\ldots & -k_{n2} \\ \cdot & & & & \\ \cdot & & & & \\ \cdot & & & & \\ \cdot & & & & \\ -k_{1n} & -k_{2n} & -k_{3n} & \ldots\ldots & K_n \end{bmatrix} \tag{4.5}$$

is the $n \times n$ matrix of all elimination and transfer rates. In linear compartmental modeling all the values of the matrix $\underline{\underline{K}}$ are assumed to be constant.

$$\underline{q} = \begin{bmatrix} q_1 \\ q_2 \\ \vdots \\ q_n \end{bmatrix} \tag{4.6}$$

is the column vector consisting of the variables of all compartments

$$\underline{F}(t) = \begin{bmatrix} f_1(t) \\ f_2(t) \\ \vdots \\ f_n(t) \end{bmatrix} \tag{4.7)}$$

is the column vector of all the feeding rates, and

$$\underset{=0}{q} = \begin{bmatrix} q_1(0) \\ q_2(0) \\ \vdots \\ q_n(0) \end{bmatrix} \tag{4.8}$$

is the value of the column vector Q at the beginning of the experiment, i.e., $t=0$. The solution to the *Equation 4.4*, with the initial conditions Q_0 will be

$$q(t) = e^{-\underline{\underline{K}}t} q_0 + e^{-\underline{\underline{K}}t} \int e^{\underline{\underline{K}}\tau} F(\tau) d\tau \tag{4.9}$$

where by definition of Taylor series expansion

$$e^{-\underline{\underline{K}}t} = I - t\underline{\underline{K}} + \frac{t^2 \underline{\underline{K}}^2}{2!} - \frac{t^3 \underline{\underline{K}}^3}{3!} + \ldots\ldots \tag{4.10}$$

and I is the $n \times n$ identity matrix and. The eigenvalues of the K are important since the properties of exponential matrix $e^{-\underline{\underline{K}}t}$ are determined by them.

In most cases, radiotracers are administered to a central compartment and the other compartments exchange this amount of activity administered at $t=0$ without having any feed from outside after that time. In this case, the input matrix given in *Equation 4.7* is a zero matrix,

$$\underline{\underline{F}}(t) = \underline{\underline{0}}. \tag{4.11}$$

If all eigenvalues of matrix $\underline{\underline{K}}$ are real and distinct (or nonrepetitive), then there always exist a nonsingular matrix $\underline{\underline{L}}$ such that [32]

$$\underline{\underline{K}} = \underline{\underline{L}}^{-1} \underline{\underline{\Lambda}}\ \underline{\underline{L}}. \tag{4.12}$$

where $\underline{\underline{\Lambda}}$ is the matrix whose elements are the eigenvalues, λ_i, are the eigenvalues of matrix $\underline{\underline{K}}$.

$$\underline{\underline{\Lambda}} = \begin{bmatrix} \lambda_1 & 0 & \cdots & 0 \\ 0 & \lambda_2 & & 0 \\ \vdots & & & \vdots \\ 0 & 0 & \cdots & \lambda_n \end{bmatrix} \tag{4.13}$$

Equation 4.9 can then be expressed as

$$Q(t) = Q_0\, e^{-\underline{\underline{\Lambda}} t}. \tag{4.14}$$

Thus, the solution to *Equation 4.1*, in general notation, is

$$Q_i = \sum_{j=1}^{n} A_{ij}\, e^{-\lambda_j t} \,. \qquad (4.15)$$

where the coefficients A_{ij} are constants that depend on the initial conditions, and λ_j are the eigenvalues of matrix $\underline{\underline{K}}$.

Compartmental model solution involves the simultaneous solution of n set linear differential equations given in *Equation 4.3* for the coefficient A_{ij} and parameters λ_i. The numeric solution requires a well defined algorithm, generally a least squares regression algorithm such as Marquardt or Gauss-Newton algorithm, and a powerful computer to execute it. There are a number of software packages to perform compartmental tracer analysis for the biologic systems. MTLAB, BMDP, and SAAM are the examples of these computer packages [27].

Because of the various factors in data collection and the different applications of compartmental modeling, the data generated vary among the applications. For a general statistical approach, one may assume that the model satisfies the following conditions:

- The structure and the kinetic of the system must justify the use of compartmental model, i.e., identify non zero $\underline{\underline{K}}$ and $\underline{\underline{F}}(t)$ in *Equation 4.4.*

- Model must consists of a identifiable parameter set P.

- The bolus administration into only one compartment, central compartment, is assumed to be done at a single time at $t=0$. All the other compartments have no activity at the time of administration. The initial conditions are then

$$Q_1(0) = C \qquad (C \text{ stands for constant})$$
$$Q_i(0) = 0 \qquad \text{where } i=2,3,....n \tag{4.16}$$

- The sample size is large enough to make an statistical analysis. The sample size, generally depends on the nature of the problem and subjective judgment. Some factors which may effect the sample size for radiopharmaceutical biokinetic studies includes the physical and chemical characteristic of the radiopharmaceutical and the pathophysiologic condition of the patient.

- The model estimate for the amount of radioactive substance at any time point can be expressed as

$$Q_i(t) = f_i(t, \underline{P}) + \varepsilon_i(t) \tag{4.17}$$

where $\varepsilon_i(t)$ is the random error, also named as residual which designates the difference between the model estimate $f_i(t,\underline{P})$ and observed value. All measuring biases are assumed to be removed such that the mean value of $\varepsilon_i(t)$ is zero and the standard deviation is equal to σ. The distribution of error is normal with a mean of zero and standard deviation of σ, i.e., $N(0,\sigma)$ [33, 34]. The random error expectation can be given as

$$E(\underline{\varepsilon}_i) = \underline{0} \,. \tag{4.18}$$

In most cases observations are assumed to be not intercorrelated. For this case the variance covariance matrix of the observation can be expressed as

$$D = \begin{bmatrix} \sigma_{11}^2 & 0 & . & . & 0 \\ 0 & \sigma_{22}^2 & & & \\ . & & & & \\ . & & & & \\ 0 & & & & \sigma_{nn}^2 \end{bmatrix} \tag{4.19}$$

4.4 Parameter estimation

The nature of the biokinetic behavior, in general, is complex and hard to model. In most cases the quantitative determination of biokinetic parameters is quite tedious and

requires powerful computers and well-written computational algorithms. A number of factors might influence the magnitude of the error in the model parameter estimation. First consideration should be given to the validity of the model. It is essential to make sure that the nature of the problem for which a solution is sought justifies the use of the model. Before having quantitative and qualitative knowledge or judgment to validate the model, any attempt to estimate the parameters would be meaningless and a waste of time. Some of factors which shall be considered as potential sources of error in parameter estimation include the correlation between variables, data accuracy, sampling space, sampling size, weighting factor, estimation method, and the initial parameter guess. The latter is particularly important when either the nature of the problem or solution to the model appear to have nonlinearity. Convergence to a local minimum is one of the major concern of the nonlinear modeling. The modelers should be aware of the local and global minimum concept while estimating the parameters of nonlinear models. Initial guesses play an important role in the nonlinear model parameter estimation. A set of appropriate initial guesses may result in a relatively good curvefit, but it dose not guarantee a convergence to a global minimum. Indeed, it is quite likely that the modeler would not even be aware of this convergence to a local minimum on the n-dimensional error surface. Because of mentioned difficulties nonlinear problems continues to be a dilemma even for the experienced modelers.

There are several methods to deal with the nonlinear model parameter estimation including curve-peeling and least squares method. Among them, least square method has

become popular because of the availability and being easy to apply. There are many commercial least square softwares available for analyzing data sets [35, 36]

Least square fitting and adjustment procedure was introduced by Gauss more than a century ago. The beauty of this principle is that it allows a variety of interpretations like "Best Fit", "Bayesian Estimation", "Maximum Likelihood", "Minimum Variance Estimation", and "Chi-square Method" [37]. Least squares method involves curve fitting of the experimental data to a mathematical function so that the sum of the squares of the distance from the curve, deviation (δ_y) or residual error ε, is minimized, where the distance is measured in the vertical direction (the y-direction).

$$\varepsilon_i = \delta y_i = y_i - f_i(t, p) \tag{4.20}$$

where y_i is the observed value and $f_i(t, p)$ is the model estimate.

The type of function such as sine function, polynomial, or exponential functions may be suggested by the nature of the problem. It is also possible to compute statistical information such as the estimation of parameter uncertainties in the form of a variance-covariance matrix with the least squares analysis method. One of the main advantage of the least squares is the reduction of uncertainties in the parameter estimation. Stallman states this idea as "The main advantage of the least squares method lies not so much in the possible adjustment of measured values, but in the reduction of uncertainties due to

the combination of information" [37]. The least squares method is based on a normal and linear relationship between variables. If the model equations are strongly nonlinear, least squares estimators are questionable. Therefore, the least squares method is not guaranteed to converge if the model is nonlinear. The main task of the generalized least squares method (GLS) is to estimate $\hat{\underline{P}}$, the parameter vector, such that the sum of squared deviations is minimum. The model solution which minimizes the total variation can be expressed by sum of squared residuals

$$SS_{Res} = \sum_{i} (\varepsilon_i)^2 = \sum_{i=1} \left[Q_i - f_i(\hat{\underline{P}}) \right]^2 \tag{4.21}$$

Equation 4.21 can be expressed in vector form as following:

$$X^2(\hat{\underline{P}}) = \left[Q_i - f_i(\hat{\underline{P}}) \right]^T \left[Q_i - f_i(\hat{\underline{P}}) \right] \tag{4.22}$$

or

$$X^2(\hat{\underline{P}}) = \varepsilon^T \varepsilon \tag{4.23}$$

where X^2 represents the sum of squared residual, and $\hat{\underline{P}}$ is the optimum parameter vector which minimize sum of squared error.

On the other hand, weighted least squares (WLS) estimates are used where the

knowledge of error associated with the measurements is available and when the variability in the measurements are quite large. In this case the solution is the one which minimizes the weighted sum of squared residuals and can be expressed as

$$X^2(\hat{\underline{P}}) = \left[\underline{Q}_i - f_i(\hat{\underline{P}})\right]^T W \left[\underline{Q}_i - f_i(\hat{\underline{P}})\right] \tag{4.24}$$

or

$$X^2(\hat{\underline{P}}) = \varepsilon^T \, W \, \varepsilon \tag{4.25}$$

where W is the weighting factor. Several weighting factors shall be generated in accordance to the nature of data. The inverse of the data variance is the most commonly used weighting factor in biokinetic model parameter estimation. In this case the weighting factors can be expressed as the inverse of the S matrix, variance-covariance matrix of the measurements, which is given in *Equation 4.19.*

$$W = S^{-1} = \begin{bmatrix} \frac{1}{\sigma_{11}^2} & 0 & . & . & 0 \\ 0 & \frac{1}{\sigma_{22}^2} & & & \\ . & & & & \\ . & & & & \\ 0 & & & & \frac{1}{\sigma_{nn}^2} \end{bmatrix} \tag{4.26}$$

As it is discussed in *Section 4.2,* biokinetics of tracers or a compartmental model solution suggest that the solution can be represented by a sum of exponentials

$$q(t) = \sum_j A_{ij}\, e^{-\lambda_j t}\,. \tag{4.27}$$

In order to estimate the optimal parameter set of $\left(A_{ij}\ ,\lambda_i\right)$, one needs to minimize the following:

$$SS_{Res} = \sum \left[Q_i - \sum_j A_{ij}\, e^{-\lambda_j t} \right]^2. \tag{4.28}$$

The minimization of any equation is performed by taking the partial derivatives of the equation with respect to its parameters and setting each derivative to zero.

$$\frac{\partial\, SS_{res}}{\partial\, A_{ij}} = \sum_i \left[Q_i - \sum_j A_{ij}\, e^{-\lambda_j t} \right] \left[e^{-\lambda_j t} \right] = 0 \tag{4.29}$$

and

$$\frac{\partial\, SS_{res}}{\partial\, \lambda_j} = \sum_i \left[Q_i - \sum_j A_{ij}\, e^{-\lambda_j t} \right] \left[-t\, A_{ij}\, e^{-\lambda_j t} \right] = 0 \tag{4.30}$$

Equation 4.29 and *4.30* are examples of nonlinear equations. These equations can only be solved by using a numeric solution method which utilizes an iterative algorithm. One can find many algorithms in the literature for the minimization of sum of squared residuals in nonlinear parameter estimation. The Gauss-Newton method is most often used in software computing algorithms for calculating the least squares estimator $\hat{\underline{P}}$ in nonlinear models [35, 36]. The Gauss-Newton method makes use of Taylor series expansions to linearize the nonlinear form of the function to be fitted. For a general case

$$y_i = f(x_i, \underline{P}) + \varepsilon_i \tag{4.31}$$

linearization of *Equation 4.31* by Taylor expansion around $P=P_0$ can be expressed as

$$f(x_i, P) \cong f(x_i, P_0) + (P_1 - P_{1,0}) \left(\frac{\partial f(x_i, P)}{\partial P_1} \right)_{P=P_0} + (P_2 - P_{2,0}) \left(\frac{\partial f(x_i, P)}{\partial P_2} \right)_{P=P_0} + \ldots\ldots$$

$$\ldots\ldots + (P_n - P_{n,0}) \left(\frac{\partial f(x_i, P)}{\partial P_n} \right)_{P=P_0} \tag{4.32}$$

or

$$f(x_i, P) - f(x_i, P_0) \cong \gamma_1 \Gamma_{1i} + \gamma_2 \Gamma_{2i} + \ldots\ldots\ldots + \gamma_n \Gamma_{ni} + \varepsilon_i \tag{4.33}$$

where

$$\Gamma_{ji} = \left(\frac{\partial f(x_i, \underline{P})}{\partial P_j} \right)_{P=P_0} \tag{4.34}$$

is the derivative of the nonlinear function with respect to the jth parameter. The derivatives are evaluated at all starting values.

$$\gamma_j = P_j - P_{j,0} \tag{4.35}$$

is the regression coefficient, and

$$\boldsymbol{P_0} = (P_{1,0}, P_{2,0}, \ldots\ldots\ldots\ldots, P_{n,0}) \tag{4.36}$$

is the vector of initial estimates.

The left hand side of the equation can be considered as the residual. The derivatives are known as regressor variables, and γ is the difference between a parameter value and starting value playing the role of regression coefficient. Then a linear regression algorithm can be employed to solve *Equation 4.33* for the parameter values. The Gauss-Newton method is very sensitive to the initial guess which make this method vulnerable to uncertainty. There are several modifications of the Gauss-Newton method which are written in order to improve the method. More details in nonlinear parameter

estimation and algorithms are given in Myers, 1990, Bard, 1974, Gallant, 1975, and Hartley, 1961 [35, 36, 38, 39].

4.5 Estimation of parameter uncertainties

No general theory, in principle, applies for small sample size properties of individual parameters especially if they are known to be nonlinear in nature [32, 33]. Matis, H. M., *et al.* states that least squares method allows two approaches to investigate the properties of $\hat{\underline{P}}$ estimator, theoretic or experimental [33]. Theoretic approach may be used in cases where the number of data is large enough to assume m, the number of observation, approaches infinity. Otherwise one need to use his or her expertise, or obtain information by expert elicitation to make a decision how the shape of the distribution changes as m approaches infinity . The Sampling method is the empirical way to perform uncertainty analysis using some kind of computer sampling method such as Monte Carlo (MC) or Latin Hypercube Sampling (LHS). Besides the least squares principle one may use some other statistical estimation methods including maximum likelihood, Bayes estimation, and robust estimation techniques. Among them the Bayes approaches is believed to have some advantage over the other methods. But, it is not often used due to the difficulties of implementation especially where the model involves large number of parameters.

4.6 Statistical analysis of estimated parameters through the asymptotic approach.

More often than not, it is not possible to have the number of observations large enough to determine precisely the behavior of the biokinetic of radiopharmaceuticals. Therefore, one needs to make some assumptions to obtain statistical information of the model solution. The following idealization needs to be made in order to obtain a formalism for estimating the parameter uncertainties.

- The time interval between the observations approaches zero

- The kinetics of the radiopharmaceutical is assumed to be determined is to be determined by the function to be fitted after the last data point.

The asymptotic case will then have the following properties [33]:

1. Estimator $\hat{P}_i$ has a normal distribution with mean P_i

2. The variance covariance matrix can be calculated using information matrix obtained at the last iteration and the sum of squared residual. Here an approximation to the calculation of the variance-covariance matrix is introduced, a more detailed and complete form can be found in Stallman's work [37]. The variance-covariance matrix of $\underline{\hat{P}}$ can be approximated by

$$Var(\underline{\hat{P}}) = \left(\underline{\underline{A}}^T \underline{\underline{A}}\right)^{-1} \underline{S}^2 \qquad \text{for the GLS model}$$

$$Var(\underline{\hat{P}}) = \left(\underline{\underline{A}}^T \underline{\underline{W}} \underline{\underline{A}}\right)^{-1} \underline{S}^2 \qquad \text{for the WLS model} \tag{4.37}$$

where S^2 is the familiar sum of squared error given by

$$S^2 = \frac{\sum_{i=1}^{n} \left(y_i - f_i(t, \underline{\hat{P}})\right)^2}{n - p} \tag{4.38}$$

where n is the number of observation and the p is the number of the model parameter.

A is the matrix of partial derivatives with respect to parameters given by

$$A = \begin{bmatrix} \left.\frac{\partial f(\underline{\hat{P}})}{\partial P_1}\right|_{t_1} & \left.\frac{\partial f(\underline{\hat{P}})}{\partial P_2}\right|_{t_1} & \cdots & \left.\frac{\partial f(\underline{\hat{P}})}{\partial P_n}\right|_{t_1} \\ \left.\frac{\partial f(\underline{\hat{P}})}{\partial P_1}\right|_{t_2} & & & \\ \vdots & & & \\ \left.\frac{\partial f(\underline{\hat{P}})}{\partial P_1}\right|_{t_n} & & & \left.\frac{\partial f(\underline{\hat{P}})}{\partial P_n}\right|_{t_n} \end{bmatrix} \tag{4.39}$$

Then the variance covariance matrix of the estimator can be expressed as

$$Var(\underline{\hat{P}}) = \begin{bmatrix} \sigma_{11}^2 & \rho_{21}\sigma_1\sigma_2 & \cdots & \rho_{n1}\sigma_1\sigma_n \\ \rho_{12}\sigma_1\sigma_2 & \sigma_{22}^2 & & \\ \vdots & & & \\ \rho_{1n}\sigma_1\sigma_n & & & \sigma_{nn}^2 \end{bmatrix} \tag{4.40}$$

where the off diagonal terms are the cross-correlations, the diagonal terms are the variances of the estimators and ρ_{ij} is the correlation factor between estimators.

3. Using s_{ii}^2, the diagonal element of the variance-covariance matrix given in *Equation 4.40*, as an estimate, the following statements will be true asymptotically:

$$Var(\hat{P}_i) = s_{ii}^2 \tag{4.41}$$

100 (1-α) % confidence interval for each $\hat{P}_i$ can be given by

$$\hat{P}_i \pm t(\alpha/2, \nu)\, s_{ii} \tag{4.42}$$

where $t(\alpha,\nu)$ is the Student's t statistics and ν is the degree of freedom, which is numerical difference between the number of available data points and the model parameters *(n-p)* [32, 35, 36].

Chapter 5

DETERMINATION OF UNCERTAINTIES IN THE ABSORBED DOSE CALCULATIONS

5.1 Introduction

It is almost impossible to perform a perfect real-world experiment and measurement. There will always be some shortcomings due to the instrumentation, human factors, and the inherent probabilistic behavior of parameters. The magnitude of error may depend, in varying degrees, on any component of the experiment being performed. There are many scientists who consider an experiment or calculation incomplete if uncertainty information does not accompany the results. Uncertainty analysis has become an important part of "state-of-the-art" science. It would be more meaningful to express measurements and calculations with their uncertainty information and/or confidence intervals than to provide only results.

If the subject of the experiment is a human being and the concern is human health, the uncertainty associated with the experiment and calculations appears to be more important than experiments where human health is not at risk. The main goal of nuclear medicine is to improve the medical care given to patients. There is, however, an unavoidable risk associated with exposure to ionizing radiation which a patient or a population will receive as a result of nuclear medicine procedures. As discussed earlier, the radiation absorbed dose is calculated in order to predict the risk involved in the medical application of radioactivity. The absorbed dose calculation involves empirical data and assumptions whose uncertainties propagate through the determination of absorbed dose.

The essential data for calculating absorbed dose, namely pharmacokinetic data and the *S-value* were discussed in the previous chapters. Methodology and the determination of uncertainty in the internal dose calculations will be discussed in this chapter. Uncertainties due to the assumptions and to model identification are not included in the calculations, since they are beyond the scope of this study. However, some cognitive heuristic discussions concerning these source of uncertainties will be presented.

The absorbed dose probability distributions were determined for seven healthy individuals who have undergone a nuclear medicine brain imaging procedure with the

radiopharmaceutical ^{123}I-IPT (cocaine analog pturine). The average dose distributions of each target organ for the small patient population was also determined. Uncertainty calculation was performed in several steps in order to be able to show the significance of the each parameter's uncertainty.

This study utilized the classical approach to determine the probability distributions for radiation absorbed dose. Classical approaches define the probability as the value to which a long-run frequency converges as the number of trials increases [4]. A sampling method, Latin Hyper Cube Sampling (LHS), was used in order to generate large data samples. In most cases first order approximation of error propagation as well as LHS was used to propagate error and the results were tabulated in order to make a quantitative comparison between these two error propagation methods.

Uncertainty analysis was performed in the following four steps:

(i) A simplified biokinetic model which adequately describes the biokinetics for dosimetry was postulated.

(ii) Biokinetic data were simulated with a biexponential function. The parameter estimators for the model and their associated uncertainties were obtained through least squares regression analysis. The residence times and their

associated uncertainties were then determined using the estimated model parameters and their associated uncertainties. This calculation was simulated by the LHS sampling method at least 10,000 times in order to obtain a large sample size.

(iii) *S-value* uncertainties were determined by propagating specific absorbed fraction uncertainties through the results of the *S-values*. The first order error propagation method was utilized in the determination of *S-value* uncertainties.

(iv) Uncertainty associated with the absorbed dose estimates for each patient were determined. The absorbed dose probability distribution of the target organs for the seven-patient population were then determined with 95% confidence interval. These calculation were performed for the following two cases in order to distinguish the contribution of inter-patient biokinetic variabilities and biologic differences to the magnitude of the estimated uncertainties.

(a) considering uncertainties in the least squares parameter estimates and in the absorbed fraction calculations.

(b) incorporating inter-population organ mass variabilities into dose calculations in addition to (a).

The uncertainties associated with the calculation of residence time and *S-values* were considered in (a). The uncertainty in residence time calculations was due to the uncertainties from least squares parameter estimation, while the *S-value* uncertainties are basically from the statistical uncertainties in the determination of absorbed fraction through Monte Carlo photon transport calculations. In (b) organ mass variabilities in the American/Western population were determined and incorporated into the calculations of the *S-values*. The *S-value* calculations were then repeated in order to determine the associated uncertainties when the mass variabilities were included.

5.2 Residence time calculations

The residence time, τ, is defined as the ratio of the cumulated activity to the administered activity, A_0, and given by

$$\tau_h = \frac{\tilde{A}_h}{A_0} \tag{5.1}$$

In the determination of residence time, the only unknown is the cumulated activity $\tilde{A}_h$, and as discussed earlier, it is the total number of transitions in the source organ. The following section discusses the determination of residence time and assessment of uncertainty step-by-step.

5.2.1 Biokinetic data analysis

The fraction of the administered activity in the source organs and excreta, as a function of time, make up the biokinetic data for internal dosimetry calculations. The raw data are the scintigraphically measured counts for each region of interest. Gamma cameras, are the most frequently used devices to monitor the distribution of the radiolabeled material within the body. Data from gamma cameras consist of gross counts per counting time (generally 3 minutes) in both anterior and posterior regions of interest. The net count is the geometric mean of the image corrected counts of the anterior and the posterior counts. The image correction is carried out by introducing the transmission factor, T. The calculation of transmission factor T requires two steps. First, the total number of counts is obtained by scanning with a flat source of radioactivity underneath the patient. Secondly, the total number of counts is obtained by scanning the flat source without the patient. The transmission factor is then the ratio of the counts transmitted through the subject to the counts measured without the subject. The image correction is then carried out by dividing the number of counts by the transmission factor. The geometric mean of the corrected counts can be given by the following equation

$$C = \left(CPM_A \times CPM_P\right)^{1/2} \tag{5.2}$$

where CPM_A is the image corrected anterior count per minute, $\frac{Count_A}{T}$ and

CPM_p is the image corrected posterior count per minute, $\frac{Count_P}{T}$.

The number of counts must be corrected in order to be able to model biologic behavior of radiopharmaceutical within the body. Radioactive decay correction is performed by dividing the number of counts by the decay factor. Decay factor, *DF*, is calculated using the following equation:

$$DF = e^{-\frac{ln2}{t_{1/2}}t} \tag{5.3}$$

where $t_{1/2}$ is the half-life of the radionuclide and it is 13.2 hours for Iodine-123 (^{123}I).

Since the number of counts is a function of administered activity and residence time is defined as the cumulated activity divided by the administered activity it would be convenient to convert the counts to the percentage of the administered activity in each region of interest (ROI). This is carried out by dividing each ROI's corrected geometric mean count by that of the total body.

It is important to take enough samples to fully characterize the biodistribution of the radiopharmaceutical over the time course of the study. The following are some essential criteria to prevent potential errors in the estimation of cumulated activity with

reference to the biokinetic data:

- Catch the early peak uptake and rapid washout phase. Generally, sampling too late is the reason the uptake phase is missed. In this case, the time activity curve is assumed to pass thorough the observed points which leads to an inaccurate estimation of the cumulated activity.

- Typically, collecting data for three effective half-lives of the radiopharmaceutical is sufficient in nuclear medicine in order to observe the approximate long term behavior of the activity distribution within the region of interest.

- Consider all the paths of excretion of the radiopharmaceutical from the body (urine, feces and in some cases exhalation). This is particularly important in the estimation of the total body activity and remainder of the body activity.

In the activity measurements, it is assumed that all biases are removed such that the only uncertainty consideration is the counting statistics. The corrected counts for ROIs were between 10,000 and 300,000 in ^{123}I-IPT brain imaging. It is well known that radioactive decay can be approximated by Poisson statistics. For a Poisson distribution standard deviation is the square root of the mean count as shown in *Equation 5.4.*

$$\sigma_C = \sqrt{\bar{C}} \tag{5.4}$$

In this study, the coefficients of variation of the counts were determined to be between 0.6 and 1. The magnitude of the standard deviations associated with the count rates were not large enough to have a significant effect in parameter estimation.

A set of biokinetic data for ^{123}I-IPT brain imaging studies which had been conducted at The Hospital of the University of Pennsylvania was used in this work. This data set included uptake in the source organs and characterization of excretion which was simply urine in this case. The geometric mean correction was performed as discussed earlier, and converted into fraction of administered activity.

5.3 Methodology for the determination of residence times and associated uncertainties.

The number of total transitions in the source organ *h*, can be estimated by calculating the area under the time activity curve. There are several approaches to carry out this calculation. Direct integration methods such as the trapezoidal method are very good in estimating approximate area under the curve but provide no information about what might occur after the last observation. On the other hand one can determine the approximate long term behavior of biokinetic distribution of the radiopharmaceutical

using multiexponential curve fitting. In this approach one needs to assume that the behavior of the radiopharmaceutical beyond the last observation is determined by the function chosen to model the biokinetic behavior of the radiopharmaceutical. However, if there are source organs for which no data was collected, it is not possible to simulate the activity distribution for those organs using multiexponential curvefitting method. Multicompartmental modeling, on the other hand, eliminates this shortcoming of the two previously mentioned methods. This method not only predicts the approximate long term behavior of biokinetic distribution, but also conserves activity in the body and provides information for organs that have no available biokinetic data. Multicompartmental model is a more realistic representation of the real world situations and provide a more accurate estimate, because all parameters in a compartmental model are derived using all the available data. In curve fitting, on the other hand, the model parameters for a compartment are only functions of the data obtained for that compartment. Generally a least squares algorithm is used to execute both multicompartmental modeling and multiexponential curvefitting. However, multicompartmental modeling is more difficult and time consuming than curvefitting.

A simplified compartmental model which adequately describe the biokinetic of ^{123}I-IPT in the body was postulated and was displayed in Figure 5.1. Organs with relatively larger amounts of activity were included into the model as the source organ compartments. Source organs with insignificant amount of activity were combined into

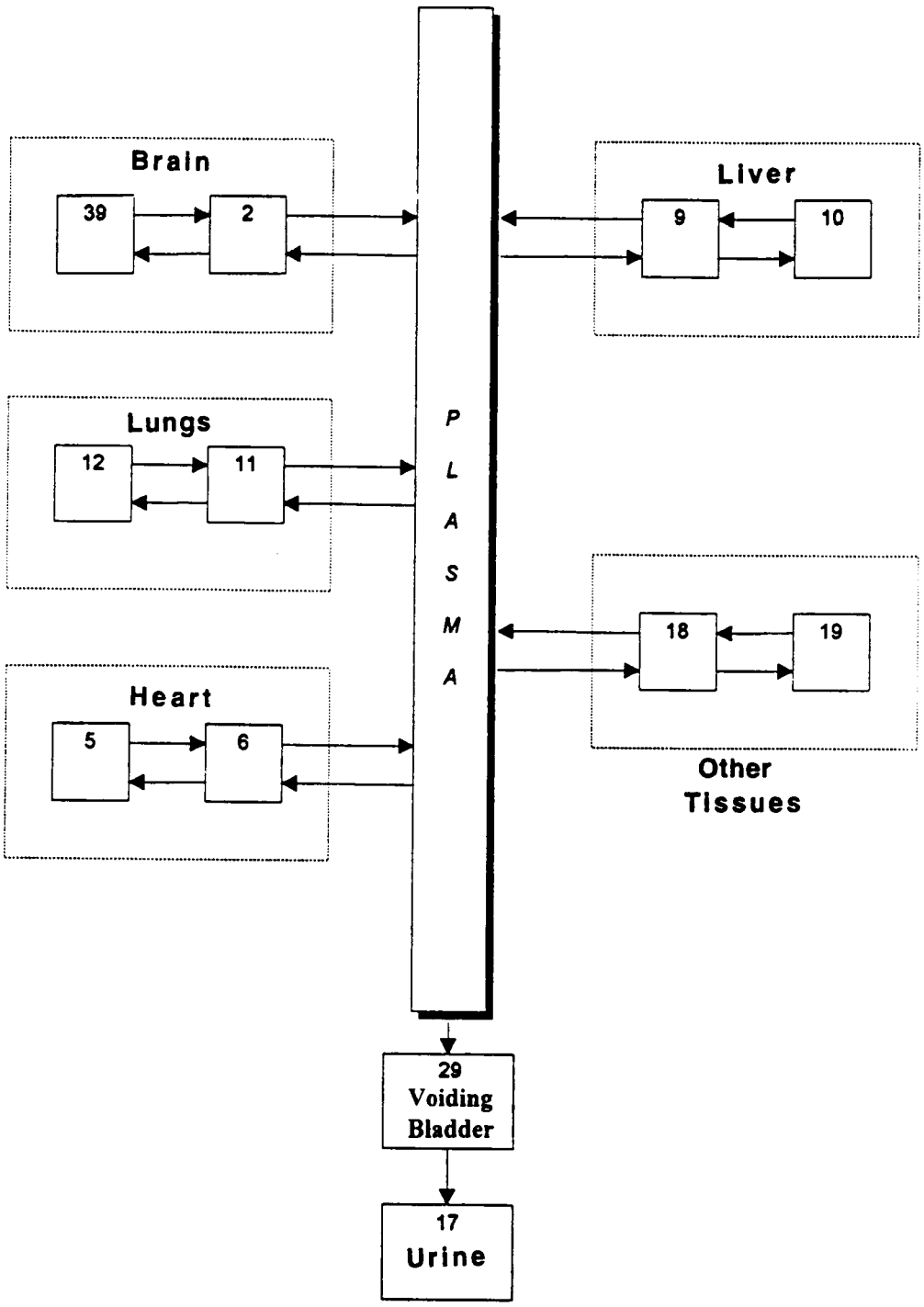

Figure 5.1 Simplified compartmental model for ^{123}I-IPT dosimetry

one compartment resulting in a six-compartment model. Liver, lungs, heart and brain were the selected source organs for this model. The remainder of the body compartment included all activity that is not excreted in the urine. The multicompartmental model represent a set of coupled, first order, linear differential equations. The model solutions for these equations simulate the observed activity distribution within the body.

For the purpose of comparison, residence times were obtained by multicompartmental modeling and multiexponential curvefitting for patient BS and were listed in Table 5.1. As shown in Table 5.1, the results of the two methods are comparable. For the sake of simplicity and in order to be appropriate for the uncertainty analysis, this present study utilized the multiexponential curve fitting in order to calculate residence times.

The SAAM (Simulation, Analysis, And, Modeling) software makes use of the least squares regression analysis method for estimating model parameters and the associated uncertainties The mathematical basis and theory of least squares parameter estimation is explained in Chapter 4. A more detailed discussion about SAAM and examples of model input are included in *Appendix A.*

The SAAM software which is a least squares regression analysis computer program is used to curvefit the data to the multiexponential function as shown in

Table 5.1 A comparison of the multiexponential curvefit and compartmental model solutions for the residence time.

	Liver	*Lungs*	*Heart*	*Brain*	*Remainder of the body*
Multicompartmental modeling	8.07E-01	1.04E+00	1.71E-01	3.26E-01	8.06E+00
Multiexponential curvefitting	8.21E-01	1.06E+00	1.74E-01	3.19E-01	8.02E+00
Difference in %	1.7	1.3	1.1	-2	-0.55

Equation 5.5.

$$\frac{A_h(t)}{A_0} = S_1\ e^{-L_1 t} + S_2\ e^{-L_2 t} \qquad (5.5)$$

The compartmental modeling and curvefitting parts of the present work were conducted at Radiation Internal Dose Information Center of Oak Ridge Associated Universities, Oak Ridge, Tennessee (RIDIC / ORAU). As discussed earlier, a good initial guess is essential for the nonlinear model parameters estimation. The initial guesses for the parameters were determined by expert elicitation method. Scientists of RIDIC/ORAU

provided initial guesses for the parameter estimates. SAAM inputs were prepared and solved for the model parameters. The SAAM software adjusts the parameters of *Equation 5.5* (eigenvalues L_1 *and* L_2, and eigenvectors S_1 *and* S_2) in order to find a better fit, in the statistical sense. The parameters for this model were iteratively adjusted using the Gauss-Newton algorithm for nonlinear regression analysis until the simulated activity distribution statistically fit the observed activity distribution. SAAM makes use of a numerical integration method to compute the residence times from the time-activity curves. As a model output, SAAM provides residence times, parameter estimates, as well as statistical information for the estimators in the form of a correlation matrix and a diagonal matrix of the parameter standard deviations. An example of the SAAM output for patient *BS* is provided in Table 5.2.

Parameter estimates and their confidence intervals for the selected source organs are displayed in. Several authors [27, 33, 35, 36] state that the confidence interval for the least squares parameter estimates can be expressed by

$$\hat{P}_i \pm t\,(\alpha/2,\ \nu)\ s_{ii} \tag{5.6}$$

where s_{ii} is the corresponding standard deviation for parameter estimate $\hat{P}_i$, $t\,(\alpha/2,\ \nu)$ is the Student's t statistic and ν is the degree of freedom, which is the numerical

Table 5.2 A SAAM output for the patient BS

```
      A SAAM30 IPT-123 FOR THE PATIENT ****BS***  09/01/95
**************
PATIENT:BS
ORGAN : BRAIN
**************
0PARAMETER VALUES
0ADJUSTABLE PARAMETERS          DEPENDENT PARAMETERS            FIXED
PARAMETERS
 L ( 0, 2)=  5.7788420E+00
 L ( 0, 3)=  3.8680229E-02
 S ( 1, 2)=  1.5090060E-01
 S ( 1, 3)=  2.7825173E-02
                          P ( 6, 0)=  5.2507576E-02
 INITIAL COMPONENT VALUES
  1=  1.7873E+01   2=  1.0000E+02   3=  1.0000E+02
0  D  C ---CAT--      T        THETA      QC           QO        QO-QC     QC/QO       WT
  1  1      0   4.2000E-01  0.0000E+00  4.07000E+00 *  4.07000E+00   0.000E+00   1.000
  2  1      0   3.0000E+00  0.0000E+00  2.47766E+00 *  2.29000E+00  -1.877E-01   1.082
  3  1      0   3.4300E+00  0.0000E+00  2.43679E+00 *  2.41000E+00  -2.679E-02   1.011
  4  1      0   4.1000E+00  0.0000E+00  2.37445E+00 *  2.46000E+00   8.555E-02   0.965
  5  1      0   4.5000E+00  0.0000E+00  2.33800E+00 *  2.29000E+00  -4.800E-02   1.021
  6  1      0   1.3400E+01  0.0000E+00  1.65705E+00 *  1.76000E+00   1.029E-01   0.942
  7  1      0   2.3509E+01  0.0000E+00  1.12078E+00 *  1.16000E+00   3.922E-02   0.966
  8  4      0   2.5000E+02  0.0000E+00  3.22456E-01    0.00000E+00  -3.225E-01      *
0 C   DATA    SS        NORM.SS     MEAN SD     MEAN FSD
  1    7   4.9517E-02  7.0739E-03  8.4106E-02  3.9166E-02
0***AN '*' FOLLOWS QC WHEN A DATUM DETERMINES AND INCORPOORATES THE FINAL
VALUES OF S AND/OR K.
 *** AN 'F' INDICATES THAT QC WAS RECALCULATED AFTER FINAL S AND/OR K VALUES
WERE DETERMINED.*14*
0SUM SQUARES AFTER    8 ITERATIONS IS  4.95171733E-02
  COMP  1=   4.9517173E-02
 SIG AFTER    8 ITERATIONS IS  9.90343466E-03
                          0.00000E+00   0.00000E+00   0.000E+00      *   0.00E+00
0                            SD          FSD      INITIAL        MIN          MAX
                                        ESTIMATE
0ADJUSTABLE PARAMETERS
  1    L ( 0, 2)=   5.7788420E+00 +OR- 8.9997925E+02    1.5574E+02 4.0282267E-01
  2    L ( 0, 3)=   3.8680229E-02 +OR- 2.9665281E-03    7.6694E-02 9.5332098E-06
  3    S ( 1, 2)=   1.5090060E-01 +OR- 2.5748274E+01    1.7063E+02 2.4775760E-03
  4    S ( 1, 3)=   2.7825173E-02 +OR- 1.0411436E-03    3.7417E-02 2.5805697E-04
0CORRELATION MATRIX
 COLUMN   1    2    3    4
 ROW 1  1.00  0.30  1.00  0.57
 ROW 2  0.30  1.00  0.30  0.75
 ROW 3  1.00  0.30  1.00  0.57
 ROW 4  0.57  0.75  0.57  1.00
```

difference between the number of available data points and model parameters. For a 95% confidence interval α will have a value of 0.05. For parameter means, 95% confidence intervals were calculated using *Equation 5.6* and are listed in Table 5.3 for brain and liver.

Several questions arise in parameter estimation. First of all, it is not possible to determine one true value of a nonlinear model parameter for living systems. Parameters of a living system may vary considerably from one species to another , one sex to another, even from one experiment to another with the same subject. Consequently, to provide the distribution of a parameter and its confidence interval might be a better way of defining a model parameter. It is essential to note that the confidence interval, in this context, should not be understood such that the true mean has a 95% probability of being within the specified interval. Rather, it means that the two quantities enclosing the interval are random variables and they have a 95% probability of enclosing the true mean. Classical approach states that the true mean is a fixed but unknown value. The Bayes' approach, on the other hand, allows the mean to be treated as a variable [4].

One of the common problems with curve fitting is obtaining an exceptionally good fit for the model with a set of parameter estimates with very large variances. In compartmental modeling, large variances may indicate the followings:

Table 5.3. Parameter estimates, associated standard deviations, and 95 % confidence intervals of mean parameter values for brain and liver.

BRAIN						
	PARAMETER	L_1	L_2	S_1	S_2	τ
PATIENTS	DF	9.17E-01	2.97E-02	3.73E-02	2.29E-02	3.20E-01
	WM	1.18E+00	4.86E-02	7.84E-02	4.24E-02	4.85E-01
	BS	1.08E+00	3.07E-02	4.11E-02	2.79E-02	3.22E-01
	PT	6.17E-01	8.86E-02	5.40E-02	3.17E-02	3.55E-01
	RF	1.38E+00	3.80E-02	7.11E-02	3.14E-02	4.16E-01
	MC	1.03E+00	5.37E-02	3.48E-02	2.58E-02	3.30E-01
	VU	1.35E+00	2.87E-02	4.27E-02	3.05E-02	4.06E-01
	MEAN	1.08E+00	4.54E-02	5.13E-02	3.04E-02	3.76E-01
	SD	1.07E-01	8.73E-03	7.03E-03	2.53E-03	2.52E-02
	95% CONFIDENCE INTERVAL	±2.63E-01	±2.14E-02	±1.72E-02	±6.20E-03	±6.18E-02
LIVER						
	PARAMETER	L_1	L_2	S_1	S_2	τ
PATIENTS	DF	2.04E-01	2.36E-02	5.62E-02	5.66E-02	1.02E+00
	WM	2.82E+00	4.01E-02	2.24E-01	1.15E-01	9.85E-01
	BS	1.60E+00	4.07E-02	6.07E-02	7.31E-02	8.22E-01
	PT	4.00E-01	7.89E-02	8.07E-02	7.01E-02	7.11E-01
	RF	2.64E+00	4.17E-02	1.94E-01	9.62E-02	1.15E+00
	MC	2.42E+00	3.75E-02	1.40E-01	6.84E-02	8.17E-01
	VU	2.79E+00	9.32E-03	2.75E-01	6.76E-02	1.20E+00
	MEAN	1.84E+00	3.88E-02	1.47E-01	7.82E-02	9.58E-01
	SD	4.61E-01	8.70E-03	3.52E-02	8.28E-03	7.45E-02
	95% CONFIDENCE INTERVAL	±1.13E+00	±2.13E-02	±8.63E-02	±2.03E-02	±1.83E-01

- The model is overparameterized: A system should be represented with as few parameters as possible. A model with a larger number of parameters generally fits data better. But there is penalty in using larger number of parameters, since the model lose its ability to represent the behavior of the real world process. The model, in this case provides a good fit to that particular set of data and does not guarantee the same good fit for another data set of the same kind.

- There was not enough data to perform a compartmental analysis. In such cases, since the data set was not large enough to perform a proper least squares analysis, large uncertainties in the estimated parameters may exist.

- The model itself is not a good representation of the system to be studied. There may be a more realistic representation of the problem being studied.

- There is non-uniqueness of the fit. In the error surface, there might be another local or minimum which would fit the data better.

- There parameters are highly interrelated. The reason for large parameter uncertainties might be the high interrelation between the parameters in terms of their influence on the model output [32].

The magnitude and the sign of the cross correlations will have some influence on the residence time distribution. Several cases are examined in order to determine the influence that the correlation coefficients may have on the residence time. It is found that the existence of negative correlations, in general, decreases the magnitude of the residence time standard deviation. Large variances with a good curvefit may indicate non-uniqueness of the solution [5]. This might be interpreted as the model parameters have a very flat surface in the area of this particular solution in *n-dimensional* error space, where n is the number of the model parameters. Table 5.4 displays an example of non-unique solutions obtained in this study. Another problem of curve fitting is the previously discussed local/global minimum concept. Most of the time one would not be aware whether a local or global minimum is obtained. Brute force method might be considered to test whether the solution is a global minimum. This method, however, is hard to perform because of the limitations of computer hardware. If a relatively good fit is obtained, the calculated residence time, in most cases, would not change considerably.

It is worthwhile to note that the goodness of fit or the magnitude of the sum of squared error is not a good indicator for the magnitude of the estimated parameter uncertainties nor for the variances of the residence times in least square analysis. Table 5.5 shows some examples of the latter case which had been obtained during the course of this study.

Table 5.4 Two SAAM parameter estimates and their associated uncertainties for BS liver, and their comparison which indicate the nonuniquenesse of the solution.

Liver (BS)	*CASE 1*		*CASE 1*	
Sum of Squared Error (SS)	2.08E-01		2.41E-02	
PARAMETER	μ	σ	μ	σ
L_1	5.65E+00	1.09E+03	1.58E+00	3.76E-01
L_2	3.73E-02	1.96E-03	4.07E-02	7.58E-04
S_1	3.48E-01	2.82E+02	6.01E-02	9.57E-03
S_2	7.15E-02	1.85E-03	7.30E-02	7.20E-04
Residence time	8.75E-01	1.22E+02	8.20E-01	1.48E-01

Table 5.5 Some examples of the parameter uncertainties and the sum of squared error of the curvefits.

CASE	*SUM OF SQUARED ERROR*	*PARAMETER VALUE (L_1)*	*PARAMETER SD*	*FSD*
Lungs (BS)	3.87E-01	2.53E+00	3.91E+04	1.55E+04
Liver (BS)	2.08E-01	5.66E+00	1.09E+03	1.92E+02
Lung (WM)	4.90E-01	2.82E+00	4.03E-01	1.43E-01
Liver (WM)	1.07E-01	8.97E-01	1.58E-01	1.76E-01
Total Body (DF)	7.36E+00	3.20E-01	4.32E-01	1.35E+00

This comparison indicates that the uncertainty information of the estimated parameters determined by a least squares method is not related to the sum of squared error or to the goodness of the fit. However, parameter uncertainties of a least square analysis can be considered as the true parameter estimates for that particular curvefit in a model parameter estimation procedure. Therefore, to obtain more accurate parameter uncertainties, one need to obtain a relatively good fit of the data and confirm that fit by comparing the other fits obtained with different starting points (initial guess).

There is no general statistical distribution theory that exists for a nonlinear model

estimator, $\hat{P}_i$, where small data samples are available [33]. Their approximate behavior can, however, be studied empirically by using Monte Carlo simulation [33, 35]. The Crystal Ball software, which is a user-friendly risk analysis program, is used to generate large data samples for the least squares parameter estimates. A detailed discussion about Crystal Ball program is given in *Appendix B*. Least squares theory assumes that the estimated parameters have normal distributions. However, lognormal distributions were assigned to represent the parameter distributions, since a negative value is not physically realizable. Source organs' residence times are calculated by the following equation:

$$\tau = \int_0^\infty \left(S_1 \, e^{-L_1 t} + S_2 \, e^{-L_2 t} \right) e^{-\lambda_p} \, dt \qquad (5.7)$$

where λ_p is the physical half-life of the radionuclide, S_1, S_2, L_1, and L_2 are the parameters of the model. The solution to the above integral can be expressed as

$$\tau = \frac{S_1}{L_1 + \lambda_p} + \frac{S_2}{L_2 + \lambda_p} \qquad (5.8)$$

The values for parameters, their associated standard deviations, and cross-correlations were used as assumptions in Crystal Ball. *Equation 5.8* was employed to simulate the residence time calculation by sampling from the parameter distributions

entered in the assumption cells. Samples for the Crystal Ball assumptions and forecasts were displayed in *Appendix B*. The residence time calculations were simulated by sampling from the parameter distributions at least 2,500 times in order to obtain a distribution of residence time for each organ. Standard deviations associated with residence time calculations were also calculated by using first order error propagation (FOEP) and are listed in order to make a comparison between the results of these two methods. The first order error propagation equation for calculating the variance of residence time given in *Equation 5.7* can be expressed as

$$Var(\tau) = \left(\frac{\partial \tau}{\partial P_1}\right)^2 \sigma_{P_1}^2 + \left(\frac{\partial \tau}{\partial P_2}\right)^2 \sigma_{P_2}^2 + \left(\frac{\partial \tau}{\partial P_3}\right)^2 \sigma_{P_3}^2 + \left(\frac{\partial \tau}{\partial P_4}\right)^2 \sigma_{P_4}^2 + 2 \sum_{i}^{4} \sum_{j=i+1}^{4} \rho_{P_i P_j} \sigma_{P_i} \sigma_{P_j} \left(\frac{\partial \tau}{\partial P_i}\right) \left(\frac{\partial \tau}{\partial P_j}\right) \tag{5.9}$$

where $\rho_{P_i P_j}$ is the correlation coefficient between i^{th} and j^{th} parameters and P_i and P_j are the parameters S_1, S_2, L_1, and L_2 of *Equation 5.8*. Since the variance of the physical decay constant is negligible, it is not included in *Equation 5.8*.

Remainder of the body residence times were calculated by utilizing the total body activities. The total body activity was calculated by subtracting cumulative urine activity from 100%.

$$\tilde{A}_{TB} = 100 - \tilde{A}_{CU} \tag{5.10}$$

The total body residence times were computed by curvefitting the total body activities. The remainder of the body residence time was then calculated by subtracting the sum of the other source organs residence times from that of total body.

$$\tau_{RB} = \tau_{TB} - \sum_{h=1}^{n} \tau_h \tag{5.11}$$

Remainder of the body uncertainties were calculated by using the first order error propagation method (FOEP).

$$\sigma_{RB} = \sqrt{\sigma_{TB}^2 + \sigma_{h1}^2 + \sigma_{h2}^2 + \ldots\ldots + \sigma_{hn}^2} \tag{5.12}$$

where n is the number of source organ in the model.

Table 5.6 displays means and standard deviations of the residence time estimates which were calculated using both "FOEP" and "Sampling Method" (LHS). The results of FOEP and sampling method were quite different. This may indicate the residence times and least squares parameter estimates were not normally distributed in this case.

Table 5.6 Residence times for the source organs and their associated standard deviations calculated by both FOEP and LHS sampling method.

ORGAN	PATIENT : DF			PATIENT : RF		
	τ	σ (LHS)	σ (FOEP)	τ	σ (LHS)	σ (FOEP)
LUNG	1.17E+00	2.02E-02	2.46E-03	1.22E+00	1.36E-01	2.50E-01
LIVER	1.02E+00	1.35E-01	2.75E-02	1.14E+00	1.36E-01	1.20E-01
BRAIN	3.20E-01	2.06E-02	2.08E-03	4.16E-01	9.72E-03	2.75E-03
HEART WALL	2.43E-01	2.04E-02	9.48E-03	2.94E-01	9.07E-03	7.00E-03
TOTAL BODY	1.07E+01	8.63E+00	1.07E+0	8.94E+00	1.08E+01	9.08E-01
REMAINDER OF THE BODY	7.96E+00	8.63E+00		5.87E+00	1.08E+01	
	PATIENT : MC			PATIENT : BS		
	τ	σ (CB)	σ (FOEP)	τ	σ (CB)	σ (FOEP)
LUNG	1.13E+00	2.37E-02	9.90E-03	1.06E+00	6.21E-02	1.28E-02
LIVER	8.19E-01	2.67E-02	7.21E-03	8.22E-01	1.48E-01	2.09E-02
BRAIN	3.30E-01	2.02E-02	1.00E-02	3.22E-01	1.77E-02	1.18E-02
HEART WALL	1.94E-01	7.71E-02	4.25E-02	1.78E-01	1.06E-02	7.60E-03
TOTAL BODY	1.14E+01	1.21E+00	2.70E-01	1.10E+01	2.27E+00	2.36E-01
REMAINDER OF THE BODY	8.93E+00	1.21E+00		8.62E+00	2.28E+00	

Table 5.6 Continued

	PATIENT : PT			PATIENT : VU		
	τ	σ (LHS)	σ (FOEP)	τ	σ (LHS)	σ (FOEP)
LUNG	4.55E-01	2.41E-01	9.78E-03	1.20E+00	1.01E-01	9.30E-02
LIVER	7.48E-01	2.24E-01	3.52E-02	7.53E-01	1.27E-02	9.90E-03
BRAIN	3.55E-01	6.71E-02	1.92E-02	4.06E-01	3.23E-03	1.71E-03
HEART WALL	2.54E-01	4.87E-02	5.43E-03	2.55E-01	4.07E-02	8.10E-03
TOTAL BODY	1.37E+01	1.37E+01	2.56E-01	1.33E+01	1.18E+00	3.2E-01
REMAINDER OF THE BODY	1.19E+01	1.37E+01		1.07E+01	1.19E+00	

LHS: Latin Hyper Cube Sampling
FOEP: First order error propagation

5.4 *S-values* and error propagation

The *S-values* and the associated uncertainties were calculated using first order error propagation. In these calculations the estimates of specific absorbed fractions for photon sources and their associated coefficient of variances (CV) published by Snyder *et al* [45] were used. This paper employed Snyder specific absorbed fraction since they were the only estimates for which the uncertainty information were available. Two sets of calculations were carried out : (i) considering only the error associated with residence time calculations and radiation transport calculations and (ii) mass uncertainties were determined from several references and were used in the *S-value* calculations in addition to the uncertainties in (i). In both cases, the mean organ masses were taken to be those listed in ICRP-23 (Reference Man) [50]

The following equation was utilized in the determination of the *S-values* and their associated uncertainties.

$$S(r_k \leftarrow r_h) = \sum_{i=1}^{N} \Delta_i \times \Phi_i(r_k \leftarrow r_h) \qquad (5.13)$$

where Δ_i is the mean energy emitted by the ith particle per nuclear transition and $\Phi_i(r_k \leftarrow r_h)$ is the specific absorbed fraction in the target organ r_k.

5.4.1 The specific absorbed fraction, Φ_i

The specific absorbed fraction in any target organ r_k is defined as the absorbed fraction in the target per unit mass of the target and is given by

$$\Phi i(r_k \leftarrow r_h) = \frac{\phi(r_k \leftarrow r_h)}{m_k} \tag{5.14}$$

where $\phi(r_k \leftarrow r_h)$ is the fraction of energy emitted from the source organ that is deposited in the target organ.

The specific absorbed fraction estimates for 12 monoenergetic photon energies for several source and target organs were obtained by Snyder *et al* and tabulated in MIRD Pamphlet 5 [20]. In their study the following idealizations were made to reduce the complexity of calculations. The uncertainties associated with these assumptions and their determinations is beyond the scope of this paper.

a) A phantom which simulated the anatomical make up of the human body was used to estimate the absorbed fraction in target organs. Each organ defined within the phantom is considered to be homogenous in composition and density, which is a simplification of real organ compositions. Three different composition and densities for lung, skeletal system and the remainder of the

phantom (soft tissues) were used to represent the body organs. The "Reference Man" phantom has a mass of 70 kg which is probably less than the current average radiation worker.

b) The source is considered to be uniformly distributed within the organs.

c) The histories of photons that originate within the source organ were determined by the Monte Carlo method.

Organs were approximated, in Snyder *et al'* s work, by homogenous elliptical and spherical sources. The most important achievement in Snyder *et al*'s study was the use of more realistic representations (e.g. size, shape, composition, and density) of normal organs compared to previous works [43]. Since the composition and density has considerable effect on both specific absorbed fraction and its variance, this study is believed to be more accurate than previous estimates [20, 43]. The Monte Carlo techniques are believed to be unreliable where the standard deviation are as large as the estimate. In such cases no estimates calculated by Monte Carlo were given. Other methods, such as build-up factor method and point kernel method were used to obtain more accurate estimates where the coefficient of variation exceeded 50% using Monte Carlo techniques. Nevertheless, the latter methods are also subject to uncertainties.

5.4.2 Statistical evaluation of the determination of absorbed dose by Monte Carlo method.

Monte Carlo is a statistical analysis method in which the fate of every individual incident and secondary particle is handled statistically on the basis of the linear attenuation coefficient and cross section for the various nuclear interactions that may occur. In such a calculation, each particle is allowed to lose energy and generate secondary electrons on a statistical basis as it does in a real interaction process. The secondary electrons are similarly transported and are allowed to produce their own secondaries until the energy of all secondaries fall below the subexcitation energy of 7.4 keV(20). The complete history, position, and identity of every photon and secondary electrons are determined and analyzed in order to calculate absorbed fraction.

For each source organ and photon energy, 60,000 photon histories were carried out by Monte Carlo transport and resulting data were compiled to obtain specific absorbed fractions. In the preliminary studies few photons were observed to penetrate to large distances. Thus, the statistics of the estimates were found to be unreliable. To obtain statistically more reliable estimates, photon histories were determined using a statistical weight method, in which each photon was given a statistical weight which was reduced with every collision in accordance with the expectation of Compton scattering in nature. This reduction of weight concept assures the probability of survival and allows

the photon to have only Compton scattering, interaction for the rest of its journey. The flight history of the photon was terminated if its energy dropped below 4 keV or its weight dropped below 10E-05. In this case the photon is assumed to absorbed by the target region. The photon histories also terminated if it left the body assuming the photon is absorbed by the target region, or if it leaves the body.

For a given source/target combination, the total energy absorbed in the target organ can be estimated by the calculation of mean energy deposited per monoenergetic photon in the target.

$$\overline{E} = \frac{1}{N}\sum_{i=1}^{N} E_i^* \qquad (5.15)$$

where E_i^* is the total energy deposited to the target region by i^{th} photon. The standard deviation of estimate $\overline{E}$ is,

$$\sigma_{\overline{E}}^2 = \frac{1}{N(N-1)}\sum_{i=1}^{N}(E_i^* - \overline{E})^2 \qquad (5.16)$$

The absorbed fraction is the mean energy deposited per photon divided by the total energy of the photon and is given by *Equation 5.16.*

$$\phi_i = \frac{\overline{E}}{\overline{E}_{total}} \tag{5.17}$$

Both, the specific absorbed fraction and the absorbed fraction are proportional to $\overline{E}$. They will then have a standard deviation differing by the same proportionality constant as $\overline{E}$. Therefore the coefficient of variation for the absorbed fraction will be the same as that of $\overline{E}$, and it can be expressed as

$$CV = \frac{\sigma_{\Phi}}{\Phi} \times 100 \tag{5.18}$$

Whenever $\overline{E}$ has an approximately normal distribution, a confidence interval can be assigned to the estimates of the mean energy. In some cases, where fewer photon interactions occur, the distribution of the mean energy would not have normal distribution. In such circumstances, a coefficient of variation larger than 50% is expected. Error of a factor of 2 to 5 can result from such a large coefficient of variation. Other methods were used in such cases in order to obtain more reliable estimates [20].

5.4.3 Methodology

The *S-values* and their associated uncertainties are calculated separately for

penetrating and nonpenetrating particles. The methodologies were presented in the following two sections.

5.4.3.1 For penetrating radiations: photons

The emitted energies and the mean energy emitted per nuclear transition for Iodine-123 (^{123}I) were obtained from the MIRD Radionuclide and Decay Schema [19]. The MIRD Radionuclide and Decay Schema contains a list of emitted particles, their energies, and the mean energy emitted per nuclear transition. This source does not contain all the emitted particles. However, the total energy of omitted radiations is only 0.3% of the total emitted radiations for Iodine-123 (^{123}I). Therefore, the uncertainties due to the omitted radiations were not included. Each emitted photon energy for Iodine-123 (^{123}I) was determined and the specific absorbed fractions for these photon energies were obtained by linear interpolation. The error associated with the interpolation of the absorbed fractions was neglected. To propagate the error through *S-value* calculations, the standard deviations of the specific absorbed fractions were calculated from the coefficients of variation by the following equation:

$$\sigma_{\Phi} = \Phi \times \frac{CV}{100} \tag{5.19}$$

Coefficients of variation were also linearly interpolated for ^{123}I spectrum. For brain specific absorbed fractions, no published statistical data were available [60]. Since the shape, size, and composition of brain is similar to that of the liver, the liver's coefficients of variation were used for brain [46].

The method for the estimation of specific absorbed fraction still continues to be of concern, particularly where the coefficient of variation exceeds the 50%. Fortunately in this work, the maximum calculated coefficient of variation was no more than 10%.

5.4.3.2 Calculations

The *S-value* is given as the sum of the product of the specific absorbed fraction, Φ_i, and the mean energy emitted per nuclear transition, Δ_i.

$$S = \sum_i \Phi_i \Delta_i \tag{5.20}$$

The standard deviations for the *S-values* are determined by propagating the error through the *Equation 5.20.*

$$S_i = \Phi_i \Delta_i \tag{5.21}$$

where

$$\Phi_i = \Phi_i + \sigma_i \tag{5.22}$$

The distributions of specific absorbed fractions and the mean energy per nuclear transition can be assumed to be normal [20]. Therefore, the first order approximation of error propagation (FOEP) would give a relatively correct result. The first order approximation of error propagation for *Equation 5.21* is presented in *Equation 5.23.*

$$\sigma_S^2 = \left(\frac{\partial S}{\partial \Phi}\right)^2 \sigma_\Phi^2 + \left(\frac{\partial S}{\partial \Delta}\right)^2 \sigma_\Delta^2 + \ \textit{correlation terms} \tag{5.23}$$

Since, the variability associated with Δ is negligible, the second term and correlations will be canceled out and *Equation 5.24* will be the error propagation formula for *S-values.*

$$\sigma_S^2 = \Delta^2 \sigma_\Phi^2 \tag{5.24}$$

Standard deviation for *S-values* can be expressed by

$$\sigma_S = \Delta\ \sigma_\Phi \tag{5.25}$$

The total *S-value* is the sum of the *S-values* for each emission and is given in *Equation 5.21.* The last step was to propagate the error through *Equation 5.21.* Using *Equation 5.23*, the following formula was obtained for the standard deviation of the *S-value.*

$$\sigma_S = \sqrt{\sigma_{S1}^2 + \sigma_{S2}^2 + \sigma_{S3}^2 + \ldots\ldots\ldots} \qquad (5.26)$$

Using the above methodology *S-values*, and their standard deviations for the target organs; heart wall, liver, brain, and lungs were calculated. An example table which is used in *S-value* calculations was displayed in Table 5.7. This table includes the specific absorbed fractions and their associated uncertainties fro discrete photon energies by Monte Carlo method, and for ^{123}I spectrum, estimated *S-values* and associated uncertainties.

5.4.4 Nonpenetrating particles

If the source and the target organ are the same, and the target organ is large compared to the mean free path of the particle, the radiations are non penetrating and are assumed to be absorbed by the source organ in which they originate. In this case there will be no consideration of the uncertainty for the estimation of the absorbed fraction. Most of the nonpenetrating emissions will be absorbed by the organ in which they originate, i.e., $\phi \cong 1$. The specific absorbed fraction for nonpenetrating particles is

Table 5.7 An example table which shows the specific absorbed fractions and associated uncertainties for discrete photon energies and for ^{123}I spectrum, S-values and their estimated uncertainties.

SPECIFIC ABSORBED FRACTIONS (1/g) AND STANDARD DEVIATIONS FOR DISCRETE PHOTON ENERGIES CALCULATED BY MONTE CARLO					
TARGET ORGAN	LUNG<-LUNG		LIVER<-LIVER		
ENERGY(MeV)	SAF (1/g)	CV(%)	SAF (1/g)	CV(%)	
0.02	4.71E-04	1	4.34E-04		
0.03	2.30E-04	1	2.97E-04	1	
0.05	8.99E-05	1	1.52E-04	1	
0.1	5.05E-05	1	9.15E-05	1	
0.2	5.00E-05	1	8.82E-05	1	Mean
0.5	5.01E-05	2	8.85E-05	1	Energy
1	4.55E-05	2	8.07E-05	1	per
INTERPOLATED VALUES FOR ^{123}I SPECTRUM					Transition
PHOTON ENERGY	SAF (1/g)	SD	SAF (1/g)	SD	rad g/μCi-h
0.02747	2.91E-04	2.49E-05	3.32E-04	1.04E-04	2.69E-02
0.0272	2.97E-04	2.39E-05	3.35E-04	1.05E-04	1.43E-02
0.031	2.23E-04	2.70E-05	2.90E-04	9.07E-05	5.73E-03
0.0317	2.18E-04	2.69E-05	2.85E-04	8.91E-05	1.80E-03
0.159	5.02E-05	1.54E-06	8.95E-05	2.80E-05	2.82E-01
0.197	5.00E-05	1.48E-06	8.83E-05	2.76E-05	1.00E-04
0.248	5.00E-05	1.45E-06	8.83E-05	2.76E-05	3.76E-04
0.281	5.00E-05	1.44E-06	8.83E-05	2.76E-05	4.74E-04
0.3464	5.00E-05	1.52E-06	8.84E-05	2.76E-05	9.30E-04
0.44	5.01E-05	1.39E-06	8.84E-05	2.77E-05	4.01E-03
0.5053	5.00E-05	1.37E-06	8.81E-05	2.76E-05	3.40E-03
0.529	4.97E-05	1.37E-06	8.78E-05	2.75E-05	1.57E-02
0.5385	4.96E-05	1.36E-06	8.76E-05	2.74E-05	4.38E-03
0.6246	4.89E-05	1.50E-06	8.63E-05	2.70E-05	1.11E-03
0.6879	4.83E-05	1.35E-06	8.53E-05	2.67E-05	3.91E-04
0.7358	4.78E-05	1.34E-06	8.45E-05	2.64E-05	9.66E-04
0.7836	4.74E-05	1.34E-06	8.38E-05	2.62E-05	9.92E-04
S-VALUE ESTIMATES AND ASSOCIATED UNCERTAINTIES					
S-value for photon	2.96E-05	3.94E-06	4.40E-05	2.79E-06	For np
S-value for electron	6.01E-05	1.80E-05	3.32E-05	9.21E-06	6.01E-02
S-VALUE & SD	8.97E-05	1.85E-05	7.72E-05	9.92E-06	

$$\Phi = \frac{1}{m} . \tag{5.27}$$

where m is the mass of the heart, liver, lung, and brain. Then *S-value* is,

$$S = \frac{1}{m} \times \Delta_{np} \tag{5.28}$$

where Δ_{np} is the total energy emitted for all nonpenetrating radiation for a radionuclide. For instance, Δ_{np} for ^{123}I is 6.01E-02 rad g / μCi-h [19].

The *S-value* is then the sum of the *S-values* for nonpenetrating and penetrating particles. The estimated *S-values* of this paper and MIRDose 3.1 computer code were comparable. In most cases the difference was no more than 3%. The differences between the calculated values in this work and MIRDose 3.1 calculations were probably due the use of different absorbed fractions. MIRDose 3.1 utilizes Christy and Eckerman's absorbed fractions while this paper utilized Snyder *et al* [20] specific absorbed fractions.

5.4.5 The *S-value* uncertainties with the incorporation of inter-patient mass variability

The "Reference Man" organ masses are used in the *S-value* calculations [50]. The

reference man was designed to simulate the body of an average American/Western radiation worker in 1975. The Reference Man's organ masses are represented by the mean organ masses that were determined for the average American radiation worker [50].

Table 5.8 listed the organ masses and associated uncertainties used in this work compiled from different sources.

Table 5.8 The list of the mean organ masses and their approximate standard deviations for American population.

	BRAIN [53, 54]		*HEART [50]*		*LIVER [52]*		*LUNG [51]*	
	AGE: 17-40		AGE: 25		70 kg	60 kg	70 kg	60 kg
	MALE	FEMALE	MALE	FEMALE	MALE	FEMALE	MALE	FEMALE
MEAN	1454	1220	332	253	1820	1500	1000	800
SD	110	100	83	55.7	500	350	300	240
CV	7.57	8.21	25	22	27.4	23.3	30	30

A literature search was carried out in order to determine the variability of the organ masses in American/Western population. It is found that the organ masses may

vary as a function of height, weight and age. Tanaka's studies in Japanese populations showed that there is a strong correlation between organ masses and whole body weight and/or height [51]. Unfortunately, a well conducted study could not be found for American/Western populations. Several medical doctors and scientists were interviewed to obtain insight about the variability of organ masses. The common opinion was that the liver and lung may have standard deviation of 20% to 30% of their mean values while heart and brain are believed to have a standard deviation of 10% to 15% of their mean values. There was no available reference for lung mass variabilities in American populations. Although there is considerable difference between the American population and Japanese population, the organ mass variabilities are believed to be similar [Personal communication with Mark Cristy[1]]. Consequently, the Japanese population lung mass variability was used in this work. In the literature, no information was found which discusses the variability of the brain and heart masses as a function of body weight and/or height. It is believed that brain organ mass variability is dependent mostly on age. Typical young American brain and heart mass variabilities were used in this work.

The definition of specific absorbed fraction is presented in *Equation 5.13* as

$$\Phi_i(r_k \leftarrow r_h) = \frac{\phi(r_k \leftarrow r_h)}{m_k}$$

[1] Scientist, Oak Ridge National Laboratories, Oak Ridge, Tennessee.

The standard deviation associated with the specific absorbed fraction is calculated by first order error propagation, which yields the following:

$$\sigma^2_{\Phi_i} = \left(\frac{\phi_i}{m}\right)^2 \times \left[\left(\frac{\sigma_{m_k}}{m_k}\right)^2 + \left(\frac{\sigma_{\phi_i}}{\phi_i}\right)^2\right] \tag{5.29}$$

where

$$\phi_i = \Phi_i \times m \tag{5.30}$$

and

$$\sigma_{\phi_i} = m \times \sigma_{\Phi_i} \tag{5.31}$$

For nonpenetrating particles *Equation 5.31* can be modified as

$$\sigma^2_{\Phi_{np}} = \left(\frac{1}{m_k}\right)^2 \sigma^2_{m_k} \tag{5.32}$$

where m_k is the target organ mass.

Using *Equation 5.30* and *5.32,* all calculations for determining the *S-value* standard deviations presented in previous sections were repeated in order to obtain the *S-value* uncertainties which include the inter-subject mass variabilities.

5.5 Remainder of the body correction

Total dose a target organ might receive is the sum of the organ self-dose and all the other source organ's dose contributions to that target organ. It is very common that a large contributor to an organ's dose is the remainder of the body activity. There are two methods for calculating the internal radiation dose from remainder of the body. Both methods seek the correction of one of the two components of the absorbed dose equation, i.e., source organ activity or *S-value*. Although these two methods use different approaches, they yield the same answer [57]. This work utilized the *S-value* correction method of calculating remainder of the body activity. This method was chosen since a spreadsheet program had already been written and used for computing the *S-values* and associated standard deviations as previously described.

Cloutier *et al* [56] developed the method for calculating the absorbed fraction, from the remainder of the body, $\phi(r_k \leftarrow RB)$, and based on his calculations, Snyder *et al* [57] suggested a new formalism for calculating the value of $S(r_k \leftarrow RB)$. According to this method the remainder of the body *S-value* can be calculated using the following equation:

$$S(r_k \leftarrow RB) = \frac{m_{TB}}{m_{RB}} S(r_k \leftarrow TB) - \sum_h \frac{m_h}{m_{RB}} S(r_k \leftarrow r_h) \tag{5.33}$$

Two different Crystal Ball spreadsheet were prepared. The first one was prepared to simulate the remainder of the body *S-value* calculation when the mass uncertainties were neglected. Previously calculated *S-values* for source/target organ pairs and their associated standard deviations were used as assumptions in the Crystal Ball spreadsheet. The lognormal distribution was chosen to represent the *S-value* distributions since a negative value is not physically realizable for a *S-value*. In order to determine the remainder of the body *S-values* and their associated standard deviations, the *S-value* calculations were simulated at least 2,500 times. In Table 5.9, the *S-values* and their associated uncertainties for each source/target organ pairs as well as for the remainder of the body are listed. A second Crystal Ball spreadsheet was prepared for calculating the remainder of the body *S-values* which included mass variabilities in addition to the other uncertainties. The estimated *S-values* and their associated uncertainties, where the mass variabilities were included into calculations, are presented in Table 5.10. For both cases, *Equation 5.33* was used as forecast in Crystal Ball for calculating the remainder of the body *S-values*. In the second case where the organ mass variabilities were included into calculations, the remainder of the body standard deviations showed dramatic increases. and varied between 60% to 90% of their means. This may indicate that the remainder of the body *S-values* are very sensitive to the mass variabilities.

5.6 Calculation of absorbed dose and determination of uncertainty

The total dose a target organ would receive can be calculated by using following

Table 5.9 The *S-values* and associated standard deviations for source/target organ pairs and for the remainder of the body whenmass variabilities were ignored.

S-VALUE (rad/μCi-h)	*SD*	*S-VALUE (rad/μCi-h)*	SD	*S-VALUE (rad/μCi-h)*	*SD*
LUNG <- LUNG		BRAIN <- BRAIN		BRAIN <-RB	
8.97E-05	2.98E-07	1.01E-04	3.31E-07	7.2E-07	1.75E-07
LUNG <- LIVER		BRAIN <- LUNG			
3.95E-06	1.19E-07	1.33E-07	1.33E-08		
LUNG <- BRAIN		BRAIN <- LIVER			
1.33E-07	1.33E-08	1.63E-08	1.63E-09	LUNG <- RB	
LUNG <- HEART W.		BRAIN <- HEART W.		1.76E-06	1.72E-07
8.38E-06	4.19E-07	5.01E-08	2.51E-09		
LUNG <- TB		BRAIN <- TB			
3.07E-06	1.23E-07	2.73E-06	1.64E-07		
LIVER <- LIVER		HEART W<-HEART W.		HEART W <- RB	
7.72E-05	2.73E-07	3.09E-04	6.35E-07	1.8E-06	1.42E-07
LIVER <- LUNG		HEART W.<- LIVER			
3.74E-06	1.31E-07	4.03E-06	1.41E-07		
LIVER <- BRAIN		HEART W.<- BRAIN			
1.63E-08	1.63E-09	5.01E-08	2.51E-09	LIVER <- RB	
LIVER <- HEART W.		HEART W.<- LUNG		1.23E-06	1.75E-07
4.03E-06	1.61E-07	8.19E-06	3.28E-07		
LIVER <- TB		HEART W. <- TB			
3.26E-06	9.78E-08	3.33E-06	1.33E-07		
TB <- BRAIN		TB <- LUNG		TB <- RB	
2.81E-06	8.43E-08	3.09E-06	9.27E-08	3.21E-06	3.61E-07
TB <- HEART W.		TB <- LIVER			
3.46E-06	1.38E-07	3.33E-06	1.33E-07		

SD= Standard deviation
RB= Remainder of the body.

Table 5.10 The *S-values* and associated standard deviations for source/target organ pairs and for the remainder of the body when mass uncertainties were included into calculations.

S-VALUE (rad/μCi-h)	*SD*	*S-VALUE (rad/μCi-h)*	*SD*	*S-VALUE (rad/μCi-h)*	*SD*
LUNG <- LUNG		BRAIN <-BRAIN		LUNG <- RB	FOEP
8.97E-05	1.85E-05	1.01E-04	4.90E-06	1.76E-06	1.55E-06
LUNG <- LIVER		BRAIN <- LUNG		CB	
3.95E-06	7.51E-07	1.33E-07	6.65E-09	1.87E-06	1.26E-07
LUNG <- BRAIN		BRAIN <- LIVER			
1.33E-07	2.53E-08	1.63E-08	8.15E-10	BRAIN <- RB	FOEP
LUNG<-HEART		BRAIN<-HEART		7.24E-07	5.24E-07
8.38E-06	1.56E-06	5.01E-08	2.51E-09	CB	
LUNG <- TB		BRAIN <- TB		7.73E-07	7.12E-07
3.07E-06	5.53E-07	2.73E-06	1.53E-07		
LIVER<-LIVER		HEART<-HEART		LIVER <- RB	FOEP
7.72E-05	9.60E-05	3.09E-04	7.50E-05	1.27E-06	1.07E-07
LIVER<- LUNG		HEART<-LIVER		CB	
3.74E-06	6.38E-07	4.03E-06	8.32E-07	1.31E-06	1.35E-06
LIVER<-BRAIN		HEART<-BRAIN			
1.63E-08	2.77E-09	5.01E-08	8.56E-09	HEART<- RB	FOEP
LIVER<-HEART		HEART<-LUNG		1.83E-06	1.66E-06
4.03E-06	6.87E-07	8.19E-06	1.69E-06	CB	
LIVER <- TB		HEART<-TB		1.95E-06	1.36E-06
3.26E-06	5.64E-07	3.33E-06	6.88E-07		
TB <- TB		TB <- BRAIN		TB<- RB	FOEP
3.20E-06	5.44E-07	3.09E-06	5.27E-07	3.21E-06	2.72E-06
TB <- HEART		TB <- LIVER		CB	
3.46E-06	5.90E-07	3.33E-06	6.01E-07	3.40E-06	2.12E-06

FOEP= First order error approximation
SD= Standard deviation
RB= Remainder of the body
TB= Total body
CB= Crystal Ball

equation:

$$\overline{D}_k = \sum_{h=1}^{n}\left[\tilde{A}_h \; S(r_k \leftarrow r_h)\right] + \tilde{A}_{RB} \; S(r_k \leftarrow RB) \qquad (5.34)$$

The dose per unit administered activity can be written as

$$\overline{D}_k / A_0 = \sum_{h=1}^{n} \left[\tau_h \; S(r_k \leftarrow r_h)\right] + \tau_{RB} \; S(r_k \leftarrow RB) \qquad (5.35)$$

The dose calculations were performed in two categories in order to determine the contribution of biokinetic and biologic variabilities to the absorbed dose uncertainties. In both cases *Equation 5.35* was employed as the forecast in Crystal Ball for absorbed dose calculations. Dose calculations were simulated, with a minimum of 10,000 trials, with the Crystal Ball computer program in order to obtain dose distributions for each target organ. In the calculation, Crystal Ball utilized samples from the *S-value* distributions and the residence time distributions which were computed in the previous sections.

5.6.1 Determination of uncertainty when mass variabilities were neglected.

When the organ mass variabilities were ignored, the uncertainty calculated was

mainly due to the uncertainty associated with the residence times. Residence time uncertainties were calculated by the propagating least square parameter estimate uncertainties through the residence time calculation as explained in Section 5.3. The absorbed dose calculation was simulated at least 10,000 times by sampling from the *S-value* and the residence times distributions. Data in Table 5.9 were used for the *S-values*. The *S-value* uncertainties shown in Table 5.9 were estimated by propagating uncertainty associated with absorbed fraction. The coefficients of variation of the organ doses for individual patients were found to vary between 4% and 29.9%. In most cases, the *S-value* coefficients of variation were around 1% to 4% of their mean values. This would indicate that the uncertainty calculated in this section was mostly due to the biokinetic variabilities and the uncertainty associated with the least squares parameter estimates. The organ absorbed doses (rad/μCi) and associated uncertainties for each patient are listed in Table 5.11.

The largest organ absorbed dose uncertainty was found in patient PT. The coefficients of variation of organ absorbed dose clustered around 30% for patient PT. These large uncertainties could have been caused by insufficient data to perform a good least squares analysis. For instance, patient PT's data set consisted of 7 observations for the target organs whereas the average number of measurements was about 10 for the other patients. Other patients with less than 10 measurements such as patient RF and DF also showed relatively larger organ dose uncertainties. In this study, urine data consisted

Table 5.11 The organ doses and associated standard deviations for each patient when mass variabilities were neglected.

TARGET ORGAN	*LUNG*			*LIVER*		
PATIENT	*DOSE (rad/μCi)*	*SD*	*CV(%)*	*DOSE (rad/μCi)*	*SD*	*CV(%)*
DF	7.60E-05	1.43E-05	18.82	9.36E-05	1.55E-05	16.53
MC	1.22E-04	4.90E-06	4.02	7.94E-05	3.83E-06	4.82
PT	6.96E-05	2.03E-05	29.12	6.95E-05	2.07E-05	29.86
WM	1.14E-04	7.31E-06	6.41	1.20E-04	8.04E-06	6.70
VU	9.32E-05	6.14E-06	6.59	1.10E-04	7.89E-06	7.17
RF	7.68E-05	1.51E-05	19.61	9.96E-05	1.52E-05	15.23
BS	1.15E-04	1.06E-05	9.25	7.87E-05	1.17E-05	14.89
TARGET ORGAN	***BRAIN***			***HEART***		
PATIENT	*DOSE (rad/μCi)*	*SD*	*CV(%)*	*DOSE (rad/μCi)*	*SD*	*CV(%)*
DF	3.86E-05	5.14E-06	13.32	9.26E-05	1.64E-05	17.75
MC	4.03E-05	2.71E-06	6.72	8.79E-05	3.99E-06	4.54
PT	4.46E-05	1.30E-05	29.10	1.06E-04	2.72E-05	25.66
WM	4.21E-05	1.97E-06	4.69	1.22E-04	5.63E-06	4.63
VU	4.90E-05	2.07E-06	4.22	1.07E-04	6.28E-06	5.86
RF	4.69E-05	6.26E-06	13.35	1.28E-04	1.50E-05	11.73
BS	3.90E-05	3.70E-06	9.48	8.33E-05	7.25E-06	8.70

SD: Standard deviation
CV: Coefficient of variation percent

of fewer measurements than that for the other organs, resulting in large uncertainties in the determination of the remainder of the body residence time. In most patients, coefficients of variation did not vary much between different target organs (for the same patient). There were few cases where the coefficients ofvariation were quite different such as in patients RF and BS. For instance, patient BS' absorbed dose coefficients of variation were around 9% for all target organs except liver which had a coefficient of variation of 15.2%. This was because of a large residence time uncertainty for the liver compare to that of the other target organs. The residence times and associated uncertainties were listed in Table 5.6. The liver in patient BS had the same number of observations as the other source organs. There might be several possible causes for the large liver absorbed dose uncertainty. The model used to simulate liver activity might be too simplistic to accurately describe the true kinetics for patient BS. For instance, in the biokinetic modeling, Gastrointestinal (GI) tract excretion was ignored. Another reason could be the overlap from abdominal cavity and other organs' activity during the time of biokinetic data collection.

Large organ dose uncertainty, on the other hand, might be caused by the convergence to a local minimum or global minimum where the parameter and residence time uncertainty are large. As it is discussed earlier, there might be a local or global minimum in *n-dimensional* error surface which could fit better the data and, at the same time, result in smaller parameter and residence time uncertainties.

The mean organ doses and associated standard deviations for each target organ were computed by sampling from each patient's organ dose distribution using Crystal Ball and first order error propagation method (FOEP) and are listed in Table 5.12. The standard deviation of the estimated mean organ dose for the population was, at maximum, 5.5% of the mean.

The mean organ doses calculated by the two methods, FOEP and LHS, were comparable. FOEP is used to propagate error when a variable is assumed to be distributed in a Gaussian fashion. Since the two methods resulted in comparable results, one may assume that the mean organ dose distributions of the seven patient population are Gaussian. For a Gaussian distribution, the standard deviation of the mean is calculated by dividing the standard deviation of the set by the square root of the sample number. Standard deviation of the population can then be calculated by

$$\sigma_D = \sqrt{7} \times \sigma_{\bar{D}}. \tag{5.36}$$

Standard deviations of the target organ absorbed doses for the seven-patient study group were calculated using Equation 5.36 and are listed in Table 5.12. Dose distributions for the seven-patient population were then simulated by the use of Crystal Ball and 95% confidence intervals were determined for each target organ. The target organ dose distributions are displayed in Figure 5.2-5.5. These figures illustrate 95%

Table 5.12 The mean organ doses for the seven-patient population and associated uncertainties for the mean doses and population doses when mass variabilities were neglected.

TARGET ORGAN	*LUNG*			*LIVER*		
	MEAN	*SD OF THE MEAN*	*CV(%)*	*MEAN*	*SD OF THE MEAN*	*CV(%)*
FOEP	9.52E-05	4.67E-06	4.91	9.30E-05	4.91E-06	5.28
LHS(CB)	9.52E-05	4.73E-06	4.97	9.32E-05	4.89E-06	5.11
	MEAN	*SD OF THE POPULATION*	*CV(%)*	*MEAN*	*SD OF THE POPULATION*	*CV(%)*
LHS(CB)	9.52E-05	1.26E-05	13.23	9.31E-05	1.29E-05	13.85
TARGET ORGAN	*BRAIN*			*HEART*		
	MEAN	*SD OF THE MEAN*	*CV(%)*	*MEAN*	*SD OF THE MEAN*	*CV(%)*
FOEP	4.29E-05	2.35E-06	5.46	1.04E-04	5.29E-06	5.10
LHS(CB)	4.29E-05	2.32E-06	5.40	1.04E-04	5.35E-06	5.15
	MEAN	*SD OF THE POPULATION*	*CV(%)*	*MEAN*	*SD OF THE POPULATION*	*CV(%)*
LHS(CB)	4.29E-05	6.15E-06	14.34	1.04E-04	1.41E-05	13.55

FOEP: First Order Error Propagation. LHS: Latin Hypercube Sampling.

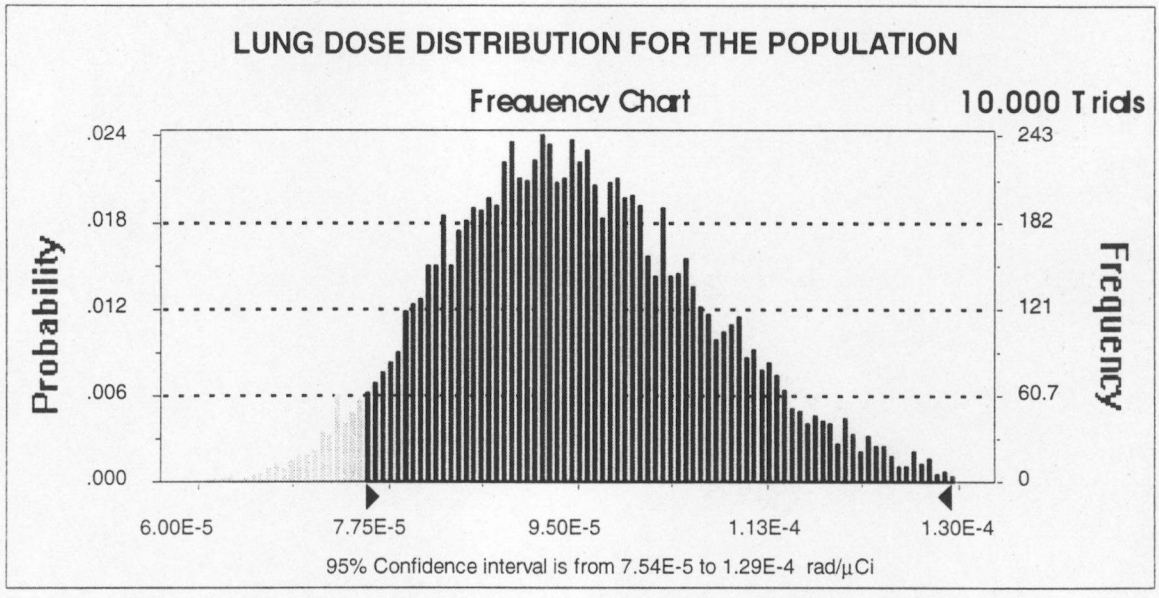

Figure 5.2 Illustration of the lung dose distribution for the seven-patient population with 95% confidence interval (mass variabilities were neglected).

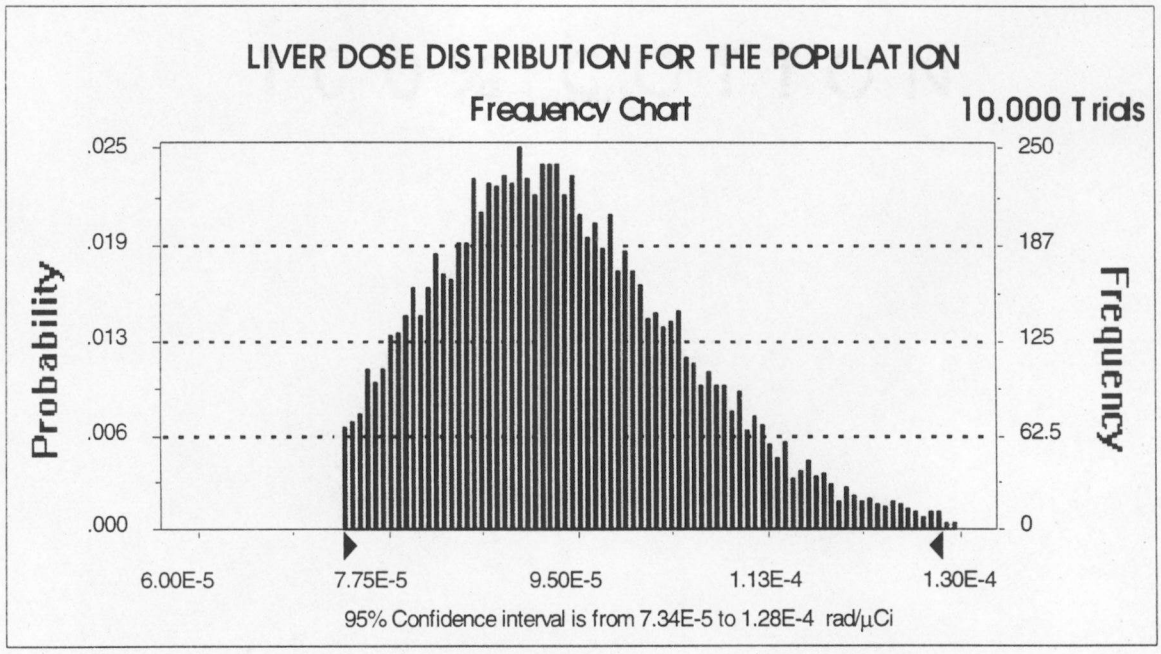

Figure 5.3 Illustration of the liver dose distribution for the seven-patient population with 95% confidence interval (mass variabilities were neglected).

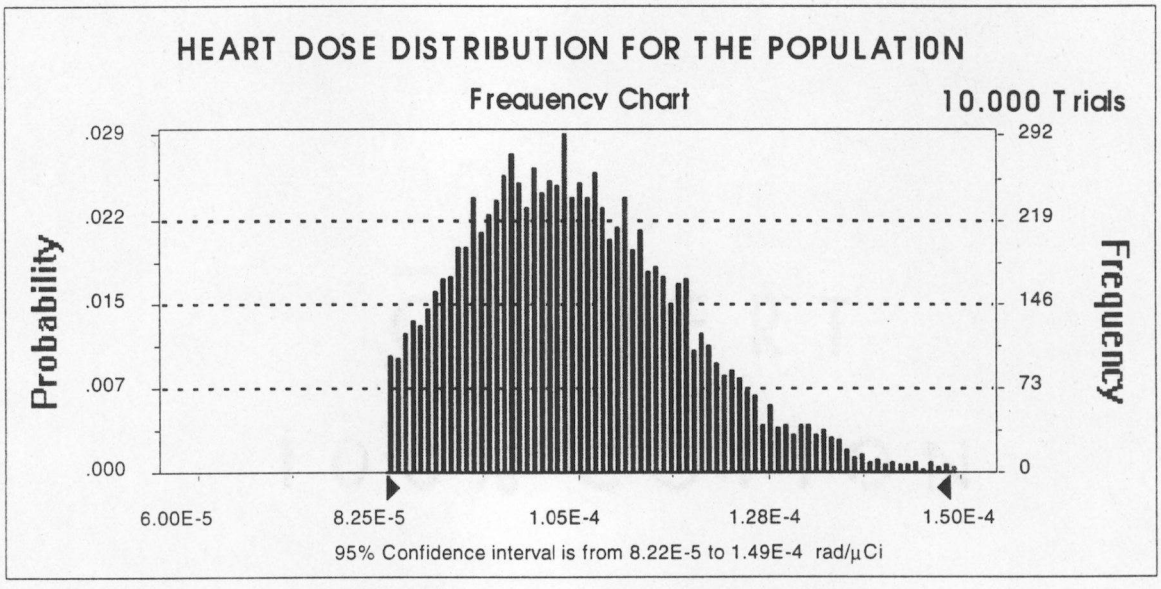

Figure 5.4 Illustration of the heart dose distribution for the seven-patient population with 95% confidence interval (mass variabilities were neglected).

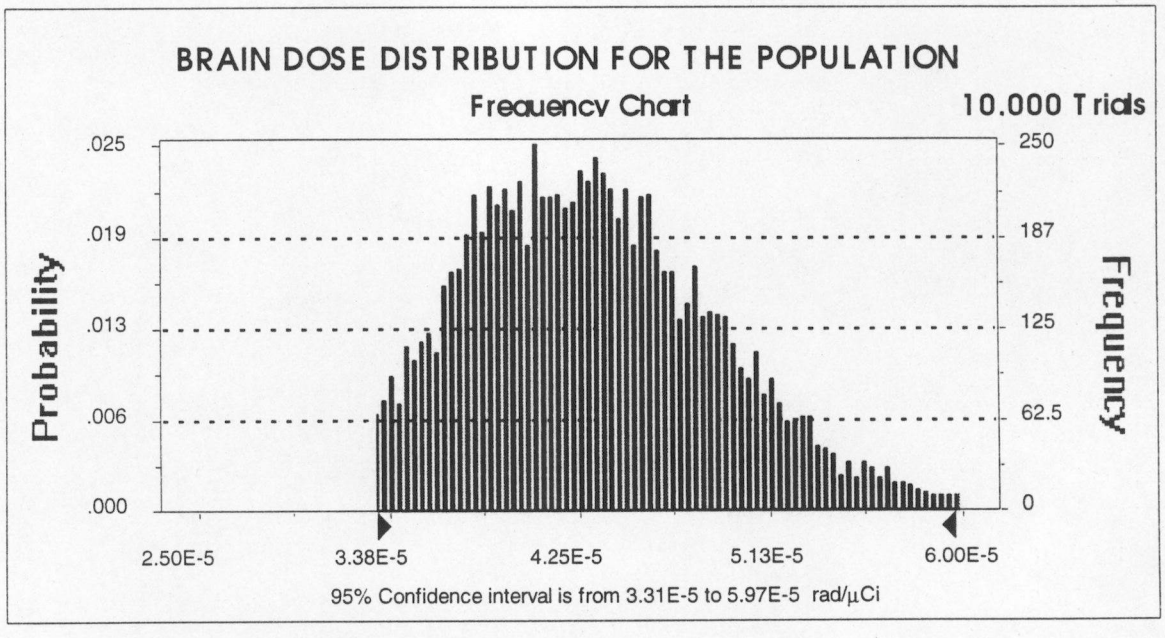

Figure 5.5 Illustration of the brain dose distribution for the seven-patient population with 95% confidence interval (mass variabilities were neglected).

confidence intervals for the target organ dose distributions and show how large the uncertainty could be due to the inter-patient biokinetic variability and least squares parameter estimation procedure.

Table 5.13 displays the mean target organ doses, minimum and maximum absorbed dose values of the 95% confidence interval for each target organ that a patient would receive if the inter-patient biokinetic variabilities and uncertainty associated with curvefitting procedures are considered as the major sources of uncertainties in absorbed dose calculations.

Table 5.13 The maximum and minimum target organ doses for the seven-patient population with 95% confidence when mass variabilities were neglected.

TARGET ORGAN	DOSE (rad/μCi)		
	MINIMUM	POPULATION MEAN	MAXIMUM
LUNG	7.54E-05	9.51E-05	1.29E-04
LIVER	7.34E-05	9.30E-05	1.28E-04
HEART	8.22E-05	1.04E-04	1.49E-04
BRAIN	3.31E-05	4.29E-05	5.97E-05

In Table 5.13, the heart is the organ with the larger organ dose uncertainty. The maximum value of 95% confidence interval of the heart dose was found to be 45% more than its mean value. It would suggest that a patient may receive an absorbed dose of 45% more than the estimated mean with 95% confidence when inter- patient biokinetic variabilities and uncertainty associated with the least squares parameter estimate considered as the major sources of uncertainty in calculations. This calculation was performed for a fairly homogenous patient population. Therefore, the magnitude of the uncertainty could be much larger for a more diverse patient population due to possibly larger biokinetic variabilities between patients.

5.6.2 Determination of uncertainties when mass variabilities were considered as an additional source of uncertainty.

Another Crystal Ball spreadsheet was prepared which consists of the residence times, S-values and their standard deviations. In this case, the *S-values* and uncertainty estimates of Table 5.10 were utilized, since in their calculation, mass variabilities as well as absorbed dose uncertainties had been included.

Section 5.6.1 were repeated in order to determine target organ doses and their associated uncertainties with new *S-value* distributions which also included mass variabilities. Table 5.14 lists the target organ doses and associated uncertainties.

Table 5.14 List of the organ doses and associated uncertainties for each patient when the mass variabilities were included in uncertainty calculations.

TARGET ORGAN	*LUNG*			*LIVER*		
PATIENT	*DOSE (rad/μCi)*	*SD*	*CV(%)*	*DOSE (rad/μCi)*	*SD*	*CV(%)*
DF	7.59E-05	1.99E-05	26.15	9.22E-05	2.76E-05	29.93
MC	1.22E-04	2.41E-05	19.79	7.90E-05	1.83E-05	23.15
PT	7.11E-05	3.50E-05	48.86	7.63E-05	4.34E-05	56.89
WM	1.14E-04	2.26E-05	19.80	1.20E-04	2.61E-05	21.73
VU	9.32E-05	1.47E-05	15.79	1.10E-04	2.15E-05	19.54
RF	7.68E-05	2.83E-05	36.85	9.96E-05	2.79E-05	29.03
BS	1.10E-04	2.25E-05	20.41	7.87E-05	2.02E-05	25.64
TARGET ORGAN	***BRAIN***			***HEART***		
PATIENT	*DOSE (rad/μCi)*	*SD*	*CV(%)*	*DOSE (rad/μCi)*	*SD*	*CV(%)*
DF	3.86E-05	9.07E-06	23.34	9.97E-05	2.50E-05	25.06
MC	4.03E-05	7.07E-06	17.54	8.96E-05	2.78E-05	31.60
PT	4.54E-05	2.12E-05	34.02	1.07E-04	3.59E-05	33.55
WM	4.21E-05	7.37E-06	17.50	1.81E-04	3.71E-05	20.61
VU	4.90E-05	8.21E-06	16.75	1.09E-04	1.93E-05	17.71
RF	4.69E-05	1.39E-06	29.66	1.12E-04	2.86E-05	23.25
BS	3.90E-05	8.11E-06	20.79	8.28E-05	1.48E-05	17.89

SD: Standard deviation CV: Coefficient of variation percent

Mean target organ doses for the seven-patient population, and their associated uncertainties were determined by sampling from individual patient's dose distributions. Then standard deviation for the population were calculated using Equation 5.35. The results are listed in Table 5.15. The absorbed dose coefficients of variation were found to vary between 17% and 57% for individual patients. As expected patient PT had the largest absorbed dose uncertainty. Figure 5.6 displays the liver dose distribution for patient PT. The 95% confidence interval of the PT's liver dose distribution was between 2.79E-05 rad/μCi and 1.88E-04 rad/μCi with a mean of 7.63E-05 rad/μCi. It indicate that the dose a patient would receive could be, at maximum, 2.5 times larger than the mean absorbed dose estimate for an individual patient (with the 95% confidence).

The mean target organ absorbed doses were very similar to the ones calculated without considering mass variability. However, coefficients of variation of the organ absorbed doses were increased by a factor ranging from 2 to 5. The largest increases were observed in patients MC, WM, and VU. For these three patients, the least squares parameter estimates and residence time uncertainty estimates were very small compared to that of the other patients. This was probably because of the availability of the better biokinetic data set for a good least square analysis and having a local or global minimum which resulted in small uncertainties in parameter and residence time estimation.

Incorporation of the mass variabilities almost doubled the 95% confidence

Table 5.15 The mean organ doses for the seven-patient population and associated uncertainties for mean doses and population doses when mass variabilities were included.

TARGET ORGAN	*LUNG*			*LIVER*		
	MEAN	*SD OF THE MEAN*	*CV(%)*	*MEAN*	*SD OF THE MEAN*	*CV(%)*
FOEP	9.48E-05	9.86E-06	10.41	9.32-05	1.04E-05	11.17
LHS(CB)	9.47E-05	9.81E-06	10.37	9.31-05	9.99E-06	10.73
	MEAN	*SD OF THE POPULATION*	*CV(%)*	*MEAN*	*SD OF THE POPULATION*	*CV(%)*
LHS(CB)	9.47E-05	2.59E-05	27.35	9.31E-05	2.63E-05	28.26
TARGET ORGAN	*BRAIN*			*HEART*		
	MEAN	*SD OF THE MEAN*	*CV(%)*	*MEAN*	*SD OF THE MEAN*	*CV(%)*
FOEP	4.29E-05	3.65E-06	8.27	1.11E-04	1.13E-05	9.64
LHS(CB)	4.29E-05	3.52E-06	8.19	1.11E-04	1.06E-05	9.54
	MEAN	*SD OF THE POPULATION*	*CV(%)*	*MEAN*	*SD OF THE POPULATION*	*CV(%)*
LHS(CB)	4.29E-05	9.31E-06	21.72	1.11E-04	2.81E-05	25.23

FOEP: First Order Error Propagation. CB: Crystal Ball.

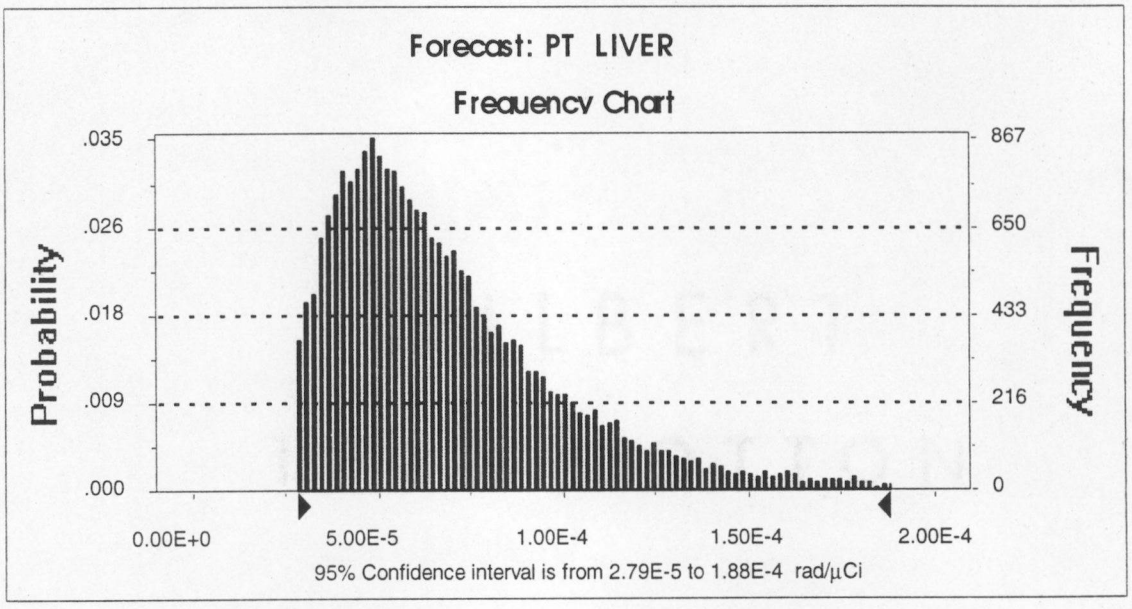

Figure 5.6 The 95% confidence interval of the liver absorbed dose distribution for patient PT (mass uncertainty is included).

interval of the organ absorbed dose of patients who had already relatively larger absorbed dose uncertainty. The largest increases were observed in patients who had relatively smaller absorbed dose uncertainty. Since their previous absorbed dose uncertainties were small, the incorporation of mass variabilities resulted in a larger absorbed dose uncertainty increase. Although, the incorporation of mass variabilities caused significant absorbed dose uncertainty increase in these three patients, their absorbed dose uncertainties were still less than that of the others.

When including mass variabilities, the uncertainties associated with the mean target organ doses were almost doubled. The coefficients of variation were found to be around 10%. The maximum coefficient of variation of 11.17% was observed for the mean dose estimate. The mass variability of the liver was smaller than that of the lung and was almost the same as that of the heart. Therefore a large dose uncertainty in mean liver dose might have been caused by inter-patient biokinetic variabilities rather than the inter-patient mass variabilities.

The standard deviations for the seven patient population dose distributions were calculated using *Equation 5.35*. The dose distributions and 95% confidence intervals were then determined by the use of Crystal Ball sampling program. The dose distributions for the target organ, liver, lung, brain, and heart are displayed in Figure 5.7-5.10.

Table 5.16 was designed to display mean organ doses, maximum and minimum doses, with 95% confidence, a patient who is similar to the study group could receive when the mass variabilities were considered as an additional source of uncertainty in dose calculations. These dose values of Table 5.16 could be a realistic representation of the minimum and maximum absorbed dose values for the next patient who resembles members of the population assuming no correlation between absorbed dose fraction and the source/target organ pair properties.

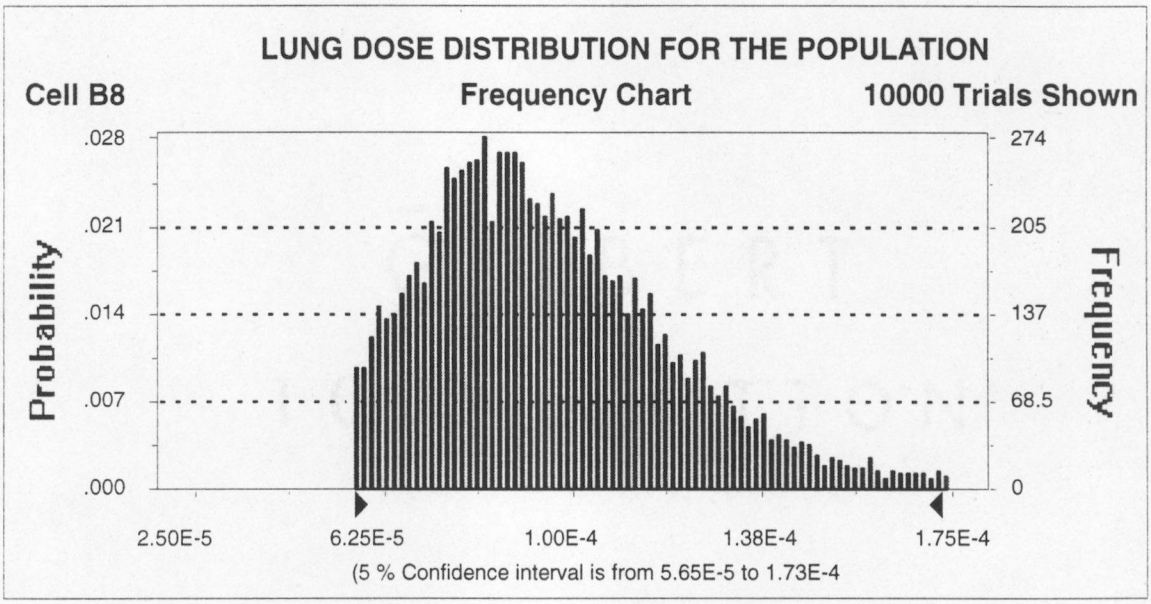

Figure 5.7 Illustration of the lung dose distribution for the seven-patient population with 95% confidence interval (mass variabilities were included).

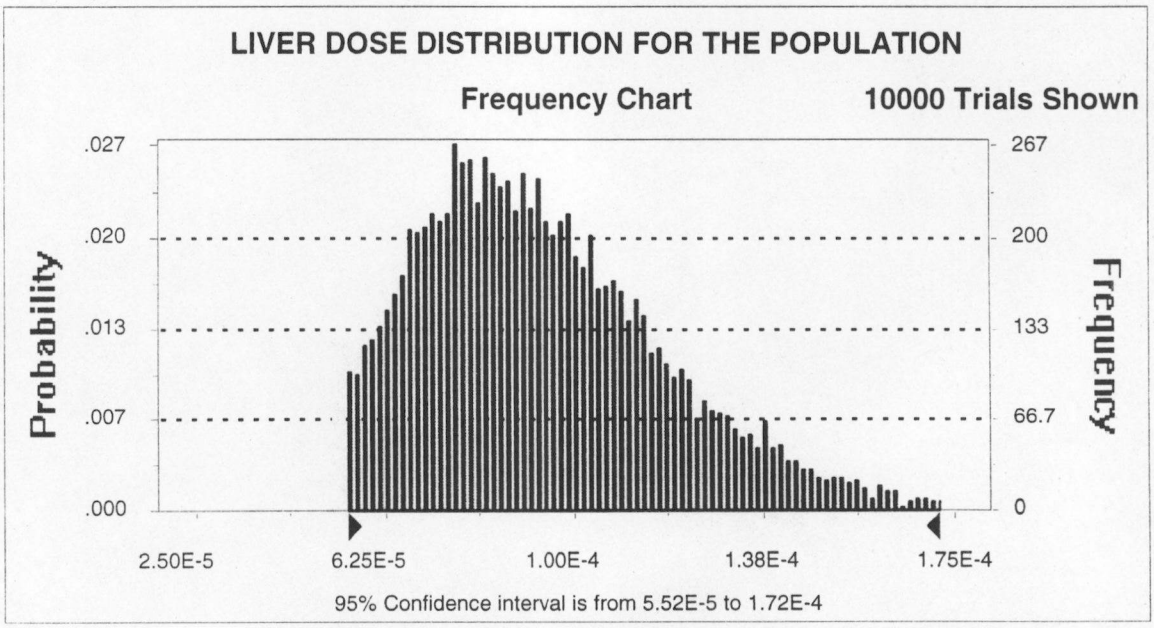

Figure 5.8 Illustration of the liver dose distribution for the seven-patient population with 95% confidence interval. (mass variabilities were included).

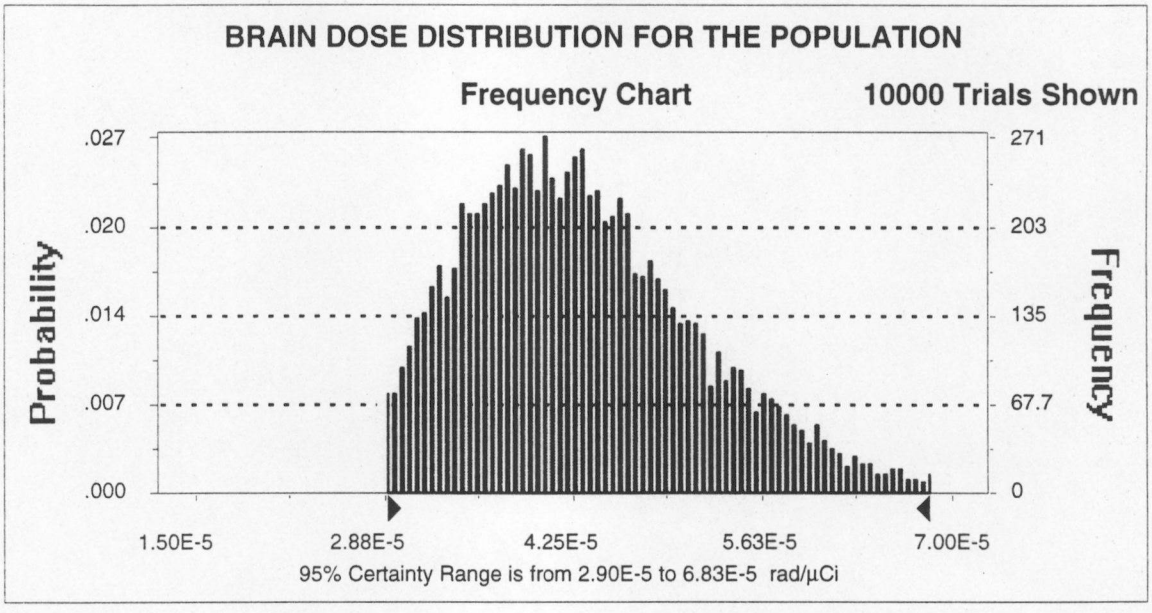

Figure 5.9 Illustration of the brain dose distribution for the seven-patient population with 95% confidence interval (mass variabilities were included).

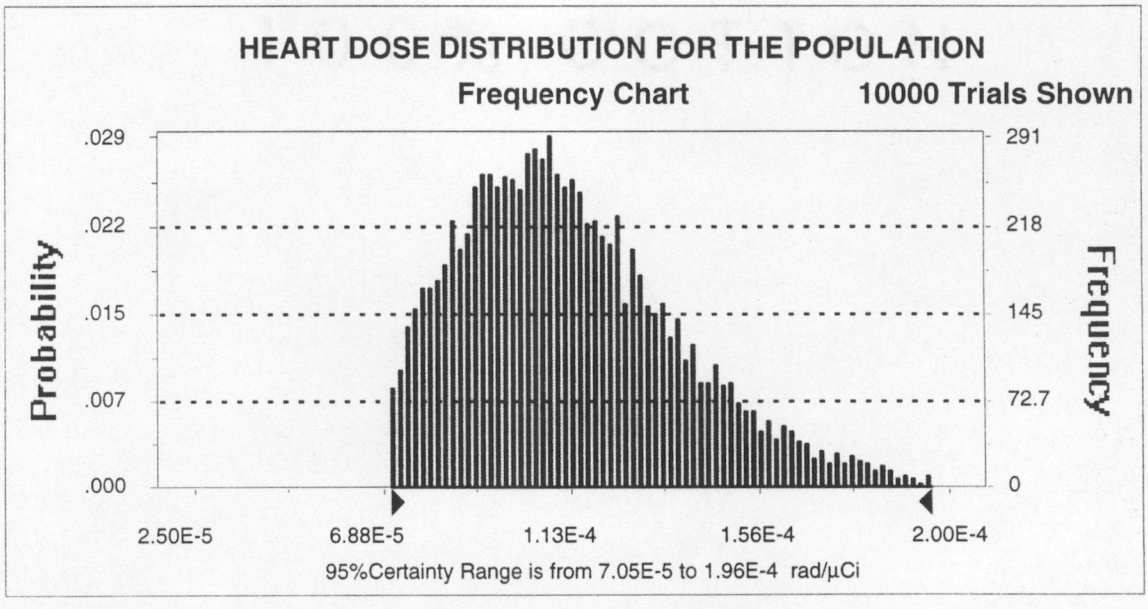

Figure 5.10 Illustration of the heart dose distribution for the seven-patient population with 95% confidence interval (mass variabilities were included).

Table 5.16 The maximum and minimum target organ doses for the seven-patient population with 95% confidence when the mass variabilities were considered as an additional source of uncertainty.

TARGET ORGAN	DOSE (rad/μCi)		
	MINIMUM	POPULATION MEAN	MAXIMUM
LUNG	5.65E-05	9.47E-05	1.73E-04
LIVER	5.52E-05	9.31E-05	1.72E-04
HEART	7.05E-04	1.12E-04	1.96E-04
BRAIN	2.90E-05	4.30E-05	6.83E-05

Incorporation of the organ mass variabilities into the uncertainty calculations almost doubled the 95% confidence intervals of the dose distributions. The upper bound of the 95% confidence interval of the absorbed dose distribution was found to be 1,7 times larger than its mean. Based on this calculation, one may conclude (with 95% confidence) that the maximum absorbed dose a patient might receive could be about twice as large as the estimated mean absorbed dose of the population.

The mean target organ doses and their standard deviations were also obtained by the first order error propagation method (FOEP) for comparison purposes. The results are

listed in Table 5.11-5.15. One of the interesting results of the sampling is that as the sample size (number of patients in this case) gets larger, the distributions generally converge to a normal distribution no matter what the underlying assumptions or distribution of the variables [4]. This may indicate that the result of the sampling method can be assumed to be normally distributed where the sample size is large. The mean organ doses which were calculated by the two methods (FOEP and LHS) were comparable. FOEP is used to propagate error when the underlying assumptions of the variables are Gaussian. Since the two methods resulted in comparable results, it can be assumed that the mean organ dose distributions of the seven patient population are Normal. It is essential to note that, the uncertainty associated with a mean is reduced as the sample size increases. It is a fact that the more information (i.e., more measurements of a variable) obtained about a variable, lower the uncertainty associated with that variable will be. For instance, although the absorbed dose coefficient of variation for liver was between 17% to 57% for individual patients, the coefficient of variation of the mean liver dose was around 11% for the seven-patient population.

The Table 5.17 is designed to summarize the results of this work in one table by including all the information lists in Table 5.11-5.16.

In this work, the sources of uncertainty were restricted to the uncertainty in least squares parameter estimates, inter-patient biokinetic variabilities, and inter-patient mass

Table 5.17 Comparison of the absorbed dose uncertainties and 95% confidence intervals when including and neglecting mass variabilities.

Dose estimates neglecting mass variabilities(rad/mci)					
Case	**Mean**	**Minimum**	**Maximum**	**SD**	**%CV**
POUPULATION					
Lung	0.10	0.08	0.13	0.00	13.60
Liver	0.09	0.07	0.13	0.01	13.50
Heart	0.01	0.08	0.15	0.00	13.60
Brain	0.04	0.03	0.06	0.01	14.30
INDIVIDUAL PATIENT					
PT Liver	0.07	0.00	0.13	0.02	29.90
Dose estimates including mass variabilities(rad/mci)					
Case	**Mean**	**Minimum**	**Maximum**	**SD**	**%CV**
POUPULATION					
Lung	0.09	0.06	0.17	0.03	27.40
Liver	0.09	0.06	0.17	0.03	28.30
Heart	0.11	0.07	0.20	0.03	21.70
Brain	0.04	0.03	0.07	0.01	25.20
INDIVIDUAL PATIENT					
PT Liver	0.08	0.03	0.19	0.04	56.90

variabilities. It was found that a dose estimate could have a coefficient of variation as large as 14.3% when the only source of uncertainty was considered to be inter-patient biokinetic variability and the uncertainty associated with the curvefitting procedures. The 95% confidence interval of the target organ dose distributions indicated that a patient might receive almost 50% more absorbed dose than the estimated mean absorbed dose. For instance, the 95% confidence interval of the heart dose distribution of the population was between 8.22E-05 and 1.49E-04 rad/μCi with a mean absorbed dose of 1.04E-04 rad/μCi.

When mass variabilities were considered as an additional source of uncertainty in the calculations, the magnitude of the uncertainty almost doubled. The increase in the upper limits of the 95% confidence intervals of the dose distributions were around 40% for liver, heart and lung. This work showed that the dose a patient would receive (with 95% confidence could be lager by a factor of two in a homogenous patient population. For instance, the liver dose a patient might receive would be (with 95% confidence) between 5.52E-05 rad/μCi and 1.72E-04 rad/μCi. The brain showed the smallest absorbed dose uncertainty increase when brain mass variabilities were included in calculations. The upper bound of the 95% confidence interval of the brain dose distribution was determined to be 60% larger than its mean. As shown in Table 5.8, brain was the organ with the smallest mass variability in this study. As a result of the incorporation of organ mass variabilities, the upper limit of the 95 % confidence interval

of the absorbed dose distribution increased from 5.97E-05 rad/μCi to 6.83E-05 rad/μCi with an increase of 15%.

This study did not include uncertainties for absorbed fraction estimates other than the statistical uncertainties associated with the Monte Carlo photon transport calculations. It is understood that the properties and geometry of source/target organ pair are the major factors in the determination of the absorbed fraction calculations. Therefore one should assume that there is a correlation between absorbed fraction and size, mass, and geometry of the source/target organ pair. To obtain a better absorbed dose uncertainty estimate, one should determine these correlations. This may increase the absorbed dose uncertainties considerably for a study group.

Chapter 6

CONCLUSIONS AND RECOMMENDATIONS FOR FUTURE STUDIES

6.1 Conclusions

The use of radiopharmaceuticals in medical applications has some risk. The radiation exposure involved in nuclear medicine procedures may cause somatic and/or genetic effects in patients. Absorbed dose is calculated in order to estimate the risk involved in nuclear medicine procedures. However, given inter-patient biokinetic variabilities, organ mass variabilities, and anatomical differences it is not possible to estimate the exact absorbed dose a patient would receive. Although it is known that the absorbed dose estimation is vulnerable to uncertainties, no work was found by the author in which the absorbed dose uncertainties were calculated or discussed. This study was conducted in order to establish a method and to determine the degree of uncertainties in the absorbed dose calculations from internally deposited radioactive sources. The inter-

patient biokinetic variabilities, organ mass variabilities, uncertainty associated with the least squares parameter estimates, and uncertainty associated with the specific absorbed fraction estimates were considered as the sources of uncertainty in absorbed dose calculations.

In this work, absorbed dose and uncertainty calculations were performed for the brain imaging agent ^{123}I-IPT. It is well known that the dose delivered in most diagnostic imaging procedures is well below the level which would entail significant risk. However, it is indeed vital to know the maximum dose that might be delivered to a patient during a radionuclide therapy. In most therapeutic nuclear medicine procedures, the absorbed dose is well above the level which does not entail a health risk, and physicians decide if the benefits outweigh the risk. But, it is seldom considered that the dose a patient would receive can be much larger than the estimated dose. Even when it is considered, it is difficult to determine the uncertainty associated with the absorbed dose estimates, since there was no scientific study of how large the uncertainty could be in absorbed dose.

This study established a method and determined the absorbed dose uncertainty in a study group. Uncertainty associated with the absorbed dose was determined in two categories. In the first category the uncertainty due to the biokinetic variabilities in a study group was determined. It is found that the absorbed dose (with 95%) can be

approximately 50% larger than the population mean for the next patient who is similar to the study group.

In the second category, inter-patient mass variabilities were determined and incorporated into the calculation as an additional source of uncertainty. It was determined that the upper end of the 95% confidence interval of the absorbed dose can be 2.5 times larger than the estimated absorbed dose for an individual patient. For instance, dose calculation for patient PT showed that the 95% confidence interval fell between 2.79E-05 rad/μCi and 1.88E-04 rad/μCi with a mean of 7.63E-05 rad/μCi. The liver was the organ with the largest absorbed dose uncertainty. The absorbed dose to the liver for the population with 95% confidence was found to be between 5.52E-05 rad/μCi and 1.72E-04 rad/μCi with a mean of 9.31E-05 rad/μCi.

The patient population selected for this study was very homogenous. They were all young adults with no known illness. Of the seven patients, five were male, and two were female. Therefore, the result of this study should not be taken to represent a diverse population. It is expected that the uncertainty is much larger for a diverse patient population than it is for a homogenous population. In a diverse population, inter-patient biokinetic variabilities, organ mass variabilities and anatomical differences will be much larger than those of a homogenous population. Consequently, residence times and

S-values will have larger associated uncertainties which would result in larger absorbed dose uncertainties. Nevertheless, the results of this work give an indication of the lower limit of the uncertainty in the determination of the absorbed dose. For other compounds and different populations results could be different. Future work could repeat this study for other compounds.

In therapy, similar studies can be conducted in order to determine the absorbed dose distributions for a patient population. Patients can be categorized according to their physical and pathologic states. The dose distributions for each patient group can then be determined. For the next patient who will undergo the same nuclear medicine procedure, physicians may predict the maximum absorbed dose the patient would receive with 95% confidence. In the prediction, having the knowledge of physical and pathological state of the new patient, the physician will decide which study group best represents the patient. Then, the absorbed dose distribution of that population might be used to determine the absorbed dose estimate and associated uncertainty for the next patient. This will provide the maximum absorbed dose a patient might receive with the desired confidence (i.e., 90%, 95%) as a result of the nuclear medicine procedure. Then, the physician can decide more reasonably whether the benefit would outweigh the risk by considering the patient's previous radiation load, and the maximum dose that the patient might receive.

In conclusion, this work showed the necessity of uncertainty analysis in absorbed

dose estimations, provided the ground work for future absorbed dose uncertainty analysis, established a method for absorbed dose uncertainty analysis, determined the uncertainty associated with individual patient organ absorbed doses and determined the uncertainty associated with a homogeneous patient population's organ absorbed doses.

6.2 Recommendations for future studies

This paper did not include the uncertainty due to the anatomy of the patients which probably is an important source of uncertainty in internal absorbed dose calculations. There is no published study which investigates the uncertainty associated with the anatomy of the patient. It is understood that there is a correlation between the mass of the organ and absorbed dose fraction. Therefore for a complete uncertainty analysis one should consider this correlation in the absorbed dose uncertainty calculations. It would involve considerable work and requires patient specific dosimetry calculations. To accomplish this, one would need to repeat the Monte Carlo radiation transport calculations using each patient's specific anatomy. Anatomic information for a patient can be obtained by MRI or CT scans. Once the anatomic properties of a patient are determined, specific absorbed fractions can be determined by Monte Carlo transport calculations. Then, patient specific *S-values* can be calculated and used in absorbed dose calculation. The result is the patient specific absorbed dose estimate. Such a calculation is difficult and time consuming, but it is the only way of estimating absorbed dose with

high accuracy for an individual patient.

The method of the present work could be used to construct absorbed dose uncertainty data bases for frequently used therapeutic agents in order to predict the absorbed dose the next patient might receive. This could save the patient and medical institute time and money. A more important result of such a study might be a more reasonable prediction of the risk a patient may incur as a result of a nuclear medicine procedures.

REFERENCES

REFERENCES

1. United Nations Scientific Committee on the Effect of Atomic Radiation; UNSCEAR 1993 Report to the general assembly with scientific annexes. *Sources and effects of the ionizing radiation.* United Nations Publication , New York, 1993

2. Johnson O. and Dailey V. The 1994 information almanac: *The ultimate browser's reference*, pp. 3. Hougthn Mifflin Company, New York, 1994

3. Loevinger R., Budinger T.F., Watson .E., *MIRD primer for absorbed dose calculations*, revised edition. The Society of Nuclear Medicine, New York, 1991.

4. Morgan M.G. and Henrion M., *Uncertainty: A guide to dealing with uncertainty in quantitative Risk and policy analysis.* Cambridge University Press 1990.

5. Berman M. and Weiss M. F, *The SAAM user manual.* US Dew Publication No: (NIH) 78-180, Washington, D.C.

6. Sander P. and Badoux, R., *Bayesian method in reliability.* Kluwer Academic Publisher, 1991. pp. 24.

7. *Crystal Ball, Version 3.0, User manual, Decisioneering*, 1993.

8. Turner J.E., *Atoms, radiation and radiation protection.* McGraw-Hill, Inc., 1992.

9. Webb S., *The physics of medical imaging.* IOP Publishing Ltd., 1988 pp. 188.

10. Sorenson A.J. and Phelps M.E., *Physics in nuclear medicine.* W.B. Saunders Company, 1987.

11. Sharp P.F., H.G. Gemmell F.W. Smith., *Practical Nuclear Imaging.* IRL Press at Oxford University Press, 1989.

12. NCRP Report No. 70, *Nuclear medicine factors influencing the choice and use of radionuclides in diagnosis and therapy.* National Council on Radiation Protection and Measurements, 1982.

13. Hladik W. B., Saha G. B., Study K. T., *Essential of nuclear medicine science.* Williams & Wilkons, 1987.

14. Loevinger R., Holt J.G., and Hine G.J., Internally administered radioisotopes. In: *Radiation Dosimetry*, Academic Press, 1956.

15. Loevinger R. and Berman M., A revised schema for calculating the absorbed dose from biologically distributed radionuclides. The Society of Nuclear Medicine, New York, 1976.

16. ICRP Publication 26, Recommendation of the International Commission on Radiological Protection. The International Commission of Radiological Protection, Pergamon Press, Oxford, England, 1977.

17. Snyder W.S. and Ford M.R. "S, Absorbed dose per unit cumulated activity for selected radionuclides and organs. MIRD Pamphlet No 11. The Society of Nuclear Medicine, New York, 1975

18. Christy M. and Eckerman K.F., "Specific absorbed fractions of energy at various ages from internal photon sources: 1. Methods. ORNL / TM-8381 / v1. pp. 1-9. Oak ridge National Laboratory, 1987.

19. Weber A.W., Eckerman K.F., Dilman T.L., Ryman J.C., *MIRD: Radionuclide and Decay Schemes.* pp. 217. The Society of Nuclear Medicine, Inc., 1989

20. Snyder W.A., Ford M.R, Warner G.G., Fisher H.L., *Estimates of specific absorbed fractions for photon sources uniformly distributed in various organs of a heterogeneous phantom. MIRD Pamphlet No 5.* The Society of Nuclear Medicine, New York, 1969

21. Snyder W.A.., Ford M.R, Warner G.G., *Estimates of specific absorbed fractions for photon sources uniformly distributed in various organs of a heterogeneous phantom. MIRD Pamphlet No. 5 Revised.* The Society of Nuclear Medicine, New York, 1978.

22. Loevinger R., Distributed radionuclide sources. Attix F.F., and Tochilin E., *Radiation dosimetry,* 2nd edition, pp. 51-90. Vol. III. New York; Academia Press, 1969.

23. Kaul A., Roedler H.D., and Henriches K., "Radionuclide biokinetics and internal dosimetry in nuclear medicine." *La Ricerca Clin. Lab.* 10:629, 1980.

24. Landaw E.M. and DiStefano III. J.J., "Multiexponential, Multicompartmental, and noncompartmental modeling II. Data analysis and statistical considerations." *Am. J. Physiology* 246 R665-R667, 1984

25. DiStefano III. J.J. and Landaw E.M., Multiexponential, Multicompartmental, and noncompartmenatal modeling I. Methodological limitations and physiological interpretations. *Am. J. Physiology* 246 R651-R664, 1984

26. Andrews J.G., McLone R.R., *Mathematical modeling.* pp. 1-12. Butterworth & Co-Publishers Ltd., London, 1976.

27. Robertson J.S., *Compartmental distribution of radiotracers.* CRC Press, Inc., 1983.

28. Hevesy G. "Historical progress of the isotopic methodology and its influences an the biologic sciences." *Minerva Nuclear* , 1, 182, 1957

29. Notari R.E., *Biopharmaceuticals and pharmacokinetics: an introduction.* Second edition. Marcel Dekker , New York, 1975.

30. Torell T., "Kinetics of distribution of substances administered to the body, I. The extravascular modes of administration." *Arch. Internal. Pharmacodynamic,* pp. 57, 205, 1937

31. Torell T., "Kinetics of distribution of substances administered to the body, II. The intravascular modes of administration." *Arch. Internal. Pharmacodynamic,* pp. 57, 205, 1937

32. Stabin G.M, Patient dose from diagnostic and therapeutic radiopharmaceuticals. Raabe O.G., eds., *Internal radiation dosimetry.* Health Physics Society, Medical Physics Publishing, 1994.

33. Matis J.H., Wehrly T.E., Gerald K.B., "The statistical analysis of pharmacokinetics data.", Lambrecht R.M. and Rescigno A., eds., *Lecture notes in biomathematics:*

Tracer kinetics and physiologic modeling. Springer-Verlag Berlin Heidelberg, 1983. pp. 1-57

34. Thakur A., "Some statistical principles in compartmental analysis.", Robertson, J., eds., *Compartmental distribution of radiotracers.* RC Press, Inc. 1983

35. Myers R.H., *Classical and modern regression with applications.* Second edition pp. 425-450. PWS-KENT Publishing, 1986

36. Bard Y., *Nonlinear parameter estimation.* New York Academic, 1974.

37. Stallmann F.W., *Theory and practice of general adjustment and model fitting procedures.* NUREG/CR-2222, ORNL/TM-7869. US Nuclear Regulatory Commission Office of Nuclear Regulatory research, 1981.

38. Gallant A.R., "Non linear regression.", *American Statistician,* 29: 73-81, 1975

39. Hartley H.O., "The modified Gauss-Newton method for fitting nonlinear regression functions by least squares. *Techometrics* 3: 269-280. 1961.

40 ICRU Report 32 , *Methods of assessment of absorbed dose in clinical use of radionuclides.* International Commission on Radiation Units and Measurement, ICRU Publications, Washington, D.C., 1979.

41. ICRP Publication 30, *Limits for intakes of radionuclides by workers.* The International Commission of Radiological Protection, Pergamon Press, Oxford, England, 1979.

42. ICRP Report 53, *Radiation dose to patients from radiopharmaceuticals.* The International Commission of Radiological Protection, Pergamon Press, Oxford, England, 1988.

43. Stabin G.M, Patient dose from diagnostic and therapeutic radiopharmaceuticals. Raabe, O.G., eds., *Internal radiation dosimetry.* Health Physics Society, Medical Physics Publishing, 1994.

44. Jacquez A.J., *Compartmental analysis in biology and medicine: Kinetics of distribution of tracer-labeled materials.* Elsevier Publishing Company, Amsterdam, 1972.

45. Snyder W.A., Ford M.R, Warner G.G., Fisher H.L., *Estimates of specific absorbed fractions for photon sources uniformly distributed in various organs of a heterogeneous phantom. MIRD Pamphlet No 5.* The Society of Nuclear Medicine, New York, 1969

46. Personal communication with Dr. James Stubbs. RIDIC/ORAU.

47. Coffey J.L., Cristy M., Warner G.G. MIRD pamphlet No. 13 - Specific absorbed fractions for photon sources uniformly distributed in the heart chambers and heart wall of a heterogeneous phantom. *J Nucl Med* 22: 65-71, 1981

48 Stabin M.G., MIRDose - The personal computer software for internal dose assessment in nuclear medicine. *J Nucl Med*, in press (1995)

49. Snyder W.S., Ford M.R, Eckerman K.F., Dilman T.L., Poston J.W., Watson S.B., Bernard S.R., Radionuclide transformations, energy and intensity of emissions. ICRP Publication 30, Pergamon Press, 1983.

50. Snyder W.S., Nasset E.S., Karhausen L.R., Howells G.P., Tipton I.H., *Report of the task group reference man.* The international Commission on radiological protection. Pergamon Press Inc., New York, 1975.

51. Tanaka G., Reference Japanese. Vol. 2, Regression analysis of organ weights vs. body weight and/or body height--20-49 years old. Safety analysis report, National Institute of radiological sciences, Chiba, Japan, 1994.

52. DeLand F.H. and North A.W., " Relationship between liver size and body size." *Radiology* 91:1195-1198, December 1968.

53. Blinkov S.M., *The human brain in figures and tables: A quantitative handbook.* pp. 337. Basic Books Inc., Publishers, Plenum Press, 1968.

54. Keneeth D.B, *Growth and development of child, Part II.* Report of the committee on growth and development, pp. 18.

55. Feller P.A., "CAMIRD/II- Computer software to facilitate absorbed dose calculations," *Radiopharmaceutical Dosimetry Symposium*, HEW Publication (FDA) 76-8044, 1976, pp. 119-126.

56. Cloutier R.J., Watson E.E., Rohrer R.H., and Smith E. M., *Journal of Nuclear Medicine.* pp. 14, 53, 1973

57. Snyder W.S.,, M.R. Ford G.G., Warner A., and Watson E.E., "Specific absorbed dose per unit cumulated activity for selected radionuclides and organs," *NM/MIRD Pamphlet No. 11*, 1975

58. Coffey J.C. and Watson E.E., "Calculating dose from remaining body activity; A comparison of two methods," *Medical Physics*: 6(4) Jul./Aug. 1979

59. Loevinger R. and Berman M., "A revised schema for calculating the absorbed dose from biologically distributed radionuclides," *NM/MIRD Pamphlet No. 1, Revised*, 1976.

60. Boston R.C., Palm M.S., Golden P.D., Ramberg C.F., *User notes for enhancements to SAAM/CONSAM version 30.1.* Resource Center for Kinetic Analysis, 1988.

61. Berman M., Beltz W.F., Grief P.C., Chabay R., Boston R.C., *CONSAM User's guide.* US Department of Health and Human Services, 1983.

62. Foster D.M. and Boston R.C., "The use of computers in compartmental analysis: The SAAM and CONSAM programs.", Robertson J.S., eds., *Compartmental distributions of radiotracers.* CRC Press Inc., 1983.

APPENDICES

Appendix A

SAAM
(Simulation, Analysis, And Modeling)

SAAM is a general purpose computer program which is developed for the data analysis of a proposed model. Although it can be used for many scientific applications, it is mostly used to study biologic models. The SAAM dictionary and operational units are, indeed, geared for the biologic investigators. SAAM simulates the solution for a mathematical model that simulate a biologic process and fits the parameters of the model to experimental data. Model equations may be represented by a set of equations for which an analytical or numerical solution exists such as differential, integral, and polynomial equations. Batch SAAM is the current version which consists of over 300 subroutines and 40,000 FORTRAN statements. SAAM is available on the VAX 11/780 and PDP, the Univca 1100 series, and the IBM370. Except VAX, all the others requires some kind of overlay scheme to operate SAAM. SAAM requires an input deck written by its own language and format to be able to run a SAAM simulation. An input deck which is used during the course of the present study is provided as an example in Table A.1. The SAAM dictionary is displayed in Table A.2. After a successful run, SAAM provides the modeler with an output that contains plot of the estimated and measured values, statistical information, and information on convergence for nonlinear parameter adjustments if any. An example of SAAM output is presented in Table A.3.

Table A. 1 A SAAM input deck.

```
A SAAM30 IPT-123 for the patient *BS*  09/01/95
C By  Bulent  Aydogan
2  75  6                          10
H PAR
C  DECAY CONSTANTS FOR INTEGRATION (RESIDENCE TIMES)
C  I-123 DECAY CONSTANT: Tp=13.2 HR
  P(6)=.6931/13.2
CY-
C  LIVER DATA
H DAT
101                              FSD=.1
        0.42        10.27
        2.1         6.96
        3.0         6.45
        3.43        6.29
        4.1         6.25
        4.5         6.20
        13.4        4.18
        23.5        2.82
        36.0
XUF(4)=F(1)*EXP(-P(6)*T)/100
104
        250
H LAM
  L(0,2)   6.985279E+00  9.999998E-06   1.000000E+02
  L(0,3)   3.724113E-02  9.999998E-06   1.000000E+02
H SIG
  S(1,2)   9.620315E-01  9.999998E-06   1.000000E+00
  S(1,3)   8.856255E-02  9.999998E-06   1.000000E+00
c  S(1,3)=-S(1,2)
H INI
  2      100.0
  3      100.0
Y-
C  LUNG  DATA
H DAT
101                *1.875        FSD=.1
        0.42        6.52
        2.1         4.89
        3.0         4.55
        3.43        4.51
        4.1         4.15
        4.5         4.33
        13.4        2.81
        23.5         2.02
        36.0
XUF(4)=F(1)*EXP(-P(6)*T)/100
104
        250
H LAM
  L(0,2)   6.444358E-01  9.999998E-06   1.000000E+02
  L(0,3)   3.671761E-02  9.999998E-06   1.000000E+02
H SIG
  S(1,2)   4.493450E-02  9.999998E-06   1.000000E+00
  S(1,3)   8.860634E-02  9.999998E-06   1.000000E+00
```

```
c  S(1,3)=-S(1,2)
H INI
  2      100.0
  3      100.0
CY-
C  BRAIN DATA
H DAT
101                              FSD=.10
        0.42        4.07
        2.1
        3.0         2.29
        3.43        2.41
        4.1         2.46
        4.5         2.29
        13.4        1.76
        23.5        1.16
        36.0
XUF(4)=F(1)*EXP(-P(6)*T)/100
104
        250
H LAM
  L(0,2)   5.782081E+00  9.999998E-06   1.000000E+02
  L(0,3)   3.768026E-02  9.999998E-06   1.000000E+02
H SIG
  S(1,2)   1.535034E-01  9.999998E-06   1.000000E+00
  S(1,3)   2.759874E-02  9.999998E-06   1.000000E+00
c  S(1,3)=-S(1,2)
H INI
  2      100.0
  3      100.0
CY-
C  HEART DATA
H DAT
101                              FSD=.10
        0.42        1.95
        2.1         1.61
        3.0         1.45
        3.43        1.49
        4.1         1.40
        4.5         1.43
        13.4        0.93
        23.5        0.54
        36.0
XUF(4)=F(1)*EXP(-P(6)*T)/100
104
        250
H LAM
  L(0,2)   1.145356E+00  9.999998E-06   1.000000E+02
  L(0,3)   3.728468E-02  9.999998E-06   1.000000E+02
H SIG
  S(1,2)   1.131537E-02  9.999998E-06   1.000000E+00
  S(1,3)   1.654406E-02  9.999998E-06   1.000000E+00
c  S(1,3)=-S(1,2)
H INI
  2      100.0
  3      100.0
CY-
C  TOTAL BODY  DATA
H DAT
101                              FSD=.10
```

```
        0.0         100.0
        0.6         96.75
        1.8         89.250
        2.8         74.09
        3.6         79.20
        4.7         73.63
        12.2        57.42
        15.4        53.14

XUF(4)=F(1)*EXP(-P(6)*T)/100
104
        250
H LAM
  L(0,2)   4.842081E-01 9.999998E-06  1.000000E+02
  L(0,3)   3.968026E-02 9.999998E-06  1.000000E+02
H SIG
  S(1,2)   8.535034E-02 9.999998E-06  1.000000E+00
  S(1,3)   1.759874E-02 9.999998E-06  1.000000E+00
c  S(1,3)=-S(1,2)
H INI
  2      100.0
  3      100.0
cY-
C    CUMULATIVE URINE ACTIVITY
H DAT
108                          FSD=.10
        0.0
        0.6          3.25
        1.8         10.75
        2.8         15.91
        3.6         20.80
        4.7         26.37
        12.2        43.58
        15.4        46.86
H LAM
  L(0,1)   4.828425E+00 9.999998E-07  1.000000E+01
  L(0,2)   0.000000E+00
  L(0,3)   4.571976E-02 9.999998E-07  1.000000E+01
  L(0,4)   0.000000E+00
  IC(1)    1
  IC(2)    1
  IC(3)    1
  IC(4)    1
H SIG
  S(8,1)  -6.329302E-01 -1.000000E+02  0.000000E+00
  S(8,2)=-S(8,1)
  S(8,3)  -8.097461E+01 -1.000000E+02  0.000000E+00
  S(8,4)=-S(8,3)
H INI
  1      100.0
  2      100.0
  3      100.0
  4      100.0
Y
```

Table A. 2 SAAM dictionary.

Source: Berman M. and Weiss M. F, *The SAAM user manual.* US Dew Publication No: (NIH) 78-180, Washington, D.C.

Name	Definition	How entered
T	Independent variable	Data card
TH	Second independent variable	Data card
F(I,T)	Model solution value for component I at time T	(See a)
UF(I)	Functional input into differential equation $\frac{dF}{dT} = UF(I) + \cdots$	As equation in data or parameter stream
FF(I)	Forcing function for component I	As equation in data stream
DF(I)	Derivative function for F(I,T)	As equation in data stream
G(I)	Arbitrary function	As equation in data or parameter stream
K(I)	Linear parameter	(See b)
S(I,J)	Linear parameter ("summer")	Parameter card
P(I)	Nonlinear parameter	Parameter card
L(I,J)	Nonlinear parameter	Parameter card (See c)
DT(I)	Delay time for delay element I	Parameter card
DN(I)	Resolution (number of cells) of delay element I	Parameter card
UF(I)	UF(I) as a parameter	Parameter card
G(I)	G(I) as a parameter	Parameter card
IC(I)	Initial conditions in component I	Parameter card
U(I)	Steady-state input into component I	Following H STE
M(I)	Steady-state mass in component I	Following H STE
R(I, J)	Steady-state "flux" to component I from component J	Requested in the data stream
SA(I)	Specific activity: calculates F(I,T)/M(I)	Category card
QO(I)	Sets F(J,T) equal to QO(I,T)/K(I)	Category card (See d)
QF(I)	Sets F(J,T) equal to FF(I,T)	Category card (See e)
QL(I)	Calculates FF(J,T) be joining sequential data by a straight line	Category card (See f)
INF	Sets T equal to 10**36	Data card
N	Null operator	

[a] If data are available to compare with F(I,T), they are entered in the data stream associated with the component assigned to F(I,T).

[b] K(I) as a special meaning for $0 < K < 26$ and $26 < K < 100$. This will be explained later.

[c] The L(I,J) as entered are constants. A provision exists in SAAM to make them function dependent (nonlinear). This is accomplished by calculating L(I,J)*Z where Z is an expression defining the functional dependence. This is explained below in more detail.

[d] J is the compartment number to be changed, I is the compartment where QO is defined. This change takes place at the times specified by the user when QO is defined.

[e] The operation is the same as with QO(I) except here FF(I) is used.

[f] QL(I) provides a quick and easy way of defining a forcing function.

Table A. 3 An example output of SAAM.

```
A SAAM30 IPT-123 FOR THE PATIENT ****BS (ORGAN : BRAIN )***  09/01/95

0PARAMETER VALUES
0ADJUSTABLE PARAMETERS          DEPENDENT PARAMETERS            FIXED
PARAMETERS
 L ( 0, 2)=  5.7788420E+00
 L ( 0, 3)=  3.8680229E-02
 S ( 1, 2)=  1.5090060E-01
 S ( 1, 3)=  2.7825173E-02
                                P ( 6, 0)=  5.2507576E-02
 INITIAL COMPONENT VALUES
  1=  1.7873E+01   2=  1.0000E+02   3=  1.0000E+02
0  D  C ---CAT--      T       THETA      QC          QO        QO-QC     QC/QO       WT
FSD
  1  1      0   4.2000E-01  0.0000E+00  4.07000E+00 *  4.07000E+00   0.000E+00   1.000
  2  1      0   3.0000E+00  0.0000E+00  2.47766E+00 *  2.29000E+00  -1.877E-01   1.082
  3  1      0   3.4300E+00  0.0000E+00  2.43679E+00 *  2.41000E+00  -2.679E-02   1.011
  4  1      0   4.1000E+00  0.0000E+00  2.37445E+00 *  2.46000E+00   8.555E-02   0.965
6.27E-01   1.525E-02
  5  1      0   4.5000E+00  0.0000E+00  2.33800E+00 *  2.29000E+00  -4.800E-02   1.021
7.23E-01   1.799E-02
  6  1      0   1.3400E+01  0.0000E+00  1.65705E+00 *  1.76000E+00   1.029E-01   0.942
1.22E+00   1.566E-02
  7  1      0   2.3509E+01  0.0000E+00  1.12078E+00 *  1.16000E+00   3.922E-02   0.966
2.82E+00
1   7   4.9517E-02  7.0739E-03  8.4106E-02  3.9166E-02
0***AN '*' FOLLOWS QC WHEN A DATUM DETERMINES AND INCORPORATES THE FINAL
VALUES OF S AND/OR K.
 *** AN 'F' INDICATES THAT QC WAS RECALCULATED AFTER FINAL S AND/OR K VALUES
WERE DETERMINED.*14*
0SUM SQUARES AFTER    8 ITERATIONS IS  4.95171733E-02
     COMP  1=   4.9517173E-02
 SIG AFTER    8 ITERATIONS IS  9.90343466E-03
0                 ESTIMATE                SD              FSD          INITIAL            MIN
MAX
0ADJUSTABLE PARAMETERS
1 L( 0, 2)=  5.7788420E+00 +OR- 8.9997925E+02   1.5574E+02  4.0282267E-01
2 L ( 0, 3)=  3.8680229E-02 +OR- 2.9665281E-03   7.6694E-02   9.5332098E-06
3 S( 1, 2)= 1.5090060E-01 +OR- 2.5748274E+01   1.7063E+02   2.4775760E-03
4 S( 1, 3)=  2.7825173E-02 +OR- 1.0411436E-03   3.7417E-02   2.5805697E-04
0CORRELATION MATRIX
 COLUMN   1    2    3    4
 ROW 1  1.00  0.30  1.00  0.57
 ROW 2  0.30  1.00  0.30  0.75
 ROW 3  1.00  0.30  1.00  0.57
 ROW 4  0.57  0.75  0.57  1.00
```

Table A.3 Continued

```
                                    LOG  ACTIVITY
                 IIII
```

Operational units of SAAM allows the modeler to design a model and enter its parameters directly through that model. For instance, let us assume the model is a compartmental model which can be defined by a set of first order linear differential equations. To operate SAAM, one need to select the model code for compartmental model and enter the model parameters. SAAM will then reconstructs internally the system of differential equations for the model selection. This feature is very convenient in terms of simplicity, since as the model get larger, it is really hard to deal with the differential equations. And for the models which have more than three compartments the calculations get nasty and becomes time consuming. However, this feature has a serious drawback, in many cases investigators fail to understand biologic implication of the models that they seek a solution.

Computational structure of SAAM

The computational structure of SAAM may be classified in four steps:

1. A set of model equations is solved
2. Model solution is compared with the experimental data
3. The model parameter are adjusted in order to obtain a best fit of data.
4. Statistical data for the model solution are derived

SAAM has 12 model to chose from in order to define a mathematical model to be solved. These models are listed in Table A.4. The model equations, in biologic studies, are typically linear or nonlinear differential equations. SAAM has two numerical method to obtain solution to systems of differential equations, model 1 and 8.

Table A. 4 Available mathematical models in SAAM .

Source: Berman M. and Weiss M. F, *The SAAM user manual.* US Dew Publication No: (NIH) 78-180, Washington, D.C

Model Code 1: Ordinary linear and nonlinear differential (fourth order variable step-size Runge Kutta)
Model Code 2: Analytical solution of a special class of compartmental models
Model Code 3: Similarity transformation
Model Code 4: Solution of algebraic functions
Model Code 5: Linear combination of spectra
Model Code 6: Sum of Gaussians and exponentials
Model Code 8: Nonlinear differential equations. The method of Chu and Berman[17] is used
Model Code 10: Linear differential equations with constant coefficients. Chu and Berman method[17]
Model Code 11: Population means
Model Code 21: Runge-Kutta 4/5 method (nonstiff)
Model Code 22: Adams predictor corrector (nonstiff)
Model Code 23: Gear stiff solver

If one of the SAAM model displayed in Table A.4 is not specified in the SAAM input deck , SAAM automatically select Model 8. This is a model developed by Berman and Chu in order to speed up the numerical solution process. It is a single-step, explicit method for solving coupled linear differential equations. This method is an alternative to the Model 1 which is fourth order step-size variable Runge-Kutta method.

After obtaining a solution, SAAM compare it with the experimental data. One may either print the results and check the model solution and experimental data, or plot and see how the model solutions and measurements agree. A solution plot is provided in Table A.3. In SAAM terminology QO is the model solution and QC is the experimental observation.

If the model and its parameters are linear, then a linear regression analysis is used to obtain the parameter estimates. Otherwise, SAAM make use of Gauss-Newton method to carry out nonlinear parameter estimation. Gauss-Newton method is explained in Chapter 4. This method basically linearize the nonlinear equation and solve it numerically by linear regression analysis. In SAAM the partial derivatives of a function with respect to the model parameters are approximated by the difference between the two succeeding iterations as follows

$$QO(k) - QC(k) = \sum \frac{\Delta QC(i)}{\Delta L_{IJ}} \delta L_{IJ} \qquad \text{A.1}$$

where $\delta L_{ij} = L^{*}_{ij} - L_{ij}$, $L^{*}_{ij} = L_{ij} + \Delta L_{ij}$, and $\Delta L_{ij} = P \times L_{ij}$ (P is a default value which determines the amount of change for the derivatives between two successive calculations).

Equation A.1 is an approximation for the values of derivatives. This approximation provides a useful tool to obtain approximation on the statistical uncertainties (this approximation is used to calculate the information matrix "A matrix" known as the "Jacobian" in the determination of parameter uncertainties). The parameter adjustment is carried out as follows:

Matrix of partial derivatives of each datum with respect to each parameter is calculated. The partial derivatives are approximate d by the following approximation.

$$\frac{\delta QC(k)}{\delta L_{IJ}} \approx \frac{\Delta QC(k)}{\Delta L_{IJ}} \qquad \text{A.2}$$

Let the correction vector corresponding to L_{ij}. is X. Then the correction vector is calculated by

$$X = a^{-1} c \qquad A.3$$

where

$$a = A^T w A$$

$$c = A^T w B \qquad \text{A.4}$$

where W is a diagonal matrix of the weighting factor. It is proportional to the inverse of the standard deviation squared for that datum and B is the difference between the model solution and the observed datum given by

$$B = QC(k) - QO(k) \qquad A.5$$

The calculated correction vector X is the quantity of the correction to be made to the each L_{ij}.. As a last step, the solution based on the corrected L_{ij} .is computed.

SAAM compute the matrix of the partial derivatives only on odd-numbered iterations in order to reduce the cost and time of calculations. Therefore it is better to set the iteration number to even numbers.

SAAM calculates the Statistical information of parameters as correlation matrix and diagonal matrix of the each parameter standard deviation. Sum of squared error is also provided as a measure of goodness of fit. An example of the SAAM output is presented in Table A.3.

Conversational SAAM (CONSAM), which is the extensively used version of SAAM, incorporate a text editor, a solution and input deck saving system, a model processor, and a graphic module. The CONSAM proved a valuable aid in modeling since it is in use. More detail can be obtained from Boston et al, Berman et al, and Robertson [60 , 61, 62]

Appendix B

Crystal Ball

Crystal Ball is a user-friendly statistical risk analysis program. It runs under the Microsoft Excel. It is possible to use most of the features of the Excel spreadsheet while working with Crystal Ball. Entire program is based on three process.

- A possible range and the type of distribution of the uncertain variables of the equation must be described. These information are entered into assumption cell.

- The equation for which the most possible outcome (i.e., mean dose) is to be found should be entered into a cell known as "forecast cell."

- Crystal Ball compute the range of the possible outcomes by a process called Monte Carlo and displays the results in a forecast chart. This chart is a plot of the possible outcomes and the probability density of achieving each one of the possible outcomes.

Crystal Ball has 16 different distributions to choose from such as lognormal,

normal, Poisson, and custom distribution. One need to decide which distribution is best represent the uncertain variable. Figure B.1 depicts a picture of the Crystal Ball Distribution Gallery.

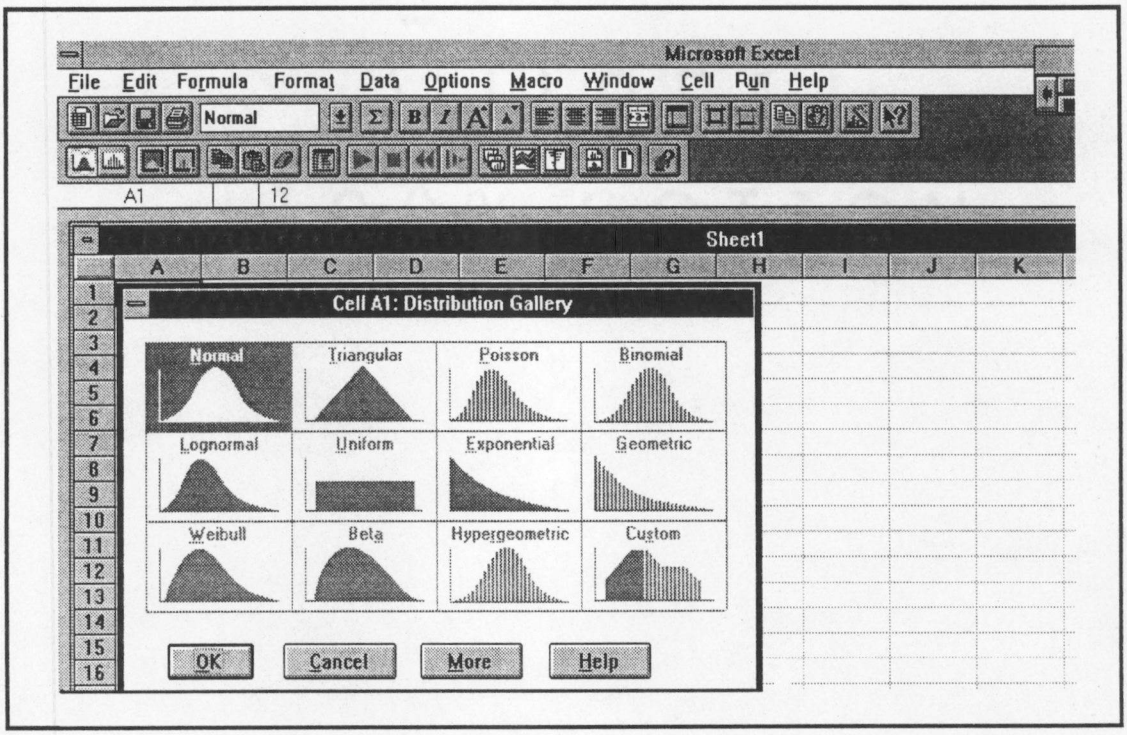

Figure B. 1 Crystal Ball distribution gallery.

Source: *Crystal Ball, Version 3.0, User manual, Decisioneering*, 1993.

Once a proper distribution is selected, the range of the distribution with the specific properties of the distributions should be specified. Each distribution requires somewhat different information to fully describe its distribution. For instance, some

distributions such as normal, binomial distributions, the knowledge of the possible range of

the variable can be specified by the mean and standard deviation of the variable, while the maximum and minimum values of a variable is to be defined to describe a uniform distribution. Figure B.2 displays an example of the assumption window for a lognormal distribution.

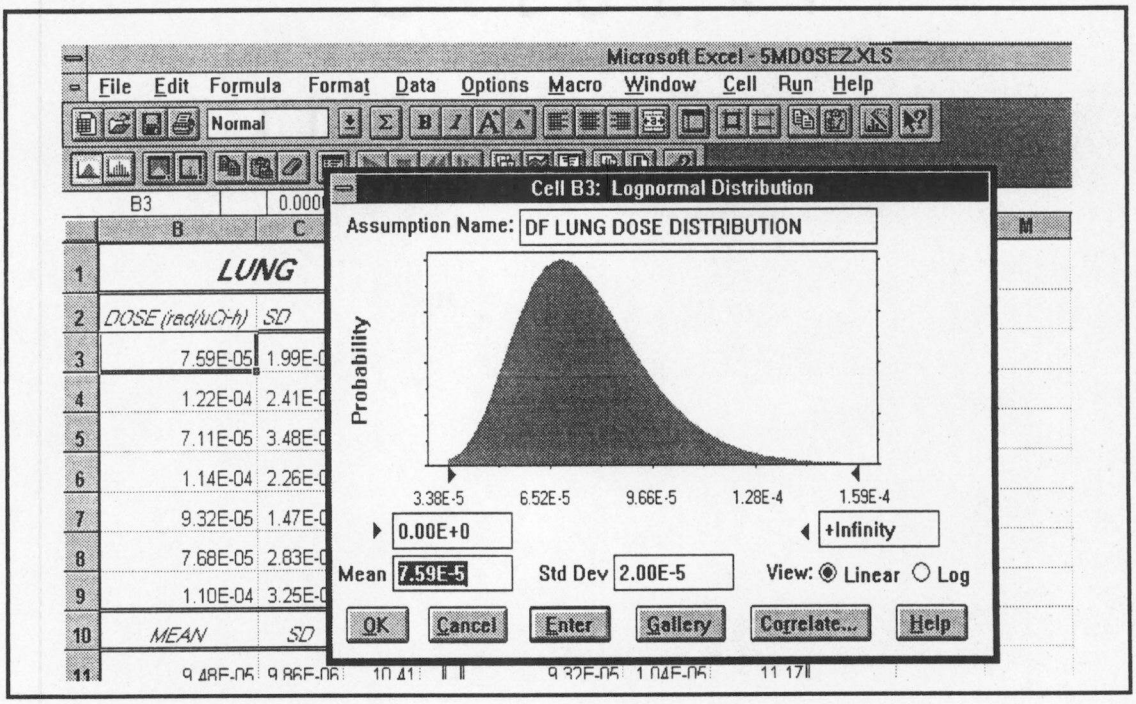

Figure B. 2 An example of assumption window for lognormal distribution.

Source: *Crystal Ball, Version 3.0, User manual, Decisioneering*, 1993.

If a variable is intercorrelated with the other variables, it is possible to define correlations between variables with Crystal Ball. Figure B.3 shows an example of Crystal Ball correlation dialog window which allow to specify correlations between variables.

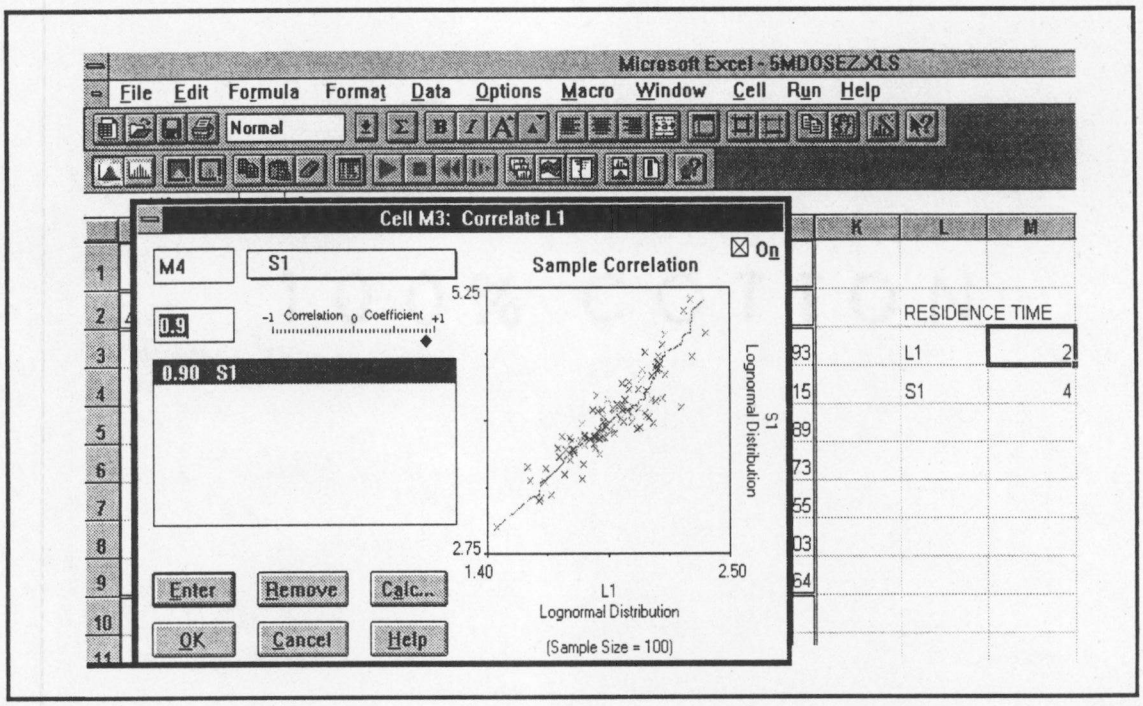

Figure B. 3 Crystal Ball correlation window.

Source: *Crystal Ball, Version 3.0, User manual, Decisioneering*, 1993.

Crystal Ball automatically calculate the correlation coefficients if the specified correlations conflicts with each other. This may occur when variables are improperly related to each other by large positive and/or negative correlation coefficients. This condition is called as inconsistent correlations. The next step is the forecast entry. The equation for which the uncertainty will be calculated should be entered and defined as

forecast. An example of the forecast window is presented in Figure B.4. The last step is to run a simulation for the equation entered as forecast.

Crystal Ball Allows to specify sampling method, number of trials, to run a

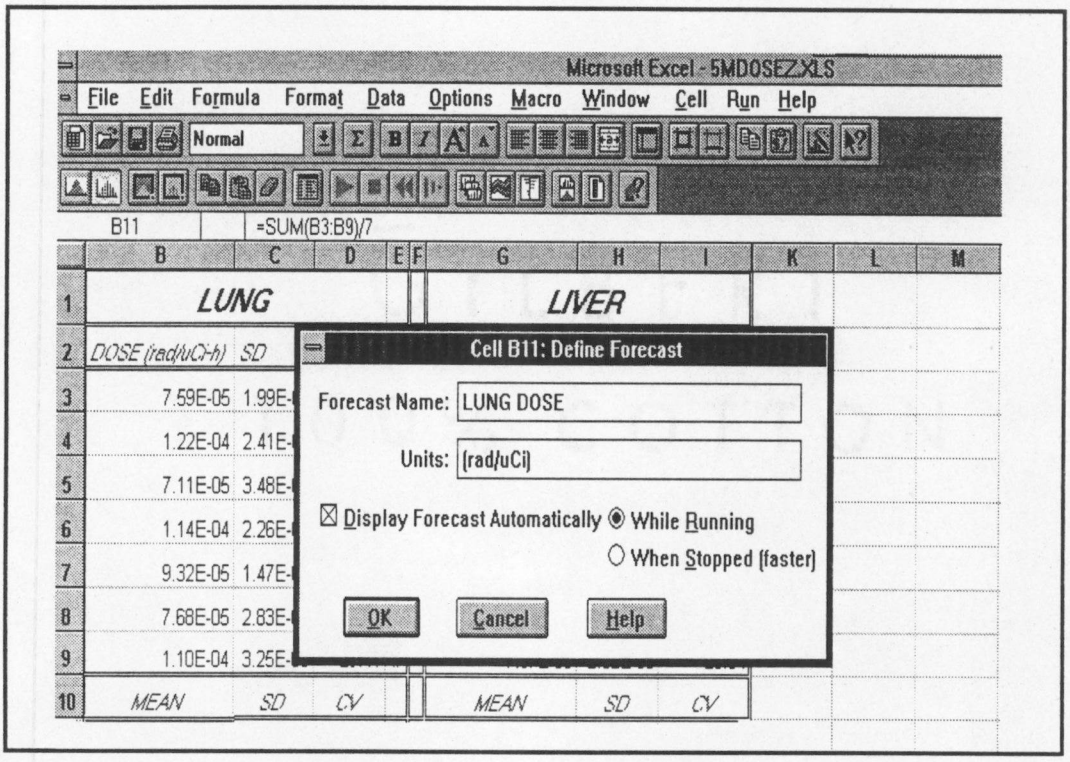

Figure B. 4 An example of Crystal Ball forecast window.

Source: *Crystal Ball, Version 3.0, User manual, Decisioneering*, 1993.

sensitivity analysis. These options shall be specified through the "Run Preferences dialog window." An example of Run Preference dialog window is displayed in Figure B.5.

Crystal Ball allows to chose either Monte Carlo or Latin Hypercube Sampling process (LHS) to run a simulation. Latin Hypercube Sampling is a stratified sampling method which is proved to be a better sampling method than Monte Carlo. However, LHS requires more memory and increase calculation time.

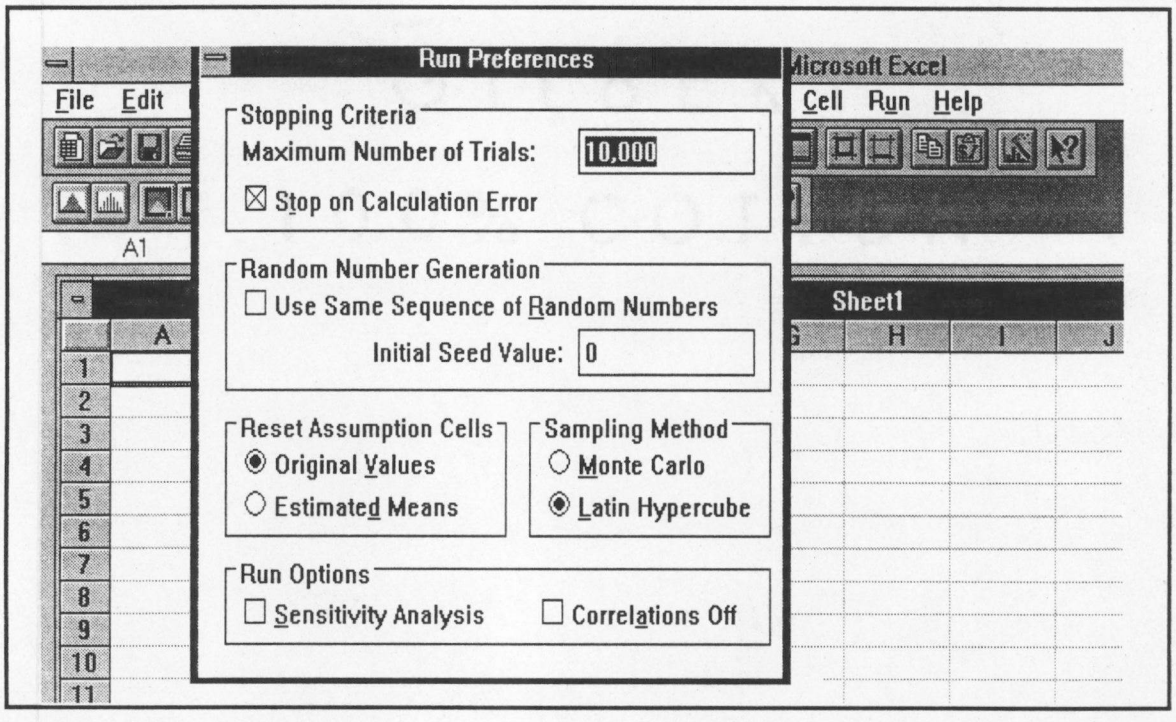

Figure B. 5 Run preference dialog window.

Source: *Crystal Ball, Version 3.0, User manual, Decisioneering*, 1993.

Crystal Ball implements Monte Carlo simulation in a three step process and repeat it for a prespecified number of trials. i) Crystal Ball generates a number from the defined distribution for each variables. ii) Crystal Ball have the spreadsheet calculate a forecast value for the selected values of the variables. iii) CB retrieves a value from the forecast

cell and adds it to the forecast chart, increasing its likelihood with every selection. A forecast chart is displayed in Figure B.6. In a forecast chart, y-axis displays the probability of occurrence for the forecast values. Crystal Ball can display results in variety forms such as cumulative chart, probability chart, trend chart, and percentiles. To obtain one of these, one need to select his choice from the preferences in forecast chart. It is also possible to display a report which includes the distributions of the variables and different statistical interpretation of the forecast. In the forecast chart, one can obtain the range of the distribution within a desired certainty by simply entering the certainty level of his choice.

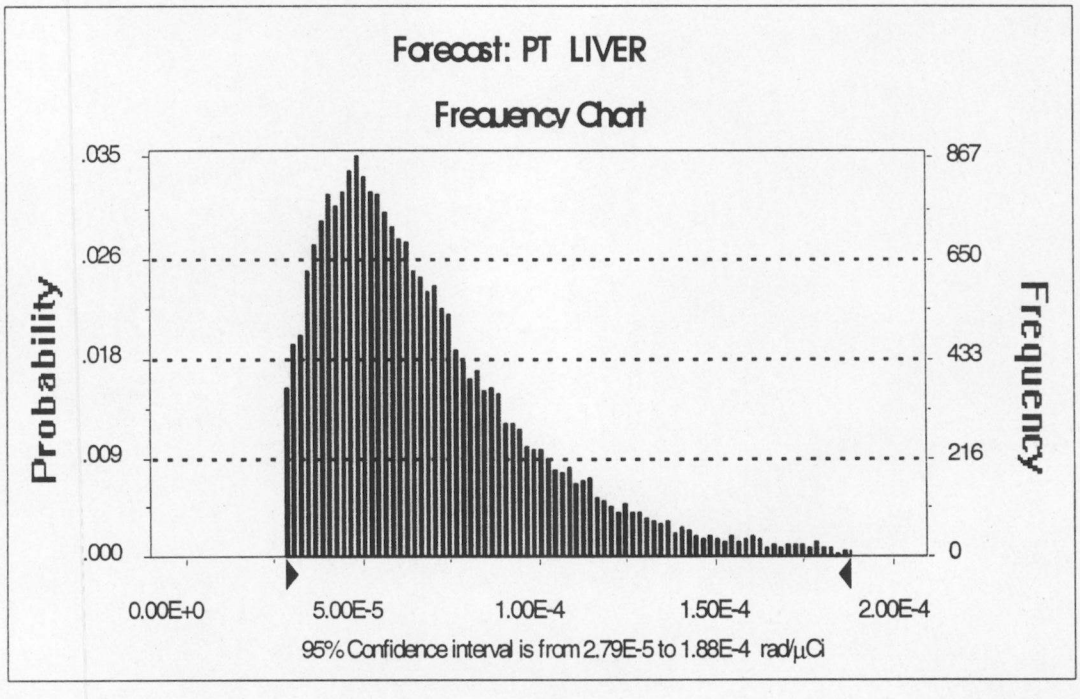

Figure B. 6 A forecast chart.

VITA

Bulent Aydogan was born in Ankara, Turkey on October 17, 1969. He attended elementary and secondary schools in Ankara, Turkiye, and graduated from Celebi Mehmet High School in June 1987. The following September he entered Middle East Technical University where he received a Bachelor of Science degree in Engineering Physics in May 1992. He, then, worked as a Physics and Mathematics teacher for one year in a private high school in Ankara, Turkey, and subsequently held a research assistant position at Balikesir University, Turkey. He received a Turkish government fellowship to pursue postgraduate degrees abroad in 1993. He entered the Physics Department of the University of Southern California in January 1994 and transferred to the Nuclear Engineering Department of The University of Tennessee, Knoxville, in August 1994 where he received a Master of Science degree with the specialty of Health Physics in Nuclear Engineering in January 1996.

He is presently a Research Assistant at the University of Florida Nuclear Engineering Department . He is currently working on his Ph.D. degree in Medical Physics.